JSCSEN 73(4)385–512(2008)

Journal of the Serbian Chemical Society

eVersion
electronic

VOLUME 73

NO 4

BELGRADE 2008

Available on line at

www.shd.org.yu/JSCS/

The full search of JSCS
is available through
DOAJ DIRECTORY OF OPEN ACCESS JOURNALS
www.doaj.org

Journal of the Serbian Chemical Society
eVersion electronic
JSCS@tmf.bg.ac.yu • www.shd.org.yu/JSCS
ISSN 0352-5139

J. Serb. Chem. Soc. Vol. 73, No. 4 (2008)

CONTENTS

Organic Chemistry and Biochemistry

Inorganic Chemistry

Theoretical Chemistry

Physical Chemistry

Geochemistry

Materials

Metallurgy

EuCheMS News

Published by the Serbian Chemical Society
Karnegijeva 4/III, 11120 Belgrade, Serbia
Printed by the Faculty of Technology and Metallurgy
Karnegijeva 4, P.O. Box 35-03, 11120 Belgrade, Serbia

Journal of the Serbian Chemical Society
eVersion eLectronic
JSCS@tmf.bg.ac.yu • www.shd.org.yu/JSCS

J. Serb. Chem. Soc. *73* (4) 385–391 (2008) UDC 542.913:546.141+547.262+547.861.3+661.333
JSCS–3720 *Original scientific paper*

A green process for the preparation of 11-{4-[2-(2-hydroxyethoxy)ethyl]-1-piperazinyl}dibenzo[*b*,*f*][1,4]thiazepine

GANESH D. MAHALE[1], ASHOK KUMAR[2], DHARMENDRA SINGH[2],
A. V. RAMASWAMY[1]* and SURESH B. WAGHMODE[1]**

[1]*Department of Chemistry, University of Pune, Pune 411 007 and* [2]*IPCA Laboratories,*
Kandivali Industrial Estate Charkop, Kandivali West, Mumbai 400 067, India

(Received 11 July, revised 19 September 2007)

Abstract: A green process for the synthesis of 11-{4-[2-(2-hydroxyethoxy)ethyl]-1-piperazinyl}dibenzo[*b*,*f*][1,4]thiazepine by the reaction of 11-(1-piperazinyl)dibenzo[*b*,*f*][1,4]thiazepine or its dihydrochloride salt with 2-(2-chloroethoxy)ethanol in the presence of an inorganic base and water is reported (conversion 99.9 % in a short time and without any impurities). The metal halides and phase transfer catalyst increase the rate of reaction, especially in water as the solvent.

Keywords: quetiapine; KI; tetrabutylammonium bromide (TBAB); 2-(2-chloroethoxy)ethanol; *N*,*N*-dimethylformamide; sodium carbonate.

INTRODUCTION

Water is a major constituent of life. It is not only inexpensive and environmentally benign but also gives completely new reactivity. Enzymatic processes in nature must occur by necessity in an aqueous environment. However, water as a solvent is uncommon for many organic reactions. Nevertheless, due to the hydrophobic effect, small size and large cohesive energy density, water not only accelerates reaction rates but also enhances reaction selectivity even when the reactants are sparingly soluble or insoluble and for water sensitive compounds.[1,2] Since the pioneering studies of the Diels–Alder reaction by Breslow, there has been increasing search for organic reactions which can proceed well in aqueous media. These offer advantages over those occurring in organic solvents. Diels–Alder,[3] pericylic,[4] carbanion[5] reactions have been reported in water with good yields and selectivity. On considering the broad applications and bright future for water as a solvent, in this study this application has been expanded to include the synthesis of pharmaceutical drugs. There has been an explosion of research acti-

---

* Present address: National Centre for Catalysis Research, Indian Institute of Technology – Madras, Chennai – 600 036, India

** Corresponding author. E-mail: suresh@chem.unipune.ernet.in

doi: 10.2298/JSC0804385M

vities in this field, which has been partially attributed to the development of the field of green chemistry.

Dibenzo[*b*,*f*][1,4]thiazepine is a class of compound used as antipsychotic drug. 11-{4-[2-(2-Hydroxyethoxy)ethyl]-1-piperazinyl}dibenzo[*b*,*f*][1,4]thiazepine (compound **I**) (trade name Quetiapine) is a typical antipsychotic drug.[6] It has been successfully employed for the treatment of schizophrenia and bipolar disorders for many years.[7] Recently, it has also been used to treat delirium and agitation.[8]

The process reported in the literature for the synthesis of **I** by the reaction of 11-(1-piperazinyl)dibenzo[*b*,*f*][1,4]thiazepine (compound **II**) or its dihydrochloride salt with 2-(2-chloroethoxy)ethanol in the presence of an inorganic base, such as sodium carbonate or potassium carbonate, in various organic solvents is well known.[9,10] The solvents used for this reaction are mainly polar aprotic and protic, such as DMF (*N*,*N*-dimethylformamide), *N*-methylpyrrolidone and methanol, ethanol, 2-propanol and *n*-hexanol or its isomers. Compound **II** may be employed in the reaction as its free base or its dihydrochloride salt (Scheme 1). The reactions were carried out in the presence of a promoter or catalyst, such as sodium iodide and tetrabutylammonium bromide (TBAB). The reaction was reportted for 24 h or more.[8,10] In another method, the reaction of 11-chlorodibenzo[*b*,*f*][1,4]thiazepine with 1-[2-(2-hydroxyethoxy)ethyl]piperazine, haloethoxypiperazine/ethyleneglycol is described.[11–13] The reaction did not precede to completion even when an excess of 2-(2-chloroethoxy)ethanol is used.

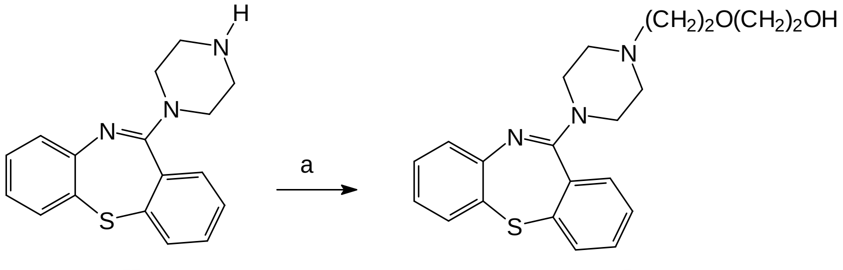

II **I**

Scheme 1. A typical reaction in water; a – 2-(2-chloroethoxy)ethanol, K_2CO_3, TBAB, KI, water.

As per pharmacopeias and drug master file requirements, the impurity level limit is very stringent.[14] This incomplete reaction gave a challenging task to attain 100 % conversion. Further purification, incurring heavy losses of the product is difficult due to the similar properties of the product and the starting material.[9,13]

A modification of the above process was reported, which deals with an attempt to reduce the reaction time and the purification procedure. According to this process, 9.7 % of unreacted **II** was found after 4 h of reaction. However, even after 17 h, only 95.5 % conversion was observed, accompanied with **II** and some other unidentified impurities. In this paper, for the first time, this reaction in aqueous medium in a shorter reaction time is described. A systematic study of the reaction parameters, such as the reaction temperature and time, the nature of the solvents and solvent to water wt. ratios (DMF:water) and the use of bases was undertaken. The typical reaction is shown in Scheme 1.

EXPERIMENTAL

The progress of the reaction was monitored by HPLC (Waters Alliance) equipped with an inertsil ODS-3, C18 (150×4.6×5 μm^3) column. The mobile phase was buffer:ACN (78:22 gradient), λ_{max} = 254 nm. ^{1}H-NMR spectroscopy of the sample was performed on a Brucker 400 MHz instrument. The ^{1}H- and ^{13}C-NMR chemical shift values are reported in ppm using TMS as the internal standard. The IR spectrum of the sample was recorded using a Perkin Elmer Spectrum 1 FTIR spectrophotometer. The mass analysis was performed on a Thermo Finnigan LCQ Advantage instrument.

*General procedure for synthesis of compound **I***

Compound **II** was prepared using the process reported by Warawa and Migler.[15,16] Then in a 100 ml four-necked round bottom flask equipped with overhead stirring, thermometer pocket and a heating oil bath, a mixture of **II** (33.30 mmol), 2-(2-chloroethoxy)ethanol (50.84 mmol), sodium carbonate (203.30 mmol) and sodium iodide (2.0 mol % w.r.t. **II**) was taken in 30 ml water and heated to about 100±2 °C. After checking the HPLC analysis, the reaction mixture was cooled to 30 °C and extracted with dichloromethane. The organic layer was washed with water, dried over anhydrous sodium sulphate and concentrated under reduced pressure to obtain compound **I** as an oil (98 %).

Anal. Calcd. for $C_{21}H_{25}N_3O_2S$: C, 65.79; H, 6.52; N, 10.96 Found: C, 65.29; H, 6.60; N, 10.82. IR (KBr, cm^{-1}): 3390, 3054, 2856, 1943, 1574, 1306, 1147, 953, 761, 699. ^{1}H-NMR (400 MHz, DMSO, δ, ppm): 2.19–2.58 (*m*, 6H, $-CH_2-N(CH_2)-CH_2$), 3.52–4.10 (*m*, 11H, $-CH_2-N(C=)-CH_2$ + $-CH_2-O-CH_2-CH_2-OH$), 6.79–7.44 (*m*, 8H, Ar). ^{13}C-NMR (400 MHz, $CDCl_3$, δ, ppm): 160.5 (C−Ar), 148.7 (C−Ar), 139.7 (C−Ar), 133.9 (C−Ar), 132.0 (C=N), 132.0 (C−Ar), 130.7 (CH−Ar), 129.0 (CH−Ar), 128.8 (CH−Ar), 128.2 (CH−Ar), 127.8 (CH−Ar), 125.2 (CH−Ar), 122.7 (CH−Ar), 72.3 (CH_2), 67.3 (CH_2), 61.6 (CH_2), 57.8 (CH_2), 52.9 (CH_2), 52.9 (CH_2), 45.6 (CH_2), 45.6 (CH_2); MS (*m*/*z*): 384 (M+1), 279, 253.

RESULTS AND DISCUSSION

The reaction reported by Warawa and Migler[9,13] in organic polar aprotic and protic solvents required 17 h under the employed reaction conditions and the yields were low (Table I, entries 1–8). Moreover, in practice, about 7 to 8 % of **II** remained unreacted even after 35 h. The reaction in water was found to be faster as compared to those in polar aprotic and protic organic solvents. The results show that water is a good solvent in combination with NaI and TBAB. The addition of TBAB slightly improved the reaction rates (Table I, entries 11 and 12). The reaction was almost completed within 30 min but trace amounts of unreacted **II** were observed up to 7 h (Table I, entry 9). However, there was no change in the concentration of **II** even after 20 h (Table I, entries 13 and 14), which depicts that after 7 h the reaction had become steady. The use of KI also gives comparable results to those obtained with NaI (Table I, entry 15).

TABLE I. A comparison of the catalytic activity of different employed catalysts and solvents. Reaction conditions: compound **II**, 33.30 mmol; 2-(2-chloroethoxy)ethanol, 50.24 mmol; K_2CO_3, 203.30 mmol; NaI or equivalent, 2 mol % to **II**; TBAB, 5 mol % to **II**; water, 30 ml

Entry	Solvents	Catalyst	Time, h	t / °C	Conversion, %
1	NMP	NaI	24	Reflux	98.7[9]
2	*n*-Propanol, NMP	NaI	24	Reflux	98.9[9]
3	Toluene	NaI	17	115–120	92.9[9]
4	Toluene	NaI/TBAB	17	115–120	99.5[9,13]
5	*n*-Butanol	NaI	17	112–115	95.7[13]
6	*n*-Butanol	NaI/TBAB	17	112–115	99.2[13]
7	DMF	NaI	4	103	90.3[13]
8	DMF	NaI/TBAB	18	103	99.3[13]
9	Water	NaI	7	98–102	99.7
10	Water	NaI	9	98–102	99.9
11	Water	NaI/TBAB	5	98–102	99.7
12	Water	NaI/TBAB	0.5	98–102	99.2
13	Water	NaI/TBAB	7	98–102	98.9
14	Water	NaI/TBAB	20	98–102	99.9
15	Water	KI	9	98–102	99.8
16	Water	NaI	7	98–102	99.8[a]
17	Water	NaI	7	98–102	99.7[b]
18	Water	KI/TBAB	7	98–102	99.9

Base: [a]triethylamine; [b]sodium bicarbonate

Different bases were employed other than sodium carbonate. The conversion of **II** in sodium bicarbonate was corroborated with the use of potassium carbonate. However, with triethylamine, the reaction mass became dark in colour and was accompanied by the formation of unidentified impurities (Table I, entry 16 and 17).

The stabilities of the compounds **I** and **II** were found to be very good under aqueous conditions. According to literature reports, the reactions were performed under inert and dry conditions.[9,13]

The influence of temperature on the reaction rate was also studied. The reactions were performed at different temperatures ranging from 30 to 102±2 °C. At lower temperatures, the conversion of **II** was very low (Table II, entry 1). However, at 50–55 °C, the conversion initially increased significantly (Table II, entry 2) but not much change was observed thereafter. At higher temperatures (100±2 °C), almost 100 % conversion was observed (Table II, entry 4).

Furthermore, the reaction was studied using different solvents and the results are summarized in Table III. In a typical reaction, water, DMF and a mixture of water and DMF were used as the solvent, in the presence of different alkali halides and TBAB. In DMF, 96.0 % conversion of **II** was observed (Table III, entry

1). The reaction mass in DMF solvent went a blackish colour. The different solvents (either DMF or water or a combination of water and DMF) at different substrate to solvent ratios were studied in order to achieve maximum conversion. The conversion increases with the water to DMF wt. ratios. At a water:DMF wt. ratio of 3:0, the maximum conversion of 99.92 % was achieved (Table III, entry 5). The reaction mass in water was of a pale yellow colour.

TABLE II. The effect of temperature on the conversion of compound **II** in water. Reaction conditions: compound **II**, 33.30 mmol; 2-(2-chloroethoxy)ethanol, 50.24 mmol; K_2CO_3, 203.30 mmol; NaI, 2 mol % to **II**; TBAB, 5 mol % to **II**; water, 30 ml

Entry	Temperature, °C (precision: ±2 °C)	Conversion, %
1	30–35	5.80
2	50–55	93.88
3	75–80	96.77
4	98–102	99.92

TABLE III. The effect of the ratio of water to DMF on the conversion of compound **II**. Reaction conditions: compound **II**, 33.30 mmol; 2-(2-chloroethoxy)ethanol, 50.24 mmol; K_2CO_3, 203.30 mmol; NaI, 2 mol % to **II**; TBAB, 5 mol % to **II**; temperature, 100±2 °C

Entry	Sub:water:DMF wt. ratio	Conversion of compound **II**, %
1	1:0:3	96.00
2	1:1:2	98.80
3	1:2:1	99.70
4	1:2.5:0.5	99.90
5	1:3:0	99.92

The quantity of water was optimized by performing the reaction at different dilution levels with respect to the **II**. The results are shown in Table IV. The reaction mass was very viscous without water and was difficult to analyze (Table IV, entry 1). As the dilution increased, the conversion decreased (Table IV). The maximum conversion was observed at a water:substrate wt. ratio 3:1 without DMF in the reaction medium (Table IV, entry 2).

TABLE IV. The effect of the concentration of water on the conversion of compound **II**. Reaction conditions: compound **II**, 33.30 mmol; 2-(2-chloroethoxy)ethanol, 50.24 mmol; base, 203.30 mmol; NaI, 2 mol % to **II**; TBAB, 5 mol % to **II**; temperature, 100±2 °C; time, 7 h

Entry	Water dilution, wt. % to **II**	Conversion, %
1	No water	RM is not uniform for analysis
2	3	99.92
3	4	99.20
4	6	98.90

A comparison of the reaction rates with and without TBAB is shown in Fig. 1. The reaction using TBAB showed a faster rate as compared to that of the reaction without TBAB. After achieving the maximum conversion in 7 h, with and without TBAB, no significant change was observed in the conversion of **II**.

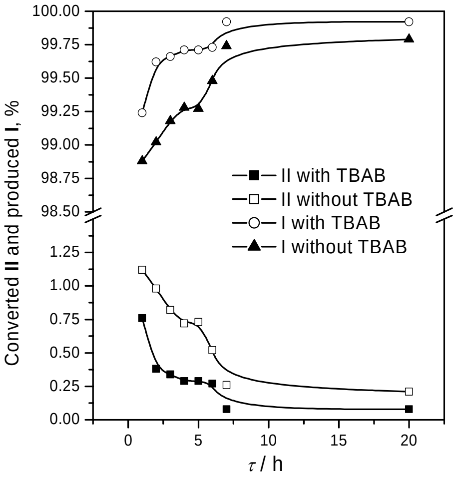

Fig. 1. The conversion to **I** and the unreacted **II**, in %, with time. Reaction conditions: Compound **II**, 33.30 mmol; 2-(2-chloroethoxy)ethanol, 50.24 mmol; base, 203.30 mmol; NaI, 2 mol % to **II**; TBAB, 5 mol % to **II**; water, 30 ml; temperature, 100±2 °C.

CONCLUSIONS

From above results, it can be concluded that the reaction in water is better than in polar aprotic and protic organic solvents. The mixture of water and DMF is also not suitable. The maximum conversion without DMF was ≈ 99.9 %. The reaction time in water was also considerably reduced, from 24 to 7 h. Phase transfer catalysts and metal halides, such as KI or NaI, were found to be important for enhancing the reaction rate.

ИЗВОД

ЕКОЛОШКИ ЧИСТО ДОБИЈАЊЕ 11-{4-[2-(2-ХИДРОКСИЕТОКСИ)ЕТИЛ]-1-ПИПЕРАЗИНИЛ}ДИБЕНЗО[*b,f*][1,4]ТИАЗЕПИНА

GANESH D. MAHALE[1], ASHOK KUMAR[2], DHARMENDRA SINGH[2],
A. V. RAMASWAMY[1] и SURESH B. WAGHMODE[1]

[1]*Department of Chemistry, University of Pune, Pune 411 007 и* [2]*IPCA Laboratories, Kandivali Industrial Estate Charkop, Kandivali West, Mumbai 400 067, India*

Описан је еколошки чист и брз поступак синтезе 11-{4-[2-(2-хидроксиетокси)етил]-1-пиперазинил}дибензо[*b,f*][1,4]тиазепина, без нечистоћа, из 11-(1-пиперазинил)дибензо[*b,f*]-[1,4]тиазепина или његове дихидрохлоридне соли и 2-(2-хлоретокси)етанола у присуству неорганске базе и воде (конверзија 99,9 %). Метални халогениди и фазни трансфер катализатор убрзавају реакцију посебно у води као растварачу.

(Примљено 11. јула, ревидирано 19. септембра 2007)

REFERENCES

1. C. J. Li, *Chem. Rev.* **93** (1993) 2023
2. L. Chen, C. J. Li, *Org. Lett.* **6** (2004) 3151
3. R. Breslow, *Acc. Chem. Res.* **24** (1991) 159
4. K. C. Nicolaou, H. Xu, M. Wartmann, *Angew. Chem. Int. Ed.* **44** (2005) 756

5. C. J. Li, *Tetrahedron* **52** (1996) 5643
6. *Merck index*, 13th Ed., p. 1439
7. B. W. Horrom, F. N. Minard, H. E. Zaugg, US 4097597 (1978)
8. R. Torres, D. Mittal, R. Kennedy, *Psychosomatics* **41** (2001) 4
9. E. J. Warawa, B. M. Migler, EP 0240228 (1987)
10. D. Dov, D. Ben-Zion, WO 076431A1 (2004)
11. J. Schmutz, F. Hunziker, US 3539573 (1970)
12. D. Diller, B. Z. Dolitzky, WO 0155125 (2001)
13. E. J. Warawa, B. M. Migler, C. J. Ohnmacht, A. L. Needles, G. C. Gatos, F. M. McLaren, C. L. Nelson, K. M. Kirkland, *J. Med. Chem*. **44** (2001) 372
14. *ICH harmonized tripartite guidelines*, (http://www.ich.org)
15. E. J. Warawa, B. M. Migler, US 4879288 (1989)
16. B. A. Charles, C. R.Jeffrey, US 0282236 (1988).

Journal of the Serbian Chemical Society

JSCS@tmf.bg.ac.yu • www.shd.org.yu/JSCS

J. Serb. Chem. Soc. 73 (4) 393–403 (2008)
JSCS–3721

UDC 577.112.383:546.11+544.35:544.4
Original scientific paper

Short hydrogen bonds in the catalytic mechanism of serine proteases

VLADIMIR LESKOVAC[1*#], SVETLANA TRIVIĆ[2#], DRAGINJA PERIČIN[1#], MIRA POPOVIĆ[2#] and JULIJAN KANDRAČ[3#]

[1]*Faculty of Technology,* [2]*Faculty of Science and* [3]*Faculty of Agriculture, University of Novi Sad, Novi Sad, Serbia*

(Received 15 May, revised 26 September 2007)

Abstract: The survey of crystallographic data from the Protein Data Bank for 37 structures of trypsin and other serine proteases at a resolution of 0.78–1.28 Å revealed the presence of hydrogen bonds in the active site of the enzymes, which are formed between the catalytic histidine and aspartate residues and are on average 2.7 Å long. This is the typical bond length for normal hydrogen bonds. The geometric properties of the hydrogen bonds in the active site indicate that the H atom is not centered between the heteroatoms of the catalytic histidine and aspartate residues in the active site. Taken together, these findings exclude the possibility that short "low-barrier" hydrogen bonds are formed in the ground state structure of the active sites examined in this work. Some time ago, it was suggested by Cleland that the "low-barrier hydrogen bond" hypothesis is operative in the catalytic mechanism of serine proteases, and requires the presence of short hydrogen bonds around 2.4 Å long in the active site, with the H atom centered between the catalytic heteroatoms. The conclusions drawn from this work do not exclude the validity of the "low-barrier hydrogen bond" hypothesis at all, but they merely do not support it in this particular case, with this particular class of enzymes.

Keywords: trypsin; serine proteases; low-barrier hydrogen bonds.

INTRODUCTION

Usually observed hydrogen bonds represent relatively weak interactions (around 10 kJ mol^{-1}). Approximate parameters for the O−H···O hydrogen bond in water are 2.8, 1.0 and 1.8 Å for the O···O ("heteroatom distance"), O−H and H···O interatomic distances, respectively.[1] However, the existence of short hydrogen bonds, or Speakman–Hadzi bonds, has been known for a long time.[2,3] In short hydrogen bonds, the overall bond becomes stronger as the heteroatom dis-

---

[*] Corresponding author. E-mail: jkandrac@polj.ns.ac.yu

[#] Serbian Chemical Society member.

doi: 10.2298/JSC0804393L

tance becomes shorter and at a distance of 2.4 Å, the hydrogen becomes centered between the heteroatoms; this is largely a covalent bond.[4]

In 1992, Cleland and Frey[1,5–9] proposed that such short, or low-barrier hydrogen bonds (LBHB), when located between the substrate and the acid-base catalyst in the active sites of enzymes, can play an important role in several cases of enzyme catalysis. The theory of LBHB has emerged in recent years and implies short (< 2.5 Å) and very strong (40–80 kJ mol^{-1}) hydrogen bonds.[5,10–12] Such hydrogen bonds are formed if the donor and acceptor atoms are close to one another and display similar pK_a values. In LBHBs, the proton is shared by the donor and acceptor in a single, low-potential energy well, which implies that the barrier for proton transfer is eliminated.[13]

The LBHB catalytic hypothesis contains the following premises:[12]

(a) In hydrogen bonds located between the substrate and the acid-base catalyst in the active site, a large increase in bond strength can occur as the enzyme–substrate complex is converted into a reactive intermediate or a transition state.[12]

(b) Strong hydrogen bonds between bases of similar proton affinities could account for much of the required differential stabilization of enzyme-bound intermediates and transition states compared to the initial enzyme–substrate complex.[12]

(c) If the hydrogen bond strength is significantly less when the proton affinities of the donor and acceptor are dissimilar (such as in the enzyme–substrate complex), the energetic cost of forming the transition state should be substantially reduced.[8,12]

(d) Thus, the strength of the hydrogen bond depends on: its length, linearity, the nature of the microenvironment and the degree to which the pK_a values of the conjugate acids and the heavy atoms sharing the proton are matched.[8]

When a mechanism involves the formation of an unstable intermediate, the transition state for forming it will closely resemble the intermediate and the LBHB will also be found in the intermediate or a closely mimicking enzyme–inhibitor complex. It was proposed that such mimics of metastable intermediates at enzymatic sites may allow the direct observation of LBHBs by crystallographic methods.[8,12,14,15]

Following this lead, the crystallographic structures of the active sites of serine proteases, in free enzymes, in preparations complexed with products of the reaction and in enzyme complexes with ligands were systematically investigated in order to observe short hydrogen bonds. Unlike other classes of enzymes, a large number of structures of serine proteases have been solved at high resolution and these proteases are exceptionally suitable for the above-mentioned task.

Protein Data Bank

The RCSB-PDB Protein Data Bank was systematically examined for three-dimensional structures of serine proteases. The data were downloaded from the website http://www.rcsb.org and are presented in Tables I and II; they summarize the free enzymes, enzyme–product complexes, and enzyme–ligand complexes

TABLE I. Summary of crystal structures of trypsin (entries 1–12) and other serine proteases (entries 13–18), at a resolution from 0.78–1.00 Å

Entry	PDB access code	Source of protease	Resolution Å	*R* value	pH[a]	Ligands bound in the active site[b]	Source
1	1PQ7	*Fusarium oxysporum* trypsin	0.80	0.109	5.0	Arginine	16
2 3	1FN8 1FY4	*Fusarium oxysporum* trypsin	0.81	0.108	6.0	Gly–Ala–Arg	17
4	1FY5	*Fusarium oxysporum* trypsin	0.81	0.124	6.0	Gly–Ala–Lys	17
5	1GDN	*Fusarium oxysporum* trypsin	0.81	0.108	6.0	Gly–Ala–Lys	17
6	1XVO	*Fusarium oxysporum* trypsin	0.84	0.108	5.0	–	18
7	1PQ5	*Fusarium oxysporum* trypsin	0.85	0.098	5.0	Arginine	16
8	1GDQ	*Fusarium oxysporum* trypsin	0.93	0.099	6.0	Arginine	17
9	1HJ9	Trysin from bovine pancreas after structural damage	0.95	0.117	8.0	–	19
10	2AYW	Trypsin from bovine pancreas	0.97	0.138	6.0	ONO, MES	20
11	1HJ8	Trypsin from atlantic salmon	1.00	0.118	5.8	–	19
12	1PQ8	*Fusarium oxysporum* trypsin	1.00	0.128	4.0	Gly–Gly– –Arg; Lys	16
13	2H5C	α-Lytic protease from *Lysobacter enzymogenes*	0.82	0.081	4.3	–	21
14	1SSX	α-Lytic protease from *Lysobacter enzymogenes*	0.83	0.087	8.0	–	22
15	2H5D	α-Lytic protease from *Lysobacter enzymogenes* complexed with MeOSuc–Ala–Ala–Pro– –Val boronic acid	0.90	0.080	8.0	MSU–Ala– –Ala–Pro–B2V	21
16	1EA7	*Bacillus sphaericus* sphericase	0.97	0.097	7.5	Sulfur atom	23
17	1GCI	*Bacillus lentus* subtilisin	0.78	0.099	5.9	–	24
18	1GVK	Porcine elastase acyl enzyme	0.94	0.122	5.0	Acetyl group	25

[a] pH of crystallization buffer; [b] most preparations contained SO_4^{2-} and Ca^{2+} and some contained bound benzamidine or glycerol. Abbreviations: ONO – 2-[2-({[4-(diaminomethyl)phenyl]amino}carbonyl)-6-methoxypyridin-3-yl]-5-{[(1-formyl-2,2-dimethylpropyl)amino]carbonyl)benzoic acid, MES – 2-(*N*-morpholino)-ethanesulfonic acid, MSU–Ala–Ala–Pro–B2V – Succinic acid monomethyl ester–Ala–Ala–Pro–Valine boronic acid

TABLE II. Summary of crystal structures of trypsin at resolution 1.02–1.28 Å

Entry	PDB access code	Source of trypsin	Resolution Å	*R* value	pH[a]	Ligands bound in the active site[b]	Source
1	1S0Q	Bovine pancreas	1.02	0.112	8.0	c	26
2	1S0R	Bovine pancreas	1.02	0.112	8.0	c	26
3	1GDU	*Fusarium oxysporum*	1.07	0.104	6.0	Gly–Ala–Arg	17
4	1XVM	*Fusarium oxysporum*	1.10	0.144	5.0	Gly–Ala–Arg	18
5	2AH4	Guanidinobenzoyl-trypsin	1.13	0.12	5.0	GBS	27
6	2AGI	Leupeptin–trypsin covalent complex	1.14	0.117	5.0	Ace–Leu–Leu–Arg	27
7	2AGE	Succinyl-AAPR-trypsin acyl-enzyme	1.15	0.12	6.0	Suc–Ala–Ala–Pro–Arg	27
8	1UTN	Bovine pancreas	1.15	0.113	8.0	TRS, benzylamine	28
9	1UTO	Bovine pancreas	1.15	0.139	8.0	2-Phenylethylamine	28
10	1UTQ	Bovine pancreas	1.15	0.138	8.0	c	28
11	1Y59	Bovine pancreas trypsin mutant complexed with inhibitor	1.20	0.123	7.0	TL1	29
12	2BLV	Bovine pancreatic trypsin before a high dose X-ray "burn"	1.20	0.107	–	c	30
13	2BLW	Bovine pancreatic trypsin after a high dose X-ray "burn"	1.20	0.108	–	c	30
14	2F91	Crayfish trypsin complexed with peptide inhibitor SGTI	1.20	0.139	4.6	Peptide inhibitor SGTI-32AA	31
15	1J8A	Bovine pancreas	1.21	1.21	7.4	TRS	32
16	1PPZ	Trypsin complexed with an inhibitor MIS	1.23	0.14	5.0	MIS	16
17	1PQA	Bovine pancreas trypsin complexed with PMSF	1.23	0.141	5.0	SEB	16
18	2A31	Bovine pancreas trypsin complexed with borate	1.25	0.14	8.0	BO4, PG3	33
19	2AGG	Succinyl-AAPK-trypsin acyl-enzyme (bovine pancreas)	1.28	0.125	6.0	Suc–Ala–Ala–Pro–Lys	27

[a] pH of crystallization buffer; [b] most preparations contained SO_4^{2-} and Ca^{2+} and some contained bound glycerol; [c] no ligand was bound in the active site. Abbreviations: GBS – 4-guanidinobenzoic acid, Ace–Leu–Leu–Arg – *N*-acetyl–Leu–Leu–Arg, Suc–Ala–Ala–Pro–Arg – succinyl–Ala–Ala–Pro–Arg, TRS – 2-amino-2-hydroxymethyl-propane-1,3-diol, TL1 – 2,5-bis-*O*-{3-[amino(imino)methyl]phenyl}-1,4:3,6-dianhydro-D-glucitol [2,5-*O*,*O*-bis-(3',3"-amidinophenyl)-1,4:3,6-dianhydro-D-sorbitol], MIS – monoisopropylphosphorylserine, PMSF – phenylmethylsulfonyl fluoride, SEB – ortobenzylsulfonyl-serine, BO4 – borate ion, PG3 – guanidine-3-propanol, Suc–Ala–Ala–Pro–Lys – succinyl–Ala–Ala–Pro–Lys

that were examined in this work. It is important to emphasize that the data were surveyed up to 1 January, 2007 and, therefore, Tables I and II present the complete crystallographic information on the active sites of serine proteases up to that date. The distances between atoms and the angles between the bonds were estimated with the aid of two computer programs; first, the Deep View/ /Swiss PDB Viewer program, v. 3.7, downloaded from the ExPASy Proteomics website (http://www.expasy.org/spdbv), and second, the RasWin Molecular Graphics, Windows Version 2.6 program, downloaded from the website of the University of Massachusetts Amherst (http://www.umass.edu/microbio/rasmol/getras.htm).

RESULTS

Mechanism of action of serine proteases

Serine proteases represent a large family of enzymes which catalyze the hydrolysis of peptide bonds in proteins and peptides or the hydrolysis of ester bonds. They include trypsin, chymotrypsin, and other serine proteases.[34]

Recently, Cleland[8] and Frey[35] proposed that the catalytic cycles of trypsin, chymotrypsin and other serine proteases proceed according to the mechanism given in Scheme 1.

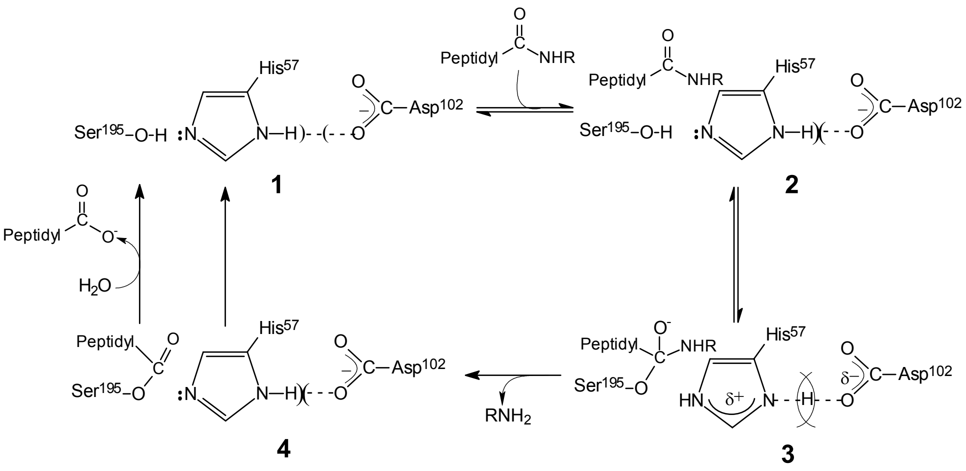

Scheme 1. Catalytic cycle of chymotrypsin, drawn according to Frey[35] and Cleland.[8]

According to Cleland,[8] upon the binding of a specific substrate, the active site of chymotrypsin undergoes a compression which brings His-57 and Asp-102 close together. The required energy is provided by the binding energy derived from specific enzyme-substrate contacts. Since the difference in pK_a between the neutral His-57 and Asp-102 is more than 10 units, the hydrogen bond remains weak and cannot relieve the strain of compression. Protonation of Nε2 permits the formation of an LBHB between His-57 and Asp-102 because the pK_a are now much more closely matched. The short hydrogen bond relieves the strain of compression (Scheme 1).

Accuracy of X-ray crystallographic data

The crystal structure of over 600 serine proteases and their complexes with substrate analogs and inhibitors have been reported and deposited in the Protein Data Bank.[36] However, only a small portion of these data was obtained at an atomic resolution (< 1 Å) or at a near atomic resolution (1.0–1.3 Å). When the crystallographic resolution becomes lower than 1.3 Å, the positioning of the hydrogen bond and the hydrogen atom becomes uncertain, because the error in estimation increases rapidly with decreasing resolution (Fig. 1). For this reason, from over 600 serine proteases reported in the literature, the crystal structure of two groups of proteases, the first group with a resolution less then 1 Å (Table I) and the second with a resolution of 1–1.3 Å (Table II), were examined in the present study.

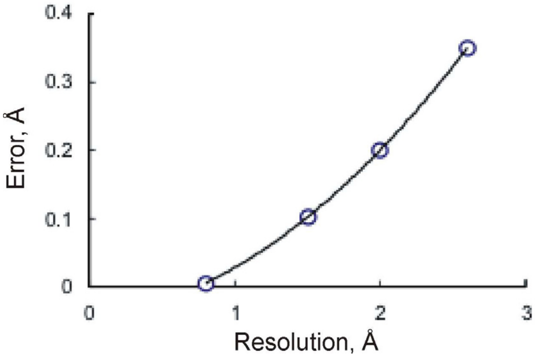

Fig. 1. Relationship between resolution and error.

Structure of serine proteases at a resolution below 1 Å

The enzyme structures analyzed in Table I were crystallized in most cases at pH 4.0–6.0, indicating that the catalytic aspartate was dissociated in most cases, while the catalytic histidine was mostly protonated. In Table I, the *R* values are in most cases below 0.12, indicating a high quality of crystallographic resolution. In the catalytic triad Ser···His···Asp (Scheme 1), the distance between the heteroatoms in Ser and His, for all structures listed in Table I, was always 2.80–3.10 Å (data not shown), indicating a normal hydrogen bonding distance between the hydroxyl oxygen of serine and imidazole nitrogen of histidine.[34]

On the other hand, the distance between the heteroatoms in histidine and aspartate in the catalytic triad was shorter, from 2.64–2.77 Å (Table III). The difference between the heteroatoms in Ser and His was always shorter than that between the heteroatoms in His and Asp. The average difference was 0.2 Å, which is significant because at this resolution the error was less than 0.02 Å.

The normally allowed van der Waals distance for interatomic contacts between oxygen and nitrogen is 2.7 Å, indicating the presence of short hydrogen bonds only in several crystal structures in Table II. Since proton imaging was feasible at this resolution, it was possible to determine in most cases the extent of linearity of the H bond; in most cases the angle was 160–170°, indicating that the H bonds were nearly linear (Table III).

TABLE III. Putative hydrogen bonds in the catalytic triad of trypsin and other serine proteases at a resolution 0.78–1.00 Å, from Table I

Entry	PDB access code	Putative hydrogen bonds between the catalytic aspartate and histidine	Distance Å	Hydrogen bond, Å		Angle deg.
				OD···H	H–ND1	
1	1PQ7	ASP99A (OD2)···HIS 56A (ND1)	2.77	1.92	0.86	166.1
2	1FN8	ASP102A (OD2)···HIS 57A (ND1)	2.75	1.92	0.86	164.0
3	1FY4	ASP102A (OD2)···HIS 57A (ND1)	2.75	1.91	0.86	162.8
4	1FY5	ASP102A (OD2)···HIS 57A (ND1)	2.75	1.92	0.86	163.1
5	1GDN	ASP102A (OD2)···HIS 57A (ND1)	2.76	1.92	0.86	163.1
6	1XVO	ASP99A (OD2)···HIS 56A (ND1)	2.75	1.91	0.86	165.6
7	1PQ5	ASP99A (OD2)···HIS 56A (ND1)	2.75	1.91	0.86	165.6
8	1GDQ	ASP102A (OD2)···HIS 57A (ND1)	2.75	1.92	0.86	166.1
9	1HJ9	ASP102A (OD2)···HIS 57A (ND1)	2.73	a	a	a
10	1AYW	ASP102A (OD2)···HIS 57A (ND1)	2.70	a	a	a
11	1HJ8	ASP102A (OD2)···HIS 57A (ND1)	2.69	a	a	a
12	1PQ8	ASP99A (OD2)···HIS 56A (ND1)	2.74	1.90	0.86	166.7
13	2H5C	ASP102A (OD1)···HIS 57A (ND1)	2.76	1.93	0.85	163.9
14	1SSX	ASP102A (OD1)···HIS 57A (ND1)	2.77	1.95	0.83	170.4
15	2H5D	ASP102A (OD1)···HIS 57A (ND1)	2.73	1.77	1.01	158.6
16	1EA7	ASP34A (OD1)···HIS 71A (ND1)	2.65	1.79	0.86	174.9
17	1GCI	ASP32 (OD2)···HIS 64 (ND1)	2.64	1.57	1.12	157.5
18	1GVK	ASP102B (OD2)···HIS 57B (ND1)	2.67	a	a	a

[a] No corresponding data were found in the Protein Data Bank

Structure of serine proteases at a resolution 1.0–1.3 Å

The structures of trypsin crystallized at pH 5.0–8.0 and solved at 1.02–1.28 Å resolution are shown in Tables II and IV. At this resolution, proton imaging was possible only in few cases. The *R* values were in most cases below 0.14, indicating a satisfactory quality of the crystallographic resolution. In the catalytic triad Ser···His···Asp (Scheme 1), the distance between the heteroatoms in Ser and His for the structures listed in Table II was always 2.8–3.1 Å (data not shown), indicating again a normal hydrogen bond distance between the hydroxyl oxygen of serine and the imidazole nitrogen of histidine.

On the other hand, the distance between the heteroatoms in histidine and aspartate in the catalytic triad was shorter, from 2.57–2.77 Å; the exceptions are entries 9, 12, 16, and 19 in Table IV, where the difference was in the opposite direction (data not shown). We have no ready explanation for these exceptions, except that the lower resolution may afford, in some cases, some degree of uncertainty. The difference between the heteroatoms in Ser and His, and in His and

Asp is this time less significant, because at this resolution the error is up to 0.06 Å. At this resolution, proton imaging is possible only in a few cases and, therefore, the linearity of the H bond can be determined in only a few cases (Table V).

TABLE IV. Crystal structures of trypsin at a resolution 1.02–1.28 Å

Entry	PDB access code	Putative hydrogen bonds between the catalytic aspartate and histidine residue	Distance Å
1	1S0Q	ASP743A (OD2)···HIS 699A (ND1)	2.76
2	1S0R	ASP84A (OD2)···HIS 40A (ND1)	2.75
3	1GDU	ASP102A (OD2)···HIS 57A (ND1)	2.72
4	1XVM	ASP99A (OD2)···HIS 56A (ND1)	2.71
5	2AH4	ASP102X (OD2)···HIS 57X (ND1)	2.78
6	2AGI	ASP102X (OD2)···HIS 57X (ND1)	2.75
7	2AGE	ASP102X (OD2)···HIS 57X (ND1)	2.75
8	1UTN	ASP102A (OD2)···HIS 57A (ND1)	2.73
9	1UTO	ASP102A (OD2)···HIS 57A (ND1)	2.76
10	1UTQ	ASP102A (OD2)···HIS 57A (ND1)	2.76
11	1Y59	ASP102T (OD2)···HIS 57T (ND1)	2.74
12	2BLV	ASP102A (OD2)···HIS 57A (ND1)	2.73
13	2BLW	ASP102A (OD2)···HIS 57A (ND1)	2.73
14	2F91	ASP102A (OD2)···HIS 57A (ND1)	2.74
15	1J8A	ASP102A (OD2)···HIS 57A (ND1)	2.72
16	1PPZ	ASP99A (OD2)···HIS 56A (ND1)	2.97
17	1PQA	ASP99A (OD2)···HIS 56A (ND1)	2.57
18	2A31	ASP102A (OD2)···HIS 57A (ND1)	2.78
19	2AGG	ASP102X (OD2)···HIS 57X (ND1)	2.81

TABLE V. Putative hydrogen bonds in the catalytic triad of trypsin at resolution 1.02–1.28 Å

Entry	PDB access code	List of putative hydrogen bonds in the catalytic triad	Distance Å	Hydrogen bond, Å		Angle deg.
				OD···H	H–ND1	
3	1GDU	ASP102A (OD2)···HIS 57A (ND1)	2.72	1.89	0.86	160.4
4	1XVM	ASP99A (OD2)···HIS 56A (ND1)	2.71	1.89	0.86	160.7
16	1PPZ	ASP99A (OD2)···HIS 56A (ND1)	2.97	1.73	1.43	140.0
17	1PQA	ASP99A (OD2)···HIS 56A (ND1)	2.57	1.82	0.86	144.4
18	2A31	ASP102A (OD2)···HIS 57A (ND1)	2.78	1.85	1.00	153.2

CONCLUSIONS

Binding of ligands. Most of the analyzed enzyme structures given in Table I (obtained at a resolution < 1 Å) were crystallized in the presence of salts and contain salt ions, sometimes bound in the active site, such as SO_4^{2-}, Na^+, Ca^{2+} or citrate, or ligands, such as glycerol, benzamidine or aniline. Detailed information concerning these ligands is not included in Table I in order to save space. Furthermore, several preparations contained arginine, lysine, or arginine peptides bound in the active site, which mimic the products of the reaction. In addition, two preparations had bound inhibitors ONO (entry 10) or valine boronic acid (entry 15). In one occasion (entry 18), the serine residue in the active site was acetylated.

The analyzed enzyme structures given in Table II (resolution 1.0–1.3 Å) contained similar ligands, including imidazole. Furthermore, some preparations contained inhibitors bound in the active site, benzylamine (entriy 8) and TL1 (entry 11). In addition, in several preparations the serine residue in the active site was acylated (entries 5, 6, 7, and 19).

Hydrogen bonds in the active site. In the catalytic triad Ser···His···Asp, there are two hydrogen bonds. In the preparations listed in Table I (resolution < 1 Å), the length of the hydrogen bonds between the heteroatoms in His···Asp were in each preparation shorter than the hydrogen bond between the heteroatoms in Ser···His, on average by 0.2±0.02 Å. In the preparations listed in Table II (resolution 1–1.3 Å), the length of the hydrogen bonds between the heteroatoms in His···Asp were in most cases shorter than the bond between the heteroatoms in Ser···His, on average by 0.2±0.06 Å; however, in a few cases, the situation was reversed, *i.e.*, the former hydrogen bonds were longer than the latter, on average by 0.1±0.06 Å (entries 9, 12, 16, and 19).

Crystallographic evidence for the mechanism in Scheme 1. In this communication, a total number of 37 enzyme structures of trypsin and other serine proteases, obtained at a resolution 0.78–1.28 Å, were examined (Tables I and II). It is interesting to note that no structure was reported in the literature for chymotrypsin with a resolution better than 1.4 Å.

The information obtained from the structures of active sites of serine proteases may be compared with the mechanism presented in Scheme 1. The normally allowed van der Waals distance for interatomic contacts between oxygen and nitrogen is 2.7 Å. There are only a few distances slightly shorter than 2.7 Å, four in Table III and one in Table IV. According to Scheme 1, short hydrogen bonds are formed between the catalytic aspartate and histidine and not between serine and histidine. Indeed, in accordance with this, the hydrogen bonds between aspartate and histidine are in most cases shorter than the hydrogen bonds between serine and histidine. The formation of an LBHB requires a hydrogen bond on a straight line between the heteroatoms, with the H atom nearly centered between them. Tables II and V indicate that the H atom is nearly collinear, the angle between the heteroatoms and the hydrogen is in most cases 160–170°. However, the H atom is nearly centered between the heteroatoms in only a few cases; this is not surprising, since the H atom is fully centered only in transition states which are unstable. In addition, the hydrogen atom is centered only when the pK_as of heteroatoms are matched, which occurs only in unstable transition state structures.

Thus, the survey performed in this work of crystallographic structures obtained at high resolution indicates that in serine proteases they do not comply with the LBHB hypothesis. Warshel and coworkers suggested earlier that LBHBs cannot be observed by crystallographic methods because the transition state structures are inherently unstable.[37–40] Also, recent quantum chemistry modeling of serine proteases do not support the LBHB concept.[41,42]

However, it must be emphasized that the findings reported in this work do not exclude the validity of the LBHB hypothesis at all, but merely show that the data do not comply with the hypothesis for this particular class of enzymes. Recently, a survey of critical hydrogen bond lengths in lactate and alcohol dehydrogenase was reported.[43] It was found that short hydrogen bonds were clustered, to a very high degree, exactly at the bond breaking position in complexes of alcohol dehydrogenase with its substrates or their analogs. This finding suggests indirectly that the LBHB hypothesis may be valid for alcohol dehydrogenases. A similar clustering of short hydrogen bonds was not found in the case of lactate dehydrogenases.

Acknowledgements. This work was financially supported by the Ministry of Science and Environmental Protection of the Republic of Serbia, Grant No. 142046.

ИЗВОД

КРАТКЕ ВОДОНИЧНЕ ВЕЗЕ У КАТАЛИТИЧКОМ МЕХАНИЗМУ СЕРИНСКИХ ПРОТЕАЗА

ВЛАДИМИР ЛЕСКОВАЦ[1], СВЕТЛАНА ТРИВИЋ[2], ДРАГИЊА ПЕРИЧИН[3],
МИРА ПОПОВИЋ[2] И ЈУЛИЈАН КАНДРАЧ[3]

[1]*Технолошки факултет,* [2]*Природно–математички факултет и* [3]*Пољопривредни факултет*
Универзитета у Новом Саду

Преглед кристалографских података из “ Protein Data Bank ” за 37 структура трипсина и других серинских протеаза на разлагању од 0,78–1,28 Å, показују присуство водоничних веза у активном центру ензима, које се образују између каталитичког серина и аспартата, и у просеку су дужине 2,7 Å. То је типична дужина за нормалну водоничну везу. Геометријска својства водоничних веза у активном центру показују да H атом није центриран између хетероатома каталитичког хистидина и аспартата. Када се све сабере, ови налази показују да се “водоничне везе ниске баријере” не образују у основном стању структура активног центра које су истражене у овом раду. Хипотеза “водоничних веза ниске баријере”, коју је недавно предложио Cleland, захтева присуство кратких водоничних веза од 2,4 Å у активном центру, са H атомом центрираним између хетероатома. Закључак овог рада никако не искључује валидност хипотезе “водоничних веза ниске баријере”, али не подупире ову хипотезу у случају испитиване класе ензима.

(Примљено 15. маја, ревидирано 26. септембра 2007)

REFERENCES

1. W. W. Cleland, *Biochemistry* **31** (1992) 317
2. J. C. Spaekman, *J. Chem. Soc.* (1949) 3357
3. D. Hadzi, *Pure Appl. Chem.* **11** (1965) 435
4. W. W. Cleland, *Arch. Biochem. Biophys.* **382** (2000) 1
5. W. W. Cleland, M. M. Kreevoy, *Science* **264 (**1994) 1887
6. W. W. Cleland, M. M. Kreevoy, *Science* **269** (1995) 104
7. P. A. Frey, *Science* **269** (1995) 104
8. W. W. Cleland, P. A. Frey, J. A. Gerlt, *J. Biol. Chem.* **273** (1998) 25529
9. D. Neidhart, Y. M. Wei, C. Cassidy, J. Lin, W. W. Cleland, P. A. Frey, *Biochemistry* **40** (2001) 2439

10. J. A. Gerlt, P. G. Gassman, *Biochemistry* **32** (1993) 11934
11. C. S. Cassidy, J. Lin, P. A. Frey, *Biochem. Biophys. Res. Comm.* **273** (2000) 789
12. J. A. Gerlt, M. M. Kreevoy, W. W. Cleland, P. A. Frey, *Chem. Biol.* **4** (1997) 259
13. L. Polgar, *Cell. Mol. Life Sci.* **62** (2005) 2161
14. C. S. Cassidy, J. Lin, P. A. Frey, *Biochemistry* **36** (1997) 4576
15. P. A. Frey, S. A. Witt, J. B. Tobin, *Science* **264** (1994) 1927
16. A. Schmidt, C. Jelsch, P. Ostergaard, W. Rypniewski, V. S. Lamzin, *J. Biol. Chem.* **278** (2003) 43357
17. W. R. Rypniewski, P. R. Ostergaard, M. Norregaard-Madsen, M. Dauter, K. S. Wilson, *Acta Crystallogr., Sect. D* **57** (2001) 8
18. A. Schmidt, V. S. Lamzin, *Acta Crystallogr. Sect. D* **61** (2005) 1132
19. H.-K. S. Leiros, S. M. McSweeney, A. O. Smalas, *Acta Crystallogr. Sect. D* **57** (2001) 488
20. M. Sherawat, P. Kaur, M. Perbandt, C. Betzel, W. A. Slusarchyk, G. S. Bisacchi, C. Y. Chang, B. L. Jacobson, H. M. Einspahr, T. P. Singh, *Acta Crystallogr. D, Biol. Crystallogr.* **63** (2007) 500
21. C. N. Fuhrmann, M. D. Daugherty, D. A. Agard, *J. Am. Chem. Soc.* **128** (2006) 9086
22. C. N. Fuhrmann, B. A. Kelch, N. Ota, D. A. Agard, *J. Mol. Biol.* **338** (2004) 999
23. O. Almog, A. Gonzalez, D. Klein, H. M. Greenblat, S. Braun, G. Shoham, *J. Mol. Biol.* **332** (2003) 1071
24. P. Kuhn, M. Knapp, S. M. Soltis, G. Ganshaw, M. Thoene, R. Bott, *Biochemistry* **37** (1998) 13446
25. G. Katona, R. C. Wilmouth, P. A. Wright, G. I. Berglund, J. Hajdu, R. Neutze, C. J. Schofield, *J. Biol. Chem.* **277** (2002) 21962
26. J. A. Chamorro Gavilanes, J. A. Cuesta-Seijo, S. Garcia-Granda, to be published
27. E. S. Radisky, J. M. Lee, C. J. Lu, D. E. Koshland Jr., *Proc. Natl. Acad. Sci. USA* **103** (2006) 6835
28. H.-K. S. Leiros, B. O. Brandsdal, O. A. Andersen, V. Os, I. Leiros, R. Helland, J. Otlewski, N. P. Willassen, A. O. Smalas, *Protein Sci.* **13** (2004) 1056
29. A. Di Fenza, A. Heine, G. Klebe, in *Proceeding of 22nd European Crystallographic Meeting ECM22*, Budapest, Hungary, (2004), *Acta Crystalogaphica*, (2004), A60, s163.
30. M. H. Nanao, G. M. Sheldrick, R. B. G. Ravelli, *Acta Crystallogr. Sect. D* **61** (2005)1227
31. K. Fodor, V. Harmat, R. Neutze, L. Szilagyi, L. Graf, G. Katona, *Biochemistry* **45** (2006) 2114
32. J. A. Cuesta-Seijo, S. Garcia-Granda, *Bol. R. Soc. Hist. Nat. Sec. Geol.* **97** (2002) 123
33. T. R. Transue, S. A. Gabel, R. E. London, *Bioconjugate Chem.* **17** (2006) 300
34. D. Voet, J. G. Voet, *Biochemistry, 3rd Ed.,* Wiley, New York, 2004, p. 515
35. J. Lin, W. M. Westle, W. W. Cleland, J. L. Markley, P.A. Frey, *Proc. Natl. Acad. Sci. USA* **95** (1998) 14664
36. *Protein Data Bank*, http://www.rcsb.org (January, 2007)
37. A. Warshel, A. Papazyan, *Science* **269** (1995) 102
38. A. Warshel, A. Papazyan, *Proc. Natl. Acad. Sci. USA* **93** (1996) 3665
39. J. Villa, A. Warshel, *J. Phys. Chem.* **105** (2001) 7887
40. C. N. Schutz, A. Warshel, *Proteins: Struct. Funct. Bioinf.* **55** (2004) 711
41. Y. Zhang, J. Kua, J. A. McCammon, *J. Am. Chem. Soc.* **124** (2002) 10572
42. A. V. Nemukhin, B. L. Grigorenko, A. V. Rogov, I. A. Topol, S. K. Burt, *Theor. Chem. Acc.* **111** (2004) 36
43. V. Leskovac, S. Trivić, M. Popović, *Pol. J. Chem.* **80** (2006) 1925.

Journal of the Serbian Chemical Society
JSCS@tmf.bg.ac.yu • www.shd.org.yu/JSCS

J. Serb. Chem. Soc. 73 (4) 405–413 (2008) UDC 66.061–034:582.293.378:541.132.3+544.35
JSCS–3722 *Original scientific paper*

Metal extraction from *Cetraria islandica* (L.) Ach. lichen using low pH solutions

ANA A. ČUČULOVIĆ[1]*#, MIRJANA S. PAVLOVIĆ[2]#, DRAGAN S. VESELINOVIĆ[3]#
and ŠĆEPAN S. MILJANIĆ[3]

[1]*INEP – Institute for the Application of Nuclear Energy, Banatska 31b, 11080 Zemun,*
[2]*Institute of Nuclear Science "Vinča", Department of Physical Chemistry, P. O. Box 522,*
11001 Belgrade and [3]*University of Belgrade, Faculty of Physical Chemistry,*
P. O. Box 137, 11001 Belgrade, Serbia

(Received 24 September, revised 7 November 2007)

Abstract: Extraction of metals (K, Al, Ca, Mg, Fe, Cu, Ba, Zn, Mn and Sr) from dry *Cetraria islandica* (L.) Ach. lichen was performed using solutions similar to acid rain (solution A – H_2SO_4–HNO_3–$(NH_4)_2SO_4$ and solution B – H_2SO_4–HNO_3–$(NH_4)_2SO_4$–NH_4NO_3). The pH values of these solutions were 2.00, 2.58, 2.87, 3.28, and 3.75. Five consecutive extractions were performed with each solution. In all solutions, the extracted metal content, except Cu and Ca, was the highest in the first extract. The highest percentage of the metals desorbed in the first extraction was obtained using solutions with low pH values, 2.00, 2.58, and 2.87. The lowest percentage in the first extraction was obtained using solutions with pH 3.28 and pH 3.75, indicating influence of the H^+ ion on the extraction. According to the results obtained, the investigated metals form two groups. The first group includes K, Al, Ca, Mg, and Fe. They were extracted in each of the five extractions at each of the pH values. The second group includes Ba, Zn, Mn, Cu, and Sr, which were not all extracted at each pH value. The first group yielded three types of extraction curves when the logarithms of extracted metal amounts were plotted as a function of the number of successive extractions. These effects indicate that three different positions (centres) of metal ion accumulation exist in the lichen (due to sorption, complex formation, or other processes present in the tissues).

Keywords: *Cetraria islandica* (L.) Ach. lichen; acid rain; extraction; heavy metals.

INTRODUCTION

Cetraria islandica (L.) Ach. lichen was taken as the model system in the present research. It is one of the 25,000 lichen species in the world and is widely used in the food industry (starch from this lichen can be used for human con-

---

* Corresponding author. E-mail: anas@inep.co.yu
# Serbian Chemical Society member.

doi: 10.2298/JSC0804405C

sumption, *e.g.*, for making bread and other starch products), the alcoholic beverage industry, the pharmaceutical industry, the cosmetic industry and in medicine and veterinary science.[1–3] In cold regions, it represents the main flora and is consumed by wild and domestic animals. This indicates that the metals present in the lichen enter the food chains.

Lichens are good bio-indicators of environmental pollution. They can absorb many elements, in concentrations that are many times higher than their physiological demand. The degree of environmental pollution can be deduced from the content of radionuclides and heavy metals in lichens.[4–6] More detail on the origin of the metals and ways of entering the lichen can be found in the cited literature. It has been established that there are two types of polluting substances bound in lichen. Their presence is predominant in ion exchange or complex formation outside the cells and, to a much lesser extent, in the ion distribution inside the cells.

Our research has confirmed that lichens are bio-indicators of environmental pollution by radionuclides, both man-made and natural.[7–9] Earlier research showed that treatment of lichens with distilled water for different durations (from 1 to 24 h, five successive extractions) successfully desorbs part of the amount of ^{137}Cs in plants (49 to 60 %).[10] These results indicate that lichen can be considered as a secondary pollution source of these radionuclides in the environment because acid rain and other types of rainfall extract pollutants from the lichen and transfer them to the surroundings.[11]

Polluting compounds such as SO_2, CO_2, NO_2, NH_4^+ and fluoride have a negative effect on the development and growth of lichens. In highly polluted environments, lichens disappear. A large amount of research has been concerned with the effect of SO_2 and fluoride, showing that the chemical form in which they are introduced into the atmosphere is of biological significance.[12–14] Most lichens are very sensitive to acid rain. A lot of experimental research has dealt with solutions of pH similar to acid rain,[15–17] ranging from pH 1.0 to pH 5.5.

The purpose of this study was to investigate K, Al, Ca, Mg, Fe, Cu, Ba, Mn, and Sr desorption from *Cetraria islandica* lichen, using acid solutions that correspond to acid rain, important in the transfer (possibility of transfer or transfer mechanism) of these elements from the lichen into the environment, *i.e.*, secondary environment pollution. These elements represent essential macroelements (K, Mg, Ca), essential microelements (Cu, Mn, Fe, Sr), and non-essential elements (Ba, Al).[18]

MATERIALS AND METHODS

Apparatus

The K content was determined using a stabilized direct current arc spectrometer built at the Institute of Nuclear Sciences, Vinča.

The other metals were determined by ICP spectrometry, employing a Spectro-flame model, Spectro-Analytical Instruments, Germany.

Furthermore, a Mettler analytical balance (sensitivity 0.1 mg) and a pH meter Iskra MA 5730 were used.

Graduated glass beakers with a volume of 2 l, glass cylinders with a volume of 100 ml (1 ml graduation) and Teflon glasses were used.

Chemicals

H_2SO_4 conc., p.a., and NH_4NO_3, p.a., Merck, HNO_3, conc., p.a., Alkaloid, $(NH_4)_2SO_4$, p.a., Euro Hemija, HF 48 %, p.a., and $HClO_4$ 70 %, p.a., Superlaboratory, pH 4.00 and 7.00 buffer solutions, Carlo Erba, and certified atomic spectral standards, J. T. Baker Analyzed, were used. The solutions were prepared in distilled water. Standard filter paper was used for filtration.

Sample

Bushy lichen *Cetraria islandica* (L.) Ach. samples were collected from the Sinjajevina Mountain, Montenegro, in 1994 for commercial purposes. The lichen samples were prepared for extraction using the procedure described previously.[12]

Extraction solutions

Two types of extraction solutions were used, with compositions similar to acid rain:

1) solution A of composition H_2SO_4–HNO_3–$(NH_4)_2SO_4$ and

2) solution B of composition H_2SO_4–HNO_3–$(NH_4)_2SO_4$–NH_4NO_3.

Both solutions had five variants, *i.e.*, five different pH values: A_1 and B_1 pH 2.00; A_2 and B_2 pH 2.58; A_3 and B_3 pH 2.87; A_4 and B_4 pH 3.28; A_5 and B_5 pH 3.75. Extraction solutions were prepared in the following way: concentrated H_2SO_4 was added to 100 ml of distilled water until the desired pH values of 2.00 (a_1), 2.58 (b_1), 2.87 (c_1), 3.28 (d_1), or 3.75 (e_1) were attained. In the same manner, concentrated HNO_3 was added to 100 ml of distilled water until solutions a_2, b_2, c_2, d_2 or e_2 attained the above pH values. Mixing of solutions a_1 with a_2, b_1 with b_2, c_1 with c_2, d_1 with d_2 and e_1 with e_2 in 1:1 volume ratios yielded solutions a, b, c, d and e with the above pH values. Solutions A_1, A_2, A_3, A_4 and A_5 were obtained by adding 1.00 g of $(NH_4)_2SO_4$ into 100 ml of each of the solutions a, b, c, d and e and subsequently adjusting the pH to the corresponding value using concentrated H_2SO_4. Solutions B_1, B_2, B_3, B_4 and B_5 were obtained by adding 0.500 g of $(NH_4)_2SO_4$ and 0.500 g of NH_4NO_3 into 100 ml of each of the solutions a, b, c, d and e, and subsequently adjusting the pH as in the case of solutions A.

Extraction procedure

Extractions were performed at room temperature (22 °C) with intermittent mixing, so that 200 ml of extraction solution was poured over 10.0 g of dry lichen mass. After the first extraction, the lichen samples were dried at room temperature until constant mass and extracted again with the corresponding solutions. Each sample was extracted five times conesquently, using 24 h as the equilibrium time for each extraction. Five successive extractions were performed for each of the A_1–A_5 and B_1–B_5 solutions. All extraction series were repeated twice.

Determining the metal content in samples

The contents of K, Al, Ca, Mg, Fe, Cu, Ba, Zn, Mn, and Sr were determined in untreated samples and in the solutions after each of the five successive extractions of the same sample. In order to determine the contents of the elements in a sample of lichen before extraction, 0.500 g of the sample was disintegrated by pouring liquid nitrogen over it. It was then completely homogenized and dissolved in a 20 ml mixture of concentrated acids HNO_3/ /$HClO_4$/HF (10:1:1) in Teflon vessels.[6] The solutions were cooled, filled up to the mark in a 100.0 ml volumetric flask and the content of each metal determined.

Procedures for determining the metal concentrations in the solutions have been published in literature.[6,19-21] The elements Ca, Al, Fe, Mg, Zn, Ba, Mn, Sr, and Cu were determined by ICP spectroscopy and K using a U-shaped DC arc plasma spectrometer. The limits of detection, in (ng dm^{-3}) were: 0.3 for K, 0.13 for Ca, 15 for Al, 3.1 for Fe, 0.1 for Mg, 1.2 for Zn, 0.9 for Ba, 0.93 for Mn, 0.28 for Sr and 6.0 for Cu. Individual deviations ranged from 10 % to 30 %, depending on the total metal concentration in the sample and on the percentage of the metal extracted. The determination error was thus taken as the standard deviation of 20 individual measurements at the same pH with same extracting agent. This was used in the construction of the curves.

RESULTS AND DISCUSSION

The results for extracting agents A and B are given in Tables I and II, respectively, as the mean values from two series of measurements. The tables contain: a) the total metal contents in the lichen samples and b) the total metal content, in %, extracted by each extraction, as well as the total amount extracted by all five partial extractions.

High amounts of Ca and K were found in the lichen, while the amounts of Cu, Sr, and Mn were low (Table I). The highest percentages of the extracted metals in the first extraction, as compared to the second extraction, were obtained for K, Mg, Zn, and Mn. These differences between these two extractions were not as high for the other metals, except for Cu. This element was not extracted in the first extraction, or in any of the extractions at pH 3.28 or 3.75. This indicates its strong bonding to the tissue components, most probably inside the cell.

The contents of the investigated metals in the lichen before desorption are given in Tables I and II. The highest concentrations in the lichen were those of Ca and K. The lowest were those of Cu, Mn, and Sr.

The change of the sorbed amount of substance, C_x, in the sorbent with the extraction number, n_x, for successive extractions with the same volume of extraction agent is given by the following equation:[10]

$$\ln C_x = \ln C_0 - a n_x \tag{1}$$

where C_0 is the content of the sorbed substance before extraction and a is a constant.

It follows from Eq. (1) that the logarithm of the amount of the sorbed substance in the solid phase is a linear function of the number of successive volumes used for extraction. In a real system, it is valid only if one type of sorption exists or if one of the types is dominant, so that the other ones can be neglected. If this is not so, a deviation from the straight line occurs, indicating that the sorbent can bind the sorbed substance through different types of sorption, *i.e.*, at different sorbent positions.

Three types of curves were obtained using Eq. (1). The first type was a straight line, with the value of ln C_0 being obtained by extrapolation and corresponding to 100 % metal content in the sorbent (lichen) before extraction, Fig. 1.

This indicated the existence of only one dominant type of sorption from which most of the metal was extracted.

TABLE I. Initial contents of metals in the lichen before desorption and percentages of desorbed metals after each successive desorption by solutions A and B

Amount of the desorbed element in successive desorption solutions relative to the initial content, %											
No. of desorption	pH	Initial content, $\mu g\ g^{-1}$									
		K		Ca		Al		Fe		Mg	
		1475±75		6880±345		450±45		265±26		260±26	
		Solutions									
		A	B	A	B	A	B	A	B	A	B
I	2.00	60	88	19	25	6.8	11	8.5	14.0	43	55
	2.58	61	89	11	16	6.0	8.1	4.8	7.0	45	57
	2.87	60	86	9.1	14	8.7	8.7	2.6	3.9	43	58
	3.28	52	89	7.7	11	4.8	8.7	1.6	2.9	35	55
	3.75	52	85	7.5	10	6.3	6.0	1.5	2.3	36	54
II	2.00	2.1	4.9	12	21	1.2	1.5	2.9	6.3	2.2	4.9
	2.58	2.5	4.9	7.8	11	1.6	1.4	3.3	5.0	3.1	4.8
	2.87	2.8	4.7	6.7	10	2.0	2.9	3.5	4.2	3.0	6.0
	3.28	2.3	3.9	4.4	6.9	1.5	2.5	1.2	2.0	3.0	6.0
	3.75	2.9	4.0	4.7	6.6	1.9	2.7	1.2	1.4	3.3	5.8
III	2.00	0.31	0.5	16	21	0.7	1.9	2.3	5.0	1.7	3.9
	2.58	0.16	0.6	8.0	12	*	1.7	2.3	3.9	1.9	3.1
	2.87	0.18	0.49	6.8	11	1.0	1.8	2.6	3.9	1.6	3.3
	3.28	0.10	0.6	5.0	6.5	0.6	0.8	1.2	2.3	1.4	3.7
	3.75	0.19	0.45	4.3	5.5	1.9	1.1	0.8	2.1	1.8	3.1
IV	2.00	0.08	0.6	16	20	0.6	1.2	1.7	4.2	1.5	3.5
	2.58	0.05	0.34	9.0	11	0.22	4.6	1.9	2.6	1.4	3.7
	2.87	0.07	0.35	6.3	10	0.6	1.6	1.9	3.6	1.3	3.5
	3.28	0.07	0.5	5.6	6.6	0.5	0.7	1.4	2.1	1.8	4.0
	3.75	0.08	0.31	5.3	5.4	0.8	1.3	0.8	1.5	2.5	3.0
V	2.00	0.19	0.5	24	18	0.8	1.1	2.1	3.0	3.1	3.9
	2.58	0.14	0.24	13	10	0.31	*	1.9	2.2	2.9	3.2
	2.87	0.12	0.42	10	9.1	1.0	0.4	2.2	2.6	4.1	4.0
	3.28	0.08	0.27	8.5	6.2	0.6	0.22	2.1	1.6	2.5	2.5
	3.75	0.12	0.24	7.0	4.7	1.0	0.53	0.8	1.1	3.9	2.1
		Total amount of the desorbed elements from lichen, %									
–	2.00	63	94	87	105	10	17	18	32	52	71
	2.58	63	95	49	60	8	16	14	21	55	72
	2.87	63	92	39	54	13	15	13	18	53	75
	3.28	55	94	31	37	8	13	8	11	44	73
	3.75	55	90	29	32	11	12	5	8	48	68

*Concentration in the extract was below the detection limit

The second type was also a straight line (Fig. 2) but with the ln C_0 value below 100 %, *i.e.*, less than the amount of the metal in the sorbent. This indicated the existence of at least two types of sorption. In one type, the metal was very strongly bound in the lichen, causing the amount of the extracted metal to be lower than in the other type of sorption.

TABLE II. Initial contents of metals in the lichen before desorption and percentages of the desorbed metals after each successive desorption by solutions 1, 2 and 3

Amount of the desorbed element in successive desorption solutions relative to the initial content, %											
No. of desorption	pH	Initial content, μg g^{-1}									
		Zn		Ba		Mn		Sr		Cu	
		30±3		13±1		10±1		10±1		6.0±0.6	
		Solutions									
		A	B	A	B	A	B	A	B	A	B
I	2.00	40	40	4.6	4.6	48	58	16	28	*	*
	2.58	42	40	4.6	3.1	52	50	14	24	*	*
	2.87	27	39	6.1	4.6	50	50	16	20	*	*
	3.28	13	20	1.5	6.1	24	46	8.0	20	*	*
	3.75	27	17	4.6	7.7	34	*	10	20	*	*
II	2.00	*	*	*	*	*	*	2.0	*	*	33
	2.58	*	*	*	*	*	*	2.0	*	*	*
	2.87	*	*	*	*	4.0	6.0	2.0	8.0	*	3.3
	3.28	*	*	*	*	*	6.0	*	*	*	*
	3.75	*	*	*	4.6	*	*	*	*	*	*
III	2.00	*	*	*	*	*	*	2.0	*	*	*
	2.58	*	*	*	*	*	*	2.0	*	*	17
	2.87	*	*	*	*	*	4.0	*	6.0	*	17
	3.28	*	*	*	*	*	*	*	*	*	*
	3.75	*	*	*	*	*	*	*	*	*	*
IV	2.00	*	*	*	*	*	*	2.0	*	*	*
	2.58	*	*	*	*	*	*	*	*	*	*
	2.87	*	*	*	*	*	4.0	6.0	6.0	*	20
	3.28	*	*	*	*	*	*	*	*	*	*
	3.75	*	*	*	*	*	*	*	*	*	*
V	2.00	13	*	*	*	*	*	6.0	*	67	*
	2.58	*	*	*	*	*	*	5.0	*	17	*
	2.87	*	*	*	*	*	*	*	8.0	17	10
	3.28	*	*	*	*	*	*	*	*	*	*
	3.75	*	*	*	*	4.0	*	4.0	4.0	*	*
		Total amount of the desorbed elements from lichen, %									
–	2.00	53	40	5	5	48	58	28	28	67	33
	2.58	42	40	5	3	52	50	23	24	17	17
	2.87	27	39	6	5	54	64	24	48	17	50
	3.28	13	20	2	6	24	52	8	20	*	*
	3.75	27	17	5	13	38	*	14	24	*	*

*Concentration in the extract was below the detection limit

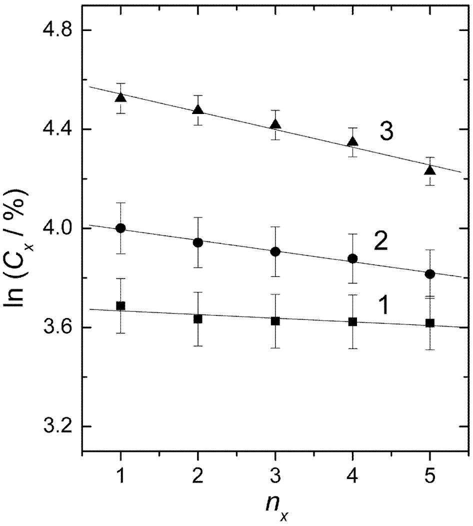

Fig. 1. Logarithm of the amount of sorbed metal *vs*. desorption number. 1) K, solution A, pH 2.00; 2) Mg, solution A, pH 2.58; 3) Ca, solution A, pH 3.28.

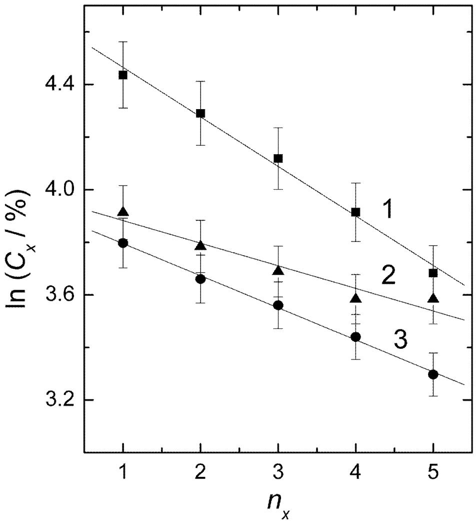

Fig. 2. Logarithm of the sorbed amount of metal *vs*. desorption number. 1) Ca, solution B, pH 2.58; 2) Mg, solution B, pH 3.28; 3) Mn, solution B, pH 2.87.

The third type of curve was not a straight line. This indicated two or more types of sorption processes, without a dominant type.

The C_0 values obtained from the straight lines according to Eq. (1) are given in Table III. In 38.0 % of the cases, a single sorption process was present, whereas two or more processes were present in 62.0 % of the cases.

TABLE III. C_0 values determined from the plots according to Eq. (1) (relative to the initial content, %)

Metal	pH	Solution A	Solution B
K	2.00	39.7	*
	2.58	38.9	*
	2.87	*	*
	3.28	*	*
	3.75	*	*
Ca	2.00	*	*
	2.58	106.7	104.6
	2.87	102.0	103.0
	3.28	101.5	98.5
	3.75	99.9	96.5
Al	2.00	93.7	90.9
	2.58	93.7	94.6
	2.87	91.8	92.3
	3.28	95.6	91.8
	3.75	94.6	94.6

TABLE III. Continued

Metal	pH	Solution A	Solution B
Fe	2.00	93.7	90.5
	2.58	97.0	95.6
	2.87	99.5	99.5
	3.28	100.5	99.0
	3.75	99.0	99.3
Mg	2.00	59.1	49.9
	2.58	56.8	47.0
	2.87	60.0	47.5
	3.28	66.4	50.2
	3.75	66.7	49.7
Sr	2.87	87.8	88.2
Mn	2.87	–	52.5

*Non-linear function

A total of 308 samples were analysed and the contents of metals determined using both types of extracting agent. The results obtained with solutions A and B are presented in Tables I and II, for five different pH values and five successive extractions. Summarising, 81.4 % of the total metal content was extracted from the lichen at the lower pH values (2.00, 2.58, and 2.87), only 3.6 % at higher pH values (3.28 and 3.75) and 15 % of the metals were equally extracted at any of the employed pH values. These results indicate an effect of H^+ ions on the extraction of metals from the lichen. This is also confirmed by the total amount of metals extracted from the lichen (Tables I and II). The highest percentages of the metals were extracted by the more acidic solutions (pH 2.00–2.87).

Acknowledgement. The Ministry of Science of the Republic of Serbia financially supported this work, projects Nos. ON 142039 and ON 142065.

ИЗВОД

ЕКСТРАКЦИЈА МЕТАЛА ИЗ ЛИШАЈА *Cetraria islandica* (L.) Ach. РАСТВОРИМА НИСКИХ pH ВРЕДНОСТИ

АНА А. ЧУЧУЛОВИЋ[1], МИРЈАНА С. ПАВЛОВИЋ[2], ДРАГАН С. ВЕСЕЛИНОВИЋ[3] И ШЋЕПАН С. МИЉАНИЋ[3]

[1]ИНЕП – Институт за примену нуклеарне енергије, Банатска 31б, Земун, [2]Институт за нуклеарне науке 'Винча', Лабораторија за физичку хемију, п. пр. 522, 11001 Београд и [3]Универзитет у Београду, Факултет за физичку хемију, п.пр. 137, 11001 Београд

Испитивана је екстракција метала K, Al, Ca, Mg, Fe, Cu, Ba, Zn, Mn и Sr сорбованих у узорцима лишаја *Cetraria islandica* (L.) Ach. киселим растворима (раствор А – H_2SO_4–HNO_3––$(NH_4)_2SO_4$ и раствор Б – H_2SO_4—HNO_3–$(NH_4)_2SO_4$–NH_4NO_3) сличним киселим кишама. pH вредности раствора су износиле 2,00; 2,58; 2,87; 3,28 и 3,75. Урађено је пет сукцесивних екстракција са сваким раствором. Најуспешније су прве екстракције наведеним растворима, осим код Cu и Ca. Највећи проценат десорпције метала је првим екстракцијама када се користе раствори ниских pH вредности 2,00; 2,58 и 2.87. Нижи проценти код првих екстракција су добијени коришћењем раствора pH 3,28 и 3,75 што указује на утицај H^+ јона на екстрак-

цију. Испитивања су показала да се десорбовани метали могу поделити у две групе. Првој групи припадају K, Al, Ca, Mg и Fe, који се десорбују свим екстракцијама растворима свих pH вредности. Другој групи припадају Ba, Zn, Mn, Cu и Sr који нису десорбовани свим екстракцијама и при свим pH вредностима. Логаритамска зависност садржаја метала у функцији од броја десорпције указује на постојање три типа кривих, тј. на три начина везивања и три јачине везе метала у лишају.

(Примљено 24. септембра, ревидирано 7. новембра 2007)

REFERENCES

1. K. O. Vartia, *The lichens,* Academic Press, New York, 1973, p. 547
2. D. H. S. Richardson, *Handbook of Lichenology* **3** (1988) 93
3. S. Kumar, K. Müller, *J. Nat. Prod.* **62** (1999) 821
4. P. Eckl, W. Hofmann, R. Türk, *Radiat. Environ. Biophys.* **25** (1986) 43
5. D. H. S. Richardson, *Pollution monitoring with lichens*, Richmond Publishing, Slough, 1992
6. E. J. Sloof, *Ph.D. Thesis*, Delft University of Technology, Delft, The Netherlands, 1993
7. A. Stanković, *M.Sc. Thesis*, Faculty of Physical Chemistry, University of Belgrade, Belgrade, Serbia, 1994 (in Serbian)
8. O. Nedić, A. Stanković, S. Stanković, *Arch. Environ. Contamin. Toxicol.* **29** (1995) 380
9. A. Stanković, S. Stanković, G. Pantelić, *Ekologija* **34** (1999) 49 (in Serbian)
10. A. Čučulović, D. Veselinović, Š. S. Miljanić, *J. Serb. Chem. Soc.* **71** (2006) 565
11. A. Čučulović, D. Veselinović, Š. S. Miljanić, *J. Serb. Chem. Soc.* **72** (2007) 673
12. M. R. D. Seaward, *Environ. Rev.* **1** (1993) 73
13. E. Nieboer, D. H. S. Richardson, K. J. Pucket, F. D. Tomassini, in *Effects of air pollutants on plants*, T. A. Mansfield, Ed., Cambridge University Press, Cambridge, 1976, p. 61
14. D. F. Perkins, R.O. Millar, *Environ. Pollut.* **47** (1987) 63
15. K. Boonppragob, T. H. Nash, C. A. Fox, *Environ. Exp. Botany* **29** (1989) 187
16. L. L. Sigal, J. W. Johnston Jr., *Environ. Exp. Botany* **26** (1986) 59
17. T. C. Hutchinson, M. Dixon, M. Scott, *Water Air Soil Pollut.* **31** (1986) 409
18. R. Kastori, *Required elements*, Nučna knjiga, Beograd, 1989 (in Serbian)
19. M. Kuzmanović, M. S. Pavlović, M. Marinković, *Spectrosc. Lett.* **29** (1996) 205
20. M. Marinković, V. G. Antonijević, *Spectrochim. Acta* **35B** (1980) 129
21. P. W. J. M. Boumans, *Line Coincidence Tables for Inductively Coupled Plasma Atomic Emission Spectrometry*, Pergamon Press, Oxford, 1980.

Journal of the Serbian Chemical Society
JSCS@tmf.bg.ac.yu • www.shd.org.yu/JSCS

J. Serb. Chem. Soc. 73 (4) 415–421 (2008) UDC 542.9+547.571+547.551:547.665:547.288.2:615.281
JSCS–3723 *Original scientific paper*

Biologically active new Fe(II), Co(II), Ni(II), Cu(II), Zn(II) and Cd(II) complexes of *N*-(2-thienylmethylene)methanamine

C. SPÎNU*, M. PLENICEANU and C. TIGAE

University of Craiova, Faculty of Chemistry, Department of Inorganic Chemistry, A. I. Cuza no. 13, Craiova, Romania

(Received 2 April, revised 22 November 2007)

Abstract: Iron(II), cobalt(II), nickel (II), copper (II), zinc(II) and cadmium(II) complexes of the type ML_2Cl_2, where M is a metal and L is the Schiff base *N*-(2-thienylmethylene)methanamine (TNAM) formed by the condensation of 2-thiophenecarboxaldehyde and methylamine, were prepared and characterized by elemental analysis as well as magnetic and spectroscopic measurements. The elemental analyses suggest the stoichiometry to be 1:2 (metal:ligand). Magnetic susceptibility data coupled with electronic, ESR and Mössbauer spectra suggest a distorted octahedral structure for the Fe(II), Co(II) and Ni(II) complexes, a square-planar geometry for the Cu(II) compound and a tetrahedral geometry for the Zn(II) and Cd(II) complexes. The infrared and NMR spectra of the complexes agree with co-ordination to the central metal atom through nitrogen and sulphur atoms. Conductance measurements suggest the non-electrolytic nature of the complexes, except for the Cu(II), Zn(II) and Cd(II) complexes, which are 1:2 electrolytes. The Schiff base and its metal chelates were screened for their biological activity against *Escherichia coli*, *Staphylococcus aureus* and *Pseudomonas aeruginosa* and the metal chelates were found to possess better antibacterial activity than that of the uncomplexed Schiff base.

Keywords: Schiff base; 2-thiophenecarboxaldehyde; *N*-(2-thienylmethylene)-methanamine; antibacterial activity.

INTRODUCTION

A large number of Schiff bases and their complexes have been studied for their interesting and important properties, *e.g.*, catalytic activity[1] and transfer of the amino group,[2] photochromic properties[3] and the ability to complex some toxic metals.[4] In continuation of our work on these complexes,[5,6] the results of studies on the complexes of the Schiff base obtained through the condensation of 2-thiophenecarboxaldehyde and methylamine, *N*-(2-thienylmethylene)methanamine (TNAM), are reported herein. The presence of two potential donor atoms should render TNAM a versatile ligand. This new ligand was synthesized and its donor characteristics towards the chlorides of Fe(II), Co(II), Ni(II), Cu(II), Zn(II)

---

* Corresponding author. E-mail: spinu_cezar@yahoo.com

doi: 10.2298/JSC0804415S

and Cd(II) were examined. Tentative structures are proposed for the complexes based on analytical, spectral, magnetic and conductance data.

EXPERIMENTAL

Reagents

$CoCl_2·6H_2O$ (Merck, 99.99 %), $NiCl_2·6H_2O$ (Merck, 99.99 %), $CuCl_2·2H_2O$ (Merck, 99.99 %), 2-thiophenecarboxaldehyde (Merck, 98 %), methylamine (Merck, 98 %).

Synthesis of the bidentate Schiff base

The Schiff base was prepared by adding an ethanolic solution of 2-thiophenecaroxaldehide, 2-TFCA (0.001 mol, 25 ml) to an ethanolic solution of MA (0.001 mol, 25 ml) and refluxing for 4 h on a water bath. After the concentration of the solution, the precipitate was separated, filtered, washed with ethanol and dried over $CaCl_2$ under vacuum.

TNAM. Anal. Calcd. for C_6H_7NS: C, 57.6; H, 5.6; N, 11.2; S, 25.6. Found: C, 57.56; H, 5.70; N, 11.30; S, 25.40. ^{1}H-NMR: δ_1 9.34, δ_2 7.12. ^{13}C-NMR: δ 161.5.

Synthesis of the ML_2Cl_2 complexes

A mixture of 2-TFCA (0.002 mol, 50 ml), and MA (0.002 mol, 50 ml) in ethanol was added to an ethanolic solution of metal chlorides (0.001 mol, 50 ml). The reaction mixture was refluxed on a water bath for 6–10 h. The excess of solvent was then distilled and the compounds which separated were filtered, washed with ethanol and dried over $CaCl_2$ under vacuum.

Instruments

The ligand and complexes were analyzed for M, S and Cl by conventional methods,[7] and C, H and N by micro-analytical methods. The IR spectra were obtained in KBr discs using a Bio-Rad FTS 135 spectrophotometer. The UV–Vis spectra were recorded on a Unicam UV–Vis UV-4 spectrophotometer in DMF solution. The ^{1}H-NMR spectra (in $CDCl_3$) were recorded on a Varian T60 and the ^{13}C-NMR spectra were obtained using a Bruker WH 270 spectrophotometer. The Mössbauer spectrum of iron compound was measured at 293 K on an ECIL MBS 35 spectrometer using ^{57}Co in a Pd matrix as the source. The ESR spectra of polycrystalline samples were recorded on an ART 5 spectrophotometer at room temperature. The magnetic moments were determined by the Faraday method. A digital conductometer K 612 was used to measure the molar conductivities in DMF solution.

Antibacterial studies

The synthesized metal complexes, in comparison to the uncomplexed Schiff base ligand, were screened for their antibacterial activity against the pathogenic bacterial species: *Escherichia coli*, *Staphylococcus aureus* and *Pseudomonas aeruginosa*. The paper disc diffusion method[8] was employed for the determination of the antibacterial activity.

RESULTS AND DISCUSSIONS

The complex combinations of Co(II), Ni(II) and Cu(II) with *N*-(2-thienylmethylene)methanamine (TNAM) (Fig. 1) appeared as powders with high melting points. They were not soluble in ethanol, diethyl ether or chloroform but were soluble in acetone and more soluble in DMF.

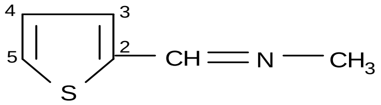

Fig. 1. The structure of *N*-(2-thienylmethylene)methanamine (C_6H_7NS) (TNAM).

Elemental analysis data

Anal. Calcd. for $Fe(TNAM)_2Cl_2$: Fe, 14.82; C, 38.22; N, 7.43; S, 16.98; Cl, 18.81. Found: Fe, 14.85; C, 38.19; N, 7.50; S, 16.97; Cl, 18.77. Anal. Calcd. for $Co(TNAM)_2Cl_2$: Co, 15.51; C, 37.91; N, 7.37; S, 16.84; Cl, 18.66. Found: Co, 15.48; C, 37.88; N, 7.40; S, 16.86; Cl, 18.64. Anal. Calcd. for $Ni(TNAM)_2Cl_2$: Ni, 15.46; C, 37.93; N, 7.37; S, 16.85; Cl, 18.67. Found: Ni, 15.45; C, 37.90; N, 7.34; S, 16.82; Cl, 18.69. Anal. Calcd. for $Cu(TNAM)_2Cl_2$: Cu, 16.53; C, 37.45; N, 7.28; S, 16.64; Cl, 18.44. Found: Cu, 16.56; C, 37.40; N, 7.31; S, 16.67; Cl, 18.41. Anal. Calcd. for $Zn(TNAM)_2Cl_2$: Zn, 16.92; C, 37.28; N, 7.25; S, 16.57; Cl, 18.35. Found: Zn, 16.89; C, 37.25; N, 7.29; S, 16.61; Cl, 18.34; Anal. Calcd. for $Cd(TNAM)_2Cl_2$: Cd, 25.94; C, 33.23; S, 14.77; Cl, 16.36. Found: Cd, 25.90; C, 33.21; S, 14.81; Cl, 16.33.

The elemental analysis data suggest that all the complexes have a 1:2 (metal–ligand) stoichiometry. Based on the elementary chemical analysis, the formula ML_2Cl_2 (Table I) is suggested for all the prepared complexes.

TABLE I. Analytical and physical data of the complexes[a]

Compounds	Melting point, °C	Colour	μ_{eff} / μ_B	Λ_M[b] / Ω^{-1} cm^2 mol^{-1}
$Fe(TNAM)_2Cl_2$	210	Red	5.14	10.7
$Co(TNAM)_2Cl_2$	170	Pink	4.88	11.6
$Ni(TNAM)_2Cl_2$	145	Greenish	3.19	19.2
$Cu(TNAM)_2Cl_2$	230	Purple	1.82	120.3
$Zn(TNAM)_2Cl_2$	215	Pale yellow	–	134.5
$Cd(TNAM)_2Cl_2$	185	Brownish	–	128.7

[a]All the complexes give satisfactory metal, C, H, S, N and Cl analyses; [b]in DMF solution

IR and NMR spectra

In order to obtain data revealing the manner in which the ligand were coordinated to the metal ions, IR spectra in the 400–4000 cm^{-1} range (Table II) were recorded.

TABLE II. Characteristic infrared absorption frequencies, in cm^{-1}, of the ligand and the complexes

Compound	ν(C=N)	ν(C–S–C)	ν($C–S_{sym}$)	ν($C–S_{asym}$)	Other bands		ν(M–N)
TNAM	1665	860	690	640	3075	1520	–
$Fe(TNAM)_2Cl_2$	1622	821	–	620	3071	1520	420
$Co(TNAM)_2Cl_2$	1618	826	–	617	3074	1517	422
$Ni(TNAM)_2Cl_2$	1620	828	–	625	3069	1525	415
$Cu(TNAM)_2Cl_2$	1615	811	–	615	3078	1515	419
$Zn(TNAM)_2Cl_2$	1619	817	–	605	3068	1510	424
$Cd(TNAM)_2Cl_2$	1624	825	–	610	3070	1512	427

The IR spectra of the ligands exhibit a band at 1665 cm^{-1}, assignable to the ν(C=N) of the azomethine group. This band shifted by about 35–50 cm^{-1} to a lower wavenumber region in the case of all the complexes, suggesting coordination through the N atom of the azomethine group.

The medium intensity band at ≈ 880 cm^{-1} observed in the spectrum of the free ligand, ascribed to ν(C–S–C) (ring) stretching vibration,[9] shifted to lower values by 30–40 cm^{-1} for all complexes, suggesting the involvement of the sulphur atom in the bonding with the metal ions. The band assigned to the asymmetric ν(C−S) shifted to lower frequency after complexation and the symmetric ν(C−S) completely disappeared in all the complexes. This also confirms that the sulphur atom is participating in the complex formation.[10]

Proof of coordination to the N atom is provided by the occurrence of new bands in the range 419–427 cm^{-1} in the IR spectra of the compounds.

In the ^{1}H-NMR spectra of the ligands, the formation of Schiff bases is supported by the presence of a singlet at δ 9.34 and δ 7.12 ppm, corresponding to the azomethine proton (−CH=N−) and to the H-5 proton of the thiophene ring, respectively, and a peak at δ 161.5 in the ^{13}C-NMR spectra, corresponding to the azomethine carbon. In the spectra of the ZnL_2Cl_2 and CdL_2Cl_2 complexes, these signals showed distinct downfield shifts of nearly 0.4–0.6 ppm in the ^{1}H-NMR spectrum and 3–5 ppm in the ^{13}C-NMR spectrum, clearly demonstrating the coordination of TNAM *via* the nitrogen and sulphur atoms.

Electronic, Mössbauer and ESR spectra

Two absorption bands at 40300 and 31560 cm^{-1}, assigned to the transitions $n\rightarrow\pi^*$ and $\pi\rightarrow\pi^*$, respectively, were observed in the UV spectrum of the ligand. These transitions were also found in the spectra of the complexes but they were shifted to lower frequencies ($\Delta\nu$ = 1500–2200 cm^{-1}), confirming the coordination of the ligand to the metal ions.

The information referring to the geometry of these compounds was obtained from the electronic spectra (Table III) and from the values of the magnetic moments.

TABLE III. Electronic spectra of the complexes

Compound	Absorption maxima, cm^{-1}
$Fe(TNAM)_2Cl_2$	12600; 10200
$Co(TNAM)_2Cl_2$	19520; 18140; 15200; 10020
$Ni(TNAM)_2Cl_2$	26100; 15200; 10000; 9150
$Cu(TNAM)_2Cl_2$	18500; 15400
$Zn(TNAM)_2Cl_2$	26000
$Cd(TNAM)_2Cl_2$	24500

The electronic spectrum of the iron(II) complex consisted of a pair of low intensity bands at 12600 and 10200 cm^{-1}, arising from $^5T_{2g}\rightarrow{}^5E_g$ transitions, similar to those found for distorted octahedral complexes. The doublet is attributed to a Jahn–Teller distortion in the excited state.[5] The room temperature magnetic moment (5.14 μ_B) corresponded to octahedral symmetry. In addition, in the Mössbauer spectrum, the value of isomer shift (0.871 mm s^{-1}) indicates a high spin variety for the iron(II) complex. Furthermore, the somewhat lower value of the isomer shift than expected for a perfect octahedral structure suggests distortion from octahedral geometry.[11] The lower value of the quadrupole splittings (1.72 mm s^{-1}) lead to a similar conclusion.

The electronic spectrum of the Co(II) compound exhibited three bands (Table III). The bands at 19520 and 18140 cm^{-1} arise from the $^4T_{1g}\to{}^4T_{1g}(P)$ transition, which is split in complexes of D_{4h} symmetry. That at 15200 cm^{-1} arises from the $^4T_{1g}\to{}^4A_{2g}$ transition and that at 10020 cm^{-1} from the $^4T_{1g}\to$ $\to{}^4T_{2g}$ transition.[12,13] These transitions correspond to a distorted octahedral geometry, which was also supported by the magnetic moment value (4.88 μ_B).

The electronic spectrum of the $Ni(TNAM)_2Cl_2$ could be assigned assuming pseudo-octahedral stereochemistry. The energies represent the following electronic transitions from the $^3A_{2g}(F)$ ground state to the $^3T_{2g}(F)$ (ν_1), $^3T_{1g}(F)$ (ν_2) and $^3T_{1g}(P)$ (ν_3) excited states for nickel(II). The low energy band of this complex is broad and split into two components (at 10000 and 9150 cm^{-1}), indicating tetragonal distortion. The magnetic moment (3.19 μ_B) lies in the region expected for octahedral complexes.

The $Cu(TNAM)_2Cl_2$ complex displays electronic spectral bands in the region 18500 and 15400 cm^{-1}, which may be assigned to $^2B_{1g}\to{}^2E_g$ and $^2B_{1g}\to$ $\to{}^2A_{1g}$ transitions in a square-planar stereochemistry.[14] The ESR spectrum of a polycrystalline sample of the complex measured at room temperature gave $g_{||}$ and $g_{\perp}$ values in the range of 2.147 and 2.083, respectively. The value $g_{||} > g_{\perp}$ is well consistent with a primarily $d_{x^2-y^2}$ ground state having a square-planar structure.[14] The G parameter determined as $G = [(g_{||}-2)/(g_{\perp}-2)]$ was found to be much less than 4, suggesting considerable interaction in the solid state.

The electronic spectra of the Zn(II) and Cd(II) complexes exhibit a sharp band of high intensity at 26000 and 24500 cm^{-1}, respectively, which may be due to ligand–metal charge transfer. The preference of the TNAM for bidentate chelation in the Zn(II) and Cd(II) complexes may due to the preference of these ions for tetrahedral coordination.

The molar conductance of the complexes in DMF (10^{-3} M) are in the range 10.7–15.2 Ω^{-1} cm^2 mol^{-1} for the Fe(II), Co(II) and Ni(II) complexes, indicating their non-electrolytic nature and 120.3–134.5 Ω^{-1} cm^2 mol^{-1} for the Cu(II), Zn(II) and Cd(II) complexes, which are 1:2 electrolytes.

In light of the above discussion, octahedral structures for the Fe(II), Co(II) and Ni(II) complexes, square-planar for the Cu(II) compound and tetrahedral for the Zn(II) and Cd(II) complexes is proposed. It is tentatively proposed that the Schiff base ligands coordinate through the nitrogen of the azomethine group and the sulphur of the thiophene ring, forming a stable chelate ring structure (Fig. 2).

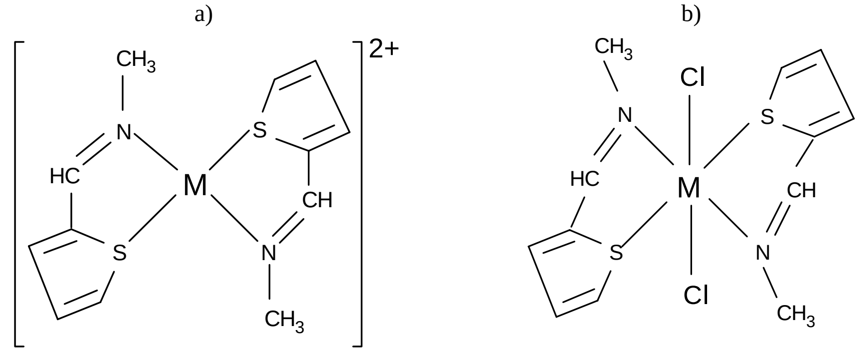

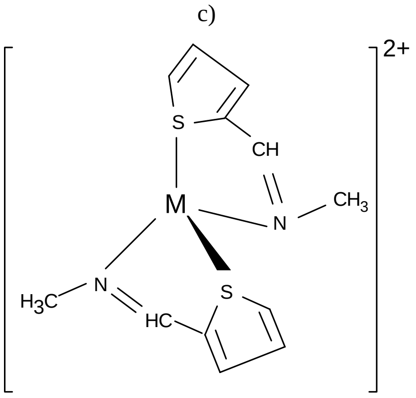

Fig. 2. The structural formulas of the complexes: a) $[Cu(TNAM)_2]Cl_2$, b) $[ML_2Cl_2]$ (M = Fe(II), Co(II), Ni(II)) and c) $[ML_2]Cl_2$ (M = Zn(II), Cd(II)).

Antibacterial activity

The antibacterial activity of the Schiff base and its complexes were studied against *Escherichia coli, Staphylococcus aureus* and *Pseudomonas aeruginosa* bacterial species. The antibacterial results are given in Table IV.

TABLE IV. Antibacterial activity data

Compound	Microbial species		
	Escherichia coli	*Staphylococcus aureus*	*Pseudomonas aeruginosa*
TNAM	+ +[a]	+	+
$Fe(TNAM)_2Cl_2$	+ + + +	+ + + +	+ + +
$Co(TNAM)_2Cl_2$	+ + + +	+ + +	+ + +
$Ni(TNAM)_2Cl_2$	+ + +	+ +	+ +
$Cu(TNAM)_2Cl_2$	+ + +	+ +	+ +
$Zn(TNAM)_2Cl_2$	+ + +	+ +	+ +
$Cd(TNAM)_2Cl_2$	+ +	+	+

[a] Inhibition zone diameter, mm (% inhibition): +, 6–10 (27–45 %); + +, 10–14 (45–64 %); + + +, 14–18 (64–82 %); + + + +, 18–22 (82–100 %). Percent inhibition values are relative to the inhibition zone (22 mm) of the most active compound with 100 % inhibition

The Schiff base and all its complexes individually exhibited varying degrees of inhibitory effects on the growth of the tested bacterial species. The biological activity of the complexes follows the order Co(II) = Fe(II) > Ni(II) = Zn(II) = = Cu(II) > Cd(II).

Furthermore, the data in Table IV show that *E. coli* were more inhibited by the Co(II) and Fe(II) complexes. The importance of this lies in the fact that these complexes could reasonably be used for the treatment of some common diseases caused by *E. coli*.

ИЗВОД

НОВИ БИЛОШКИ АКТИВНИ Fe(II), Co(II), Ni(II), Cu(II), Zn(II) И Cd(II) КОМПЛЕКСИ *N*-(2-ТИЕНИЛМЕТИЛЕН)МЕТАНАМИНА

C. SPÎNU, M. PLENICEANU и C. TIGAE

University of Craiova, Faculty of Chemistry, Department of Inorganic Chemistry,
A. I. Cuza no. 13, Craiova, Romania

У раду су добијени гвожђе(II), кобалт(II), бакар(II), цинк(II) и кадмијум(II) комплекси типа ML_2Cl_2, где је M метал, а L Шифова база *N*-(2-тиенилметилен)метанамин (TNAM) добијен кондензацијом 2-тиофенкарбоксалдехида и метиламина, и окарактерисани елементалном анализом као и магнетним и спектроскопским мерењима. Елементалне анализе указују на стехиоментрију M:L = 1:2. Подаци за магнетну сусцептибилност, повезани са електронским, ESR и Mössbauer-овим спектрима, указују на извијену октаедарску структуру Fe(II), Co(II) и Ni(II) комплекса и квадратно-планарну за Cu(II), односно тетраедарску геометрију за Zn(II) и Cd(II) комплексе. Инфрацрвени и NMR спектри комплекса одговарају координацији централног металног атома преко атома азота и сумпора. Мерења проводљивости указују на то да су комплекси неелектролити, осим Cu(II), Zn(II) и Cd(II) комплекса који су 1:2 електролити. Испитивана је биолошка активност Шифове базе и њених металних хелатних комплекса према микроорганизмима *Escherichia coli, Staphylococcus aureus* и *Pseudomonas aeruginosa*, и нађено је да су комплекси активнији од некомплексиране Шифове базе.

(Примљено 2. априла, ревидирано 22. новембра 2007)

REFERENCES

1. G. Henrici-Olive, S. Olive, *The Chemistry of the Catalyzed Hydrogenation of Carbon Monoxide,* Springer, Berlin, 1984
2. H. Dugas, C. Penney, *Bioorganic Chemistry***,** Springer, Berlin, 1981
3. J. D. Margerum, L. J. Miller, *Photochromism*, Wiley Interscience, New York, 1971
4. W. J. Sawodny, M. Riederer, *Angew. Chem. Int. Ed. Engl.* **16** (1977) 859
5. A. Kriza, C. Spinu, M. Pleniceanu, *J. Indian Chem. Soc.* **76** (2000) 135
6. C. Spinu, A. Kriza, *Acta Chim. Slov.* **47** (2000) 179
7. S. C. Mohapatra, D. V. R. Rao, *J. Indian Chem. Soc.* **57** (1980) 262
8. S. K. Srivastava, K. A. Gupta, *Acta Chim. Hung.* **118** (1985**)** 255
9. A. B. P. Lever, *Inorganic Electronic Spectroscopy*, Elsevier, New York, 1984
10. T. G. Gibb, N. N. Greenwood, *Mössbauer Spectroscopy*, Chapman & Hall, London, 1971
11. B. T. Hathaway, *Struct. Bonding* **14** (1973**)** 60
12. J. Ferguson, *J. Chem. Phys.* **32** (1960) 533
13. A. I. Vogel, *A Text Book of Quantitative Inorganic Analysis*, 3rd Ed., ELBS, London, 1961
14. Z. H. Chohan, M. Praveen, *Appl. Organomet. Chem.* **13** (2000) 376.

Journal of the Serbian Chemical Society
JSCS@tmf.bg.ac.yu • www.shd.org.yu/JSCS

J. Serb. Chem. Soc. 73 (4) 423–429 (2008)
JSCS–3724

UDC 542.9+547.571+547.551:546.742'562'472:
:547.573:543.422.25
Original scientific paper

Metal complexes of Schiff bases derived from dicinnamoylmethane and aliphatic diamines

K. KRISHNANKUTTY[1], P. SAYUDEVI[2] and MUHAMMED BASHEER UMMATHUR[3]*

[1]*Department of Chemistry, University of Calicut, Kerala-673635,* [2]*Department of Chemistry, NSS College, Manjeri, Kerala-676122 and* [3]*Department of Chemistry, Unity Women's College, Manjeri, Kerala-676122, India*

(Received 26 July, revised 10 December 2007)

Abstract: Two new Schiff bases containing olefinic linkages have been synthesized by condensing aliphatic diamines with dicinnamoylmethane under specified conditions. The existence of these compounds predominantly in the intramolecularly hydrogen bonded keto-enamine form was well demonstrated by their IR, ^{1}H-NMR and mass spectral data. Dibasic tetradentate N_2O_2 coordination of the compounds in their [ML] complexes (M = Ni(II), Cu(II) and Zn(II)) was established on the basis of analytical and spectral data.

Keywords: Schiff base; dicinnamoylmethane; metal complexes; IR spectra; ^{1}H-NMR spectra; mass spectra.

INTRODUCTION

The reactivity of carbonyl functions of 1,3-diketones and metal 1,3-diketonates towards amino-compounds has been employed in the synthesis of a large number of multidentate and macrocylic ligands.[1] These ligand systems have evoked considerable interest because of their utility as model compounds in bioinorganic studies.[2,3] Most of the reported studies are based on 1,3-diketones in which the diketo function is directly linked to alkyl/aryl groups.[4] Very few reports exist[5] on Schiff bases of 1,3-diketones in which the diketo group is linked to an alkenyl function. Such unsaturated 1,3-diketones constitute the major physiologically active principle (known generally as curcuminoids) of the traditional Indian medicinal plant turmeric (*Curcuma longa*, Linn. Zingiberaceae family) and several other related spices. Curcuminoids, their synthetic analogues and their metal complexes are known to exhibit anticancer, anti-oxidant and anti-inflammatory activities.[6,7] In this paper, the synthesis and characterization of Schiff bases of the unsaturated 1,3-diketone 1,7-diphenyl-1,6-heptadiene-3,5-dione (dicinnamoylmethane), and their metal complexes are reported.

---

* Corresponding author. E-mail: mbummathur@rediffmail.com

doi: 10.2298/JSC0804423K

EXPERIMENTAL

Methods and instruments

Carbon, hydrogen and nitrogen percentages were determined by microanalyses (Heraeus elemental analyzer) and the metal contents of the complexes by AAS (Perkin Elmer 2380). The electronic spectra of the compounds were recorded in methanolic solutions (10^{-4} M) on a 1601 Shimadzu UV–Vis spectrophotometer; the IR spectra (KBr discs) on an 8101 Shimadzu FTIR spectrophotometer; the ^{1}H-NMR spectra ($CDCl_3$ or DMSO-d_6) on a Varian 300 NMR spectrometer and the mass spectra on a Jeol/SX-102 mass spectrometer (FAB using Argon and *meta*-nitrobenzyl alcohol as the matrix). The molar conductance of the complexes was determined in DMF at 28±1 °C using approximately 10^{-3} M solutions. The magnetic susceptibilities were determined at room temperature on a Guoy type magnetic balance.

Synthesis of Schiff bases H_2ded and H_2dpd

Dicinnamoylmethane was synthesized according to the method of Pabon[8] by the condensation of benzaldehyde with acetylacetone–boron complex in the presence of tri-*sec*-butyl borate and *n*-butylamine as the condensing agents. An ethanolic solution of 1,2-diaminoethane/1,3-diaminopropane (0.01 mol, 20 ml) was added to a methanolic solution of dicinnamoylmethane (2.76 g, 0.01 mol, 30 ml) drop by drop under constant stirring. The mixture was refluxed on a boiling water bath for ≈ 3 h and left overnight. The formed crystalline precipitate was filtered, washed with water and recrystallized from hot methanol to obtain the chromatographically (TLC) pure compound.

Synthesis of Cu(II), Ni(II) and Zn(II) complexes

A solution of the metal(II) acetate (0.001 mol) in a minimum amount of water was added to a methanolic solution of the ligand (0.001 mol, 20 ml) and the mixture was refluxed for ≈ 4 h on a boiling water bath. The precipitated complex was filtered, washed with water, recrystallized from hot ethanol and dried under vacuum.

RESULTS AND DISCUSSION

The Schiff bases H_2ded and H_2dpd were formed in good yield by the condensation of dicinnamoylmethane with 1,2-diaminoethane and 1,3-diaminopropane, respectively. The compounds are crystalline in nature and soluble in common organic solvents. The elemental analytical data of the compounds (Table I) indicate that the Schiff base formation occurred in the ratio 2:1, as shown in Fig. 1. They formed stable complexes with Ni(II), Cu(II) and Zn(II) ions. The analytical data (Table I) together with their non-electrolytic nature in DMF (specific conductance < 10 Ω^{-1} cm^{-1}; 10^{-3} M solution) suggest 1:1 stoichiometry of the complexes. The Ni(II) and Zn(II) chelates are diamagnetic while the Cu(II) complexes showed normal paramagnetic moments. The observed electronic, IR, ^{1}H-NMR and mass spectral data of the complexes are fully consistent with the structure shown in Fig. 2.

Infrared spectra

Dicinnamoylmethane exists in the intramolecularly hydrogen-bonded enol form and the carbonyl stretching band is observed[9] at 1620 cm^{-1}. The IR spectra of H_2ded and H_2dpd are characterized by the presence of a strong slightly broadened band at ≈ 1660 cm^{-1}, assignable to the cinnamoyl carbonyl. This indicates that only one of the carbonyl groups is involved in the Schiff base formation. The IR spectra of the compounds show prominent bands at ≈ 1540 cm^{-1} and ≈ 1280 cm^{-1} due to NH deformation vibration and ν(C–N), respectively. The 1600–1650 cm^{-1} region of the spectra do not show any band assignable to ν(C=N). These facts together with the presence of a carbonyl band suggest the existence of the compounds in the keto-enamine form rather than in the enol-imine form.[10] The strong intramolecular hydrogen bonding present in the compounds is clearly indicated from the appearance of a broad band in the range 2700–3600 cm^{-1}. In the IR spectra of the metal complexes, this broad band and the band at ≈ 1540 cm^{-1} of the free ligands disappeared. The cinnamoyl carbonyl and ν(C–N) of the ligands also vanished and appeared as new bands at ≈ 1645 cm^{-1} and ≈ 1260 cm^{-1}, respectively. No other prominent band was present in the 1600–1800 cm^{-1} region of the spectra, indicating the involvement of the amine nitrogen and carbonyl oxygen in the coordination with the metal ion.[11] The presence of two medium intensity bands at ≈ 420 cm^{-1} and ≈ 520 cm^{-1}, assignable to ν(M–O) and ν(M–N) in the spectra of all the complexes[12] also support the structure presented in Fig. 2. Important bands that appeared in the spectra are given in Table II.

TABLE I. Physical and analytical data of H_2ded, H_2dpd and their metal complexes

Compound/empirical formula	Yield %	M.p. °C	Found(calcd.), %			
			C	H	N	M
H_2ded/$C_{40}H_{36}N_2O_2$	72	120	83.25(83.33)	6.20(6.25)	4.84(4.86)	–
H_2dpd/$C_{41}H_{38}N_2O_2$	70	148	83.54(83.39)	6.50(6.44)	4.67(4.75)	–
[Ni(ded)]/$C_{40}H_{34}N_2NiO_2$	68	236	75.64(75.86)	5.31(5.37)	4.41(4.43)	9.12(9.28)
[Ni(dpd)]/$C_{41}H_{36}N_2NiO_2$	70	240	75.91(76.08)	5.64(5.57)	4.46(4.33)	8.99(9.08)
[Cu(ded)]/$C_{40}H_{34}CuN_2O_2$	72	281	75.42(75.29)	5.28(5.33)	4.44(4.39)	9.86(9.97)
[Cu(dpd)]/$C_{41}H_{36}CuN_2O_2$	65	276	75.68(75.51)	5.46(5.52)	4.28(4.30)	9.56(9.75)
[Zn(ded)]/$C_{40}H_{34}N_2O_2Zn$	72	187	75.21(75.07)	5.44(5.32)	4.28(4.38)	10.14(10.23)
[Zn(dpd)]/$C_{41}H_{36}N_2O_2Zn$	72	189	75.14(75.30)	5.61(5.51)	4.38(4.29)	9.92(10.01)

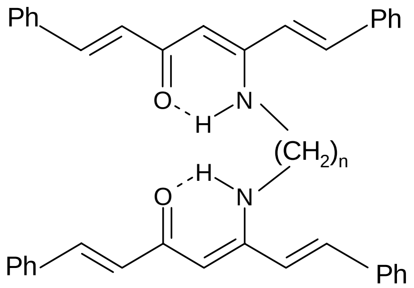

Fig. 1. Structure of the Schiff bases. For H_2ded and H_2dpd *n* equals 2 and 3, respectively.

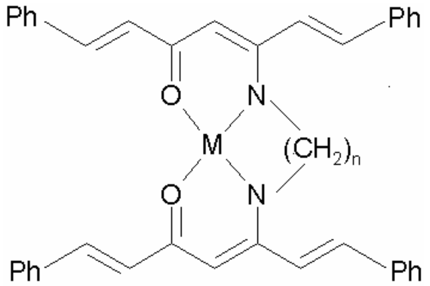

Fig. 2. Structure of the metal complexes of the Schiff bases. M = Ni(II), Cu(II), Zn(II).

TABLE II. Characteristic IR stretching bands, in cm^{-1}, of H_2ded, H_2dpd and their metal complexes

Compound	ν(C=O)	ν(C–N)	ν(N–H)	ν(C=C) phenyl/ alkenyl	ν(M–N)	ν(M–O)
H_2ded	1666	1282	1542	1596, 1590, 1588, 1580	–	–
[Cu(ded)]	1644	1262	–	1592, 1588, 1585, 1582	528	422
[Ni(ded)]	1642	1265	–	1599, 1595, 1588, 1584	526	420
[Zn(ded)]	1645	1263	–	1598, 1594, 1590, 1585	530	420
H_2dpd	1662	1280	1538	1595, 1590, 1585, 1582	–	–
[Cu(dpd)]	1640	1260	–	1596, 1588, 1585, 1580	525	418
[Ni(dpd)]	1641	1261	–	1598, 1595, 1590, 1586	518	428
[Zn(dpd)]	1640	1262	–	1598, 1594, 1591, 1588	530	420

^{1}H-NMR spectra

The ^{1}H-NMR spectra of the compounds displayed a two proton singlet at ≈ δ 13.60 ppm, assignable to hydrogen bonded amine protons.[13] The methylene protons, methine protons and olefinic protons showed signals at the expected positions. The aryl proton signals are observed in the δ range 6.80–7.80 ppm as a complex multiplet. In the ^{1}H-NMR spectra of the diamagnetic Ni(II) and Zn(II) complexes, the low field amine proton signal of the ligands disappeared, indicating its replacement by the metal cation during complexation. The methine proton signals shifted appreciably to low field compared to the shift of the olefinic protons. This may be due to the aromatic character that might have been imparted to the C_3NOM ring system of the chelates by the highly conjugated groups attached to the carbonyl moiety.[14] The integrated intensities of the methylene and olefinic protons agree well with structure of the complexes shown in Fig. 2. The assignments of the various proton signals observed are assembled in Table III.

TABLE III. ^{1}H-NMR spectral data (δ, ppm) of H_2ded, H_2dpd and their Ni(II) and Zn(II) complexes

Compound	NH	Methine	CH_2	Alkenyl
H_2ded	13.60 (2H)	5.86 (2H)	3.34 (4H)	8.13 (4H) 7.98 (4H)
[Ni(ded)]	–	6.32 (2H)	3.37 (4H)	8.18 (4H) 8.02 (4H)
[Zn(ded)]	–	6.30 (2H)	3.35 (4H)	8.17 (4H) 8.04 (4H)
H_2dpd	13.56 (2H)	5.83 (2H)	3.80 (4H) 2.87 (2H)	8.10 (4H) 7.88 (4H)
[Ni(dpd)]	–	6.36 (2H)	3.84 (4H) 2.92 (2H)	8.14 (4H) 7.94 (4H)
[Zn(dpd)]	–	6.28 (2H)	3.86 (4H) 2.94 (2H)	8.16 (4H) 7.90 (4H)

Mass spectra

The formulation of the Schiff bases as shown in Fig. 1 is clearly supported from the presence of an intense molecular ion peak in the mass spectra. Other prominent peaks are due to the elimination of CO, $[C_6H_5-CH=CH-C=O]^+$, tropylium ion, CH≡CH, *etc.*, from the parent ion and subsequent fragments.[15] The FAB mass spectra of the Cu(II) complexes showed molecular ion peaks corresponding to [CuL] stoichiometry. Peaks correspond to L^+ and fragments of L^+ are also present in the spectra. The spectra of all the chelates contain a number of fragments containing copper in the 3:1 natural abundance of ^{63}Cu and ^{65}Cu isotopes (Table IV).

TABLE IV. Mass spectral data of H_2ded, H_2dpd and their Cu(II) complexes

Compound	Mass spectral data (*m*/*z*)
H_2ded	576, 499, 473, 445, 431, 422, 396, 370, 354, 300, 288, 268, 164, 145, 131, 103
H_2dpd	590, 513, 487, 459, 445, 436, 410, 384, 368, 356, 342, 314, 300, 282, 178, 145, 131,103
[Cu(ded)]	639, 637, 576, 536, 534, 508, 506, 445, 433, 431, 422, 405, 403, 396, 375, 370, 354, 328, 300, 272, 199, 197, 169, 164, 145, 131, 103
[Cu(dpd)]	653, 651, 590, 550, 548, 522, 520, 513, 447, 445, 436, 419, 417, 389, 368, 356, 342, 286, 282, 239, 183,178, 145, 131, 103

Electronic spectra

The UV spectra of the Schiff bases show two broad bands with maxima at ≈ 390 and 260 nm, due to the various $n\rightarrow\pi^*$ and $\pi\rightarrow\pi^*$ transitions. The absorption maxima of the metal chelates bear close resemblance with those of the free ligands, which indicates that no structural alteration of the ligand occurred during complexation. However, the values are slightly shifted to longer wavelengths, indicating the involvement of the carbonyl group in metal complexation. The Cu(II) complexes showed a broad visible band, λ_{max} at ≈ 15000 cm^{-1}. This, together with the measured $\boldsymbol{\mu}_{eff}$ values (≈ 1.74 μ_B) suggests square-planar geometry.[16] In agreement with this, a broad band centred at ≈ 11000 cm^{-1} was observed in the spectra recorded in pyridine, which indicates the formation of octahedral pyridine adducts. The observed diamagnetism and broad medium-intensity band at ≈ 17500 cm^{-1} in the spectra of the Ni(II) chelates suggest their square-planar geometry. In conformity with this, the spectra of the chelates in pyridine solution (10^{-3} M) showed three bands corresponding to a configurational change to octahedral due to the association of pyridine. The three well-separated absorption bands at λ_{max} ≈ 8200, 13400 and 24400 cm^{-1} correspond to the transitions: $^3A_{2g}\rightarrow{}^3T_{2g}$, $^3A_{2g}\rightarrow{}^3T_{1g}(F)$ and $^3A_{2g}\rightarrow{}^3T_{1g}(P)$, respectively.

CONCLUSIONS

Two new Schiff base ligands have been prepared by the condensation of dicinnamoylmethane with 1,2-diaminoethane and 1,3-diaminopropane. Analytical, IR, ^{1}H-NMR and mass spectral data revealed a 2:1 product in which one of the carbonyl groups of the diketone is involved in the Schiff base formation. Analytical, physical and spectral data of the [ML] complexes of Ni(II), Cu(II) and

Zn(II) showed dibasic tetradentate N_2O_2 coordination involving the amino nitrogens and carbonyl oxygens. These compounds may exhibit interesting physiological properties compared to curcuminoids because of the presence of nitrogen donor sites. Studies in this direction are in progress.

ИЗВОД

МЕТАЛНИ КОМПЛЕКСИ СА ШИФОВИМ БАЗАМА ДОБИЈЕНИМ ОД ДИЦИНАМОИЛМЕТАНА И АЛИФАТИЧНИХ ДИАМИНА

K. KRISHNANKUTTY[1], P. SAYUDEVI[2] AND MUHAMMED BASHEER UMMATHUR[3]

[1]Department of Chemistry, University of Calicut, Kerala-673635, [2]Department of Chemistry, NSS College, Manjeri, Kerala-676122 и [3]Department of Chemistry, Unity Women's College, Manjeri, Kerala-676122, India

Две нове Шифове базе које садрже олефинске везе синтетисане су под одређеним условима кондензацијом алифатичних диамина и дицинамоилметана. Показазано је ИЦ, ^{1}H-NMR и масеним спектралним подацима да су ова једињења претежно у кето-енаминској форми, са интрамолекулском везом преко водоника. На основу аналитичких и спектралних података установљена је двобазна тетрадентатна N_2O_2 координација ових једињења у [ML] комплексима (M = Ni(II), Cu(II) and Zn(II)).

(Примљено 26. јула, ревидирано 10. децембра 2007)

REFERENCES

1. S. A. Sadeek, *J. Argent. Chem. Soc.* **93 (**2005) 165; D. Kumar, A. Syamal, A. K. Singh, *Indian J. Chem*. **42A** (2003) 280
2. M. Alaudeen, A. Abraham, P. K. Radhakrishnan, *Proc. Indian Acad. Sci. (Chem. Sci.).* **107** (1995) 123; L. Singh, G. Mohan, R. K. Parashar, S. P. Tripathi, R.C. Sharma, *Curr. Sci.* **55** (1986) 846
3. H. J. Garg, C. Prakash, *J. Pharm. Sci.* **60** (1971) 323; H. J. Garg, C. Prakash, *J. Org. Chem.* **35** (1970) 1056
4. P. D. Benny, J. L. Green, H. P. Engelbrecht, C. L. Barnes, S. S. Jurisson, *Inorg. Chem.* **44** (2005) 2381; T. D. Thangadurai, K. Natarajan, *Synth. React. Inorg. Met.-Org. Chem.* **31** (2001) 549; N. Raman, Y. Pitchaikaniraja, A. Kulandaisami, *Proc. Indian Acad. Sci. (Chem. Sci.)* **113** (2001) 183; B. S. Sankhla, S. Mathur, M. Singh, *Synth. React. Inorg. Met.-Org. Chem.* **15** (1985) 1121; B. B. Mahapatra, D. Panda, *Transition Met. Chem.* **9** (1984) 117
5. K. Krishnankutty, M. B. Ummathur, *J. Indian Chem. Soc.* **83** (2006) 663
6. V. D. John, K. Krishnankutty, *Appl. Organometal. Chem.* **20** (2006) 477; V. D. John, K. Krishnankutty, *Transition Met. Chem.* **30** (2005) 229; V. D. John, K. Krishnankutty, *Synth. React. Inorg. Met.-Org. Chem.* **33** (2003) 343
7. V. D. John, G. Kuttan, K. Krishnankutty, *J. Exp. Clin. Cancer Res.* **21** (2002) 219; S. M. Khopde, K. I. Priyadarsini, P. Venketesan, M. N. A. Rao, *Biophys. Chem.* **80** (1999) 85; S. Antony, R. Kuttan, G. Kuttan, *Immunol. Investig.* **28** (1999) 291; R. J. Anto, K. N. D. Babu, K. N. Rajasekharan, R. Kuttan, *Cancer Lett.* **94** (1995) 74
8. H. J. J. Pabon, *Recl. Trav. Chim. Pays-Bas* **83** (1964) 237
9. K. Krishnankutty, P. Venugopalan, *Synth. React. Inorg. Met-Org. Chem.* **28** (1998) 1313; K. Krishnankutty, P. Venugopalan, *J. Indian Chem. Soc.* **75** (1998) 2

10. P. Gilli, V. Bertolasi, V. Ferretti, G. Gilli, *J. Am. Chem. Soc.* **122** (2000) 1045
11. L. J. Bellamy, *The Infrared Spectra of Complex Molecules*, Chapman and Hall, London, 1980
12. K. Nakamoto, *Infrared Spectra and Raman Spectra of Inorganic and Coordination Compounds*, Wiley, New York, 1997
13. P. J. Roughley, D. A. Whiting, *J. Chem. Soc., Perkin Trans. 1* (1973) 2379
14. R. L. Lintvedt, H. F. Holtzdaw Jr., *J. Am. Chem. Soc.* **88** (1966) 2713
15. C. G. MacDonald, J. S. Shannon, *Aust. J. Chem.* **19** (1966) 1545
16. K. C. Joshi, V. N. Pathak, *Coord. Chem. Rev.* **22** (1977) 37.

Journal of the Serbian Chemical Society
JSCS@tmf.bg.ac.yu • www.shd.org.yu/JSCS
www.shd.org.yu

J. Serb. Chem. Soc. 73 (4) 431–433 (2008)
JSCS–3725

UDC 519.17+544.112:533.73:539.124
Note

NOTE

Bicyclic molecular graphs with the greatest energy

BORIS FURTULA, SLAVKO RADENKOVIĆ[#] and IVAN GUTMAN[*#]

Faculty of Science, University of Kragujevac, P. O. Box 60, 34000 Kragujevac, Serbia

(Received 6 December 2007)

Abstract: The molecular graph Q_n is obtained by attaching hexagons to the end vertices of the path graph $P_{n\text{-}12.}$ Earlier empirical studies indicated that Q_n has greatest energy among all bicyclic n-vertex (molecular) graphs. Recently, Li and Zhang proved that Q_n has greatest energy among all bipartite bicyclic graphs, with the exception of the graphs $R_{a,b}$, $a + b = n$, where $R_{a,b}$ is the graph obtained by joining the cycles C_a and C_b by an edge. This result is now completed by showing that Q_n has the greatest energy among all bipartite bicyclic n-vertex graphs.

Keywords: total π-electron energy; graph energy; bicyclic molecular graphs.

INTRODUCTION

The HMO total π-electron energy E is an important quantum-chemical characteristic of large polycyclic conjugated molecules.[1–4] A closely related quantity is the graph energy (also denoted by E), equal to the sum of the absolute values of the eigenvalues of the underlying molecular graph.[4,5] The question which molecular graph (within some pertinently defined class) has the greatest E value is of evident chemical relevance and has been much studied.[1,6–13]

In 2001, by means of a computer-aided empirical search, it was established[8] that the graph Q_n (depicted in Fig. 1) is most probably the maximum-energy specie among n-vertex bicyclic molecular graphs. Recently, Li and Zhang[11] offered a mathematical result that almost completely proved this finding. Namely, they showed that Q_n has the greatest energy among bipartite bicyclic n-vertex graphs, with the exception of the graphs $R_{a,b}$, $a + b = n$. The structures of the graphs Q_n and $R_{a,b}$ are shown in Fig. 1.

COMPLETING THE RESULT OF LI AND ZHANG

For odd n, the graphs $R_{a,b}$, $a + b = n$, are not bipartite. Therefore, for odd n, it is know that Q_n is the maximum-energy bicyclic bipartite graph and there re-

---

[#] Serbian Chemical Society member.

[*] Corresponding author. E-mail: gutman@kg.ac.yu

doi: 10.2298/JSC0804431F

mains nothing to be added to the proof of Li and Zhang. In view of this, in what follows, it is assumed that n is even.

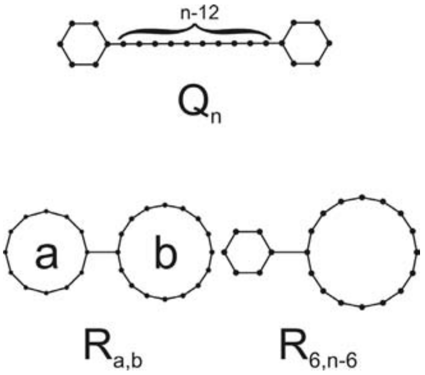

Fig. 1. The molecular graphs considered in this note. All these graphs are assumed to possess n vertices and that $n \geq 12$. Therefore $a + b = n$.

In order to complete the result of Li and Zhang,[11] appropriate computer-based investigations were undertaken. First it was necessary to determine which among the graphs $R_{a,b}$, $a + b = n$, has the greatest energy. As bipartite graphs are under consideration,[5] the parameters a and b must be even. In view of the earlier collected knowledge on the Hückel $(4m + 2)$-rule (for details see[14–16]), it could be anticipated that $E(R_{a,b})$ will be maximal for $a = 6$, $b = n - 6$ (or, what is the same: $a = n - 6$, $b = 6$). This, indeed, was confirmed by our calculations, performed until $a + b = 50$.

A comparison of the energies of Q_n and $R_{6,n-6}$ was now required. For this the quantity $\Delta(n) = E(Q_n) - E(R_{6,n-6})$, the dependence of which on n is shown in Fig. 2, was computed.

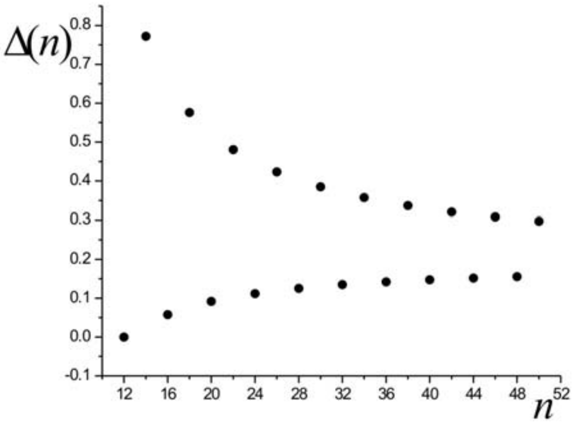

Fig. 2. The dependence of $\Delta(n) = E(Q_n) - E(R_{6,n-6})$ on the number n of vertices of the molecular graphs considered. For details see text.

As another consequence of the Hückel $(4m + 2)$-rule, the data points for $n \equiv 0 \pmod 4$, *i.e.*, for $n = 12, 16, 20, 24,\ldots$, lie below the data points for $n \equiv 2 \pmod 4$, *i.e.*, for $n = 14, 18, 22, 26,\ldots$ For $n = 12$, the molecular graphs Q_n and

$R_{6,n-6}$ coincide and therefore $\Delta(12) = 0$. For all other (even) values of n, $\Delta(n)$ is greater than zero. Moreover, as seen from Fig. 2, in the limit case $n \to \infty$, $\Delta(n)$ tends to a value that lies between 0.2 and 0.3.

By this it was verified that for all even values of n, $n > 12$, $E(Q_n) > E(R_{6,n-6})$. Consequently, $E(Q_n) > E(R_{a,b})$ for any even value of a and b, $a + b = n$. Together with the result of Li and Zhang[11], this implies that the earlier guess[8] that Q_n, the molecular graph of the α,ω-diphenylpolyene, has the greatest energy among all bicyclic graphs was correct.

ИЗВОД

БИЦИКЛИЧНИ МОЛЕКУЛСКИ ГРАФОВИ СА НАЈВЕЋОМ ЕНЕРГИЈОМ

БОРИС ФУРТУЛА, СЛАВКО РАДЕНКОВИЋ и ИВАН ГУТМАН

Природно–математички факултет Универзитета у Крагујевцу

Молекулски граф Q_n се добија додавањем по једног хексагона на крајње чворове пута P_{n-12} Ранија емпиријска проучавања указала су на то да Q_n има највећу енергију међу свим бицикличним (молекулским) графовима са n чворова. Недавно су Li и Zhang доказали да Q_n има највећу енергију међу свим бипартитним бицикличним графовима, са изузетком графова $R_{a,b}$, $a + b = n$, где је $R_{a,b}$ граф добијен повезивањем циклова C_a и C_b једном граном. Сада је овај резултат комплетиран тиме што је показано да Q_n има највећу енергију међу свим бипартитним бицикличним графовима са n чворова.

(Примљено 6. децембра 2007)

REFERENCES

1. I. Gutman, *J. Serb. Chem. Soc.* **70** (2005) 441
2. M. Perić, I. Gutman, J. Radić-Perić, *J. Serb. Chem. Soc.* **71** (2006) 771
3. I. Gutman, *J. Serb. Chem. Soc.* **72** (2007) 967
4. S. Radenković, I. Gutman, *J. Serb. Chem. Soc.* **72** (2007) 1343
5. I. Gutman, O. E. Polansky, *Mathematical Concepts in Organic Chemistry*, Springer-Verlag, Berlin, 1986
6. I. Gutman, *Theor. Chim. Acta* **45** (1977) 79
7. I. Gutman, Y. Hou, *MATCH Commun. Math. Comput. Chem.* **43** (2001) 17
8. I. Gutman, D. Vidović, *J. Chem. Inf. Comput. Sci.* **41** (2001) 1002
9. Y. Hou, I. Gutman, C. W. Woo, *Lin. Algebra Appl.* **356** (2002) 27
10. A. Chen, A. Chang, W. C. Shiu, *MATCH Commun. Math. Comput. Chem.* **55** (2006) 95
11. X. Li, J. Zhang, *Lin. Algebra Appl.* **427** (2007) 87
12. H. Hua, *MATCH Commun. Math. Comput. Chem.* **58** (2007) 57
13. I. Gutman, B. Furtula, H. Hua, *MATCH Commun. Math. Comput. Chem.* **58** (2007) 85
14. I. Gutman, S. Bosanac, *Tetrahedron* **33** (1977) 1809
15. I. Gutman, M. Stanković, *J. Mol. Struct. (Theochem.)* **309** (1994) 301
16. I. Gutman, *Monatsh. Chem.* **136** (2005) 1055.

Journal of the Serbian Chemical Society
JSCS@tmf.bg.ac.yu • www.shd.org.yu/JSCS
www.shd.org.yu

J. Serb. Chem. Soc. 73 (4) 435–451 (2008)
JSCS–3726

UDC 66.061.35:546.683.3+547.412.123:544.032.4
Original scientific paper

Rapid liquid–liquid extraction of thallium(III) from succinate media with 2-octylaminopyridine in chloroform as the extractant

SANDIP V. MAHAMUNI, PRAKASH P. WADGAONKAR[1] and MANSING A. ANUSE*

Analytical Chemistry Laboratory, Department of Chemistry, Shivaji University, Kolhapur – 416 004 and [1]Polymer Science and Engineering Division, National Chemical Laboratory, Dr. Homi Bhabha Road, Pune – 411 008, India

(Received 28 May 2007)

Abstract: A simple solvent extraction study of thallium(III) was conducted. Selective and quantitative extraction of thallium(III) by 2-octylaminopyridine (2-OAP) in chloroform occurred from aqueous sodium succinate medium (0.0075 M) at pH 3.0. Thallium(III) was back extracted with acetate buffer (pH 4.63). The effect of the concentration of succinate and 2-OAP, the role of various diluents, stripping agents, loading capacity of 2-OAP, equilibrium time and aqueous:organic volume ratio on the extraction of thallium(III) was studied. The stoichiometry of the extracted species was determined based on the slope analysis method and found to be 1: 2: 1 (metal:acid:extractant). The temperature dependence of the extraction equilibrium constant was also examined to estimate the apparent thermodynamic functions ΔH, ΔG and ΔS for the extraction reaction. The method is free from interference of a large number of cations and anions. The method was used for the selective extraction of thallium(III) from its binary mixture with Zn(II), Cd(II), Hg(II), Bi(III), Pb(II), Se(IV), Te(IV), Sb(III), Ga(III), In(III), Al(III), Tl(I) and Fe(III). The proposed method was applied to the synthetic mixtures and alloys. It is simple, selective, rapid and eco-friendly.

Keywords: liquid–liquid extraction; thallium(III); succinate media; 2-OAP; temperature effect.

INTRODUCTION

Thallium is a trace element that occurs mostly in sulphur containing ores.[1] It is a by-product metal recovered in some countries from flue dusts and residues collected in the smelting of copper, zinc and lead ores. Thallium(III) is usually present in lead(II), cadmium(II), indium(III) or zinc(II) compounds as a trace constituent.[2] Consumption of thallium metal and thallium compounds continues for most of its established end uses, such as an additive in glass to increase its refractive index and density, a catalyst or intermediate in the synthesis of organic

---

* Corresponding author. E-mail: mansinganuse@yahoo.co.in
doi: 10.2298/JSC0804435M

compounds and a component in high-density liquids for sink-float separation of minerals.[3] Thallium is a highly toxic element and Tl(I) is known to replace potassium ions in the activation of enzymes.[4] The contamination of the environment with thallium mainly results from non-ferrous mines, coal combustion and cement plants.[5] Hence, bearing all this in mind, the separation of thallium from other metal ions has been a subject of great analytical interest.

There are a few research papers on the extraction and separation of thallium(III) from associated elements. The extraction of thallium(III) and thallium(I) by solutions of carboxylic acids, such as naphthenic acid (NA), *sec*-octylphenoxy acid (CA-12) and *sec*-nonylphenoxy acetic acid (CA-100) dissolved in kerosene and acidic aqueous chloride media has been reported by X. Zhang *et. al*.[6] Various organophosphorus compounds, such as Cyanex 921,[7] Cyanex 923,[8] Cyanex 925,[9] tributyl phosphate (TBP)[10] have been found to be useful for the extraction of thallium(III). Studies on the thermodynamics of solvent extraction of thallium(I) with diethylhexylmonothiophosphoric acid (D2EHMTPA)[11] and di(2-ethylhexyl)dithiophosphoric acid[12] were conducted at an ionic strength of 0.1 mol g^{-1} in the aqueous phase containing sodium sulphate as a supporting electrolyte and at a constant initial molality of the extractant in the organic phase at temperatures from 278.15 to 303.15 K. The standard extraction constants K_0 at various temperatures were obtained by the extrapolation and the polynomial approximation methods.

Trace amounts of thallium(III) were quantitatively extracted with hexa-acetyl calix(6)arene at pH 2.0 with toluene as the diluent. However, uranium, antimony, tin and lead showed strong interference.[13] Meso-tetraspirocyclohexylcalix(4)pyrrole (TSCC4P) in 20.6 % (v/v) tetrahydrofuran was found to be an effective complexing ligand for homogeneous liquid–liquid extraction and preconcentration of thallium(I) ions at pH 5.4. The reproducibility of method was at the most 3.4 %.[14]

Thallium(III) was separated by solvent extraction into methyl isobutyl ketone (MIBK) in hydrobromic acid medium from a sample digest of geological material.[15] The extraction equilibria for the determination of ultra trace amounts of thallium(III) in a water sample by ion-pairs of the methyl-2-naphthoate (2HNpH) complex and tetrabutylammonium ion in MIBK extraction was studied by Kim and co-workers.[16] However, the percentage extraction of thallium(III) as an ion pair was 73.5 % at pH 6.0. A method was proposed for extraction of trivalent thallium from salicylate media using triphenyl arsine oxide (TPASO) dissolved in toluene as the extractant.[17] The separation of thallium(I) and thallium(III) was achieved by the difference between the distribution coefficients of thio–oxime and PAN–thallium complexes. Heavy metals such as Mn(II), Fe(III), Ni(II), Cu(II), Zn(II) needed to be masked by EDTA.[18] The kinetics of the hydrolysis of tris(thenoyltrifluoroacetonate)thallium(III) in water was studied.[19] A method for the extraction of thallium(III) with isopentyl acetate from 10 M hydrochloric acid media was proposed, whereby co-extracted iron could be removed by its re-extraction from the organic phase with 4 M H_2SO_4.[20] Trivalent thallium can be extracted from aqueous solutions at 65 °C with 2,6-bis-(1′-phenyl-3′-methyl-5′-oxo-pyrazole-4′)pyridineacyl (H_2PMBPP or H_2A) using molten paraffin wax as a diluent.[21]

The influence of module arrangements on the solvent extraction of thallium(III) from sodium chloride–sulphuric acid solution into butyl acetate was studied using laboratory-made modules consisting of hydrophobic poly(vinylidine fluoride) (PVDF) and polypropylene (PP) hollow fibres.[22–25] The distribution coefficient of thallium(III) between butyl acetate and the aqueous phase was about 1000 when the extraction was carried out from 5.0 mol dm^{-3} sulphuric acid solution containing sodium chloride, providing the molar ratio between thallium(III) and Cl^- was not less than 1:4. From this solution, thallium(III) is extracted in the form of the $HTlCl_4$ complex.[24] The extraction was found to be dispersion free.[24,25]

Gas-stirred propylene carbonate (PC) extraction has proved to be highly useful for the separation and subsequent direct polarographic estimation of thallium(III). It can be seen that selective separation of thallium(III) from other metal ions was achieved by the extraction into PC from 0.03 M hydrochloric acid. However, Fe(III) was found to be partially co-extracted with thallium(III).[26] Chung *et al.* reported a selective extraction method for thallium(III) in the presence of gallium, indium, bismuth and antimony into 2-propanol by the salting out method using sodium chloride to induce phase separation.[27] The distribution behaviour of the ion association complexes of tetrahalogenatothallate(III) ions (TlX_4^- (X^- = chloride, bromide and iodide ions)) with quaternary ammonium cations (Q^+) between three organic phases (chloroform, chlorobenzene and benzene) and an aqueous phase was examined, and the extraction constants (log K_{ex}) were determined.[28] Electrothermal atomic absorption spectrometry (ETAAS) has been used for the determination of thallium(III) in aqueous solution in conjunction with an enrichment technique such as solid-phase extraction.[29] Thallium(III) was quantitatively retained by 1,10-phenanthroline and tetraphenylborate onto benzophenone in the pH range 0–11.0 from a large volumes of aqueous solutions of various samples.[30] A selective method has been developed for extraction studies of thallium(III) with a high molecular weight carboxylic acid, SRS–100 (a liquid cation exchanger). Quantitative extraction of thallium(III) was achieved in the pH range 5.0–6.0 from acetic acid and sodium acetate solution.[31]

Solvent extractions of thallium(III) with high molecular weight amines have been investigated. A simple solvent extraction study for thallium was conducted based on the extraction of thallium as a chlorocomplex (tetrachlorothallate(III) anion) with tribenzylamine. The recovery of thallium was found to be 95 %.[32] Recently, a primary amine, *n*-octylaniline dissolved in toluene was reported to be an effective extractant for thallium(III) using salicylate media.[33]

Herein, a rapid and selective extraction procedure for thallium(III) with 2-octylaminopyridine is reported. The method permits the separation of thallium(III) from commonly associated elements and was employed to separate thallium(III) in synthetic mixtures and alloy samples.

EXPERIMENTAL

Apparatus

An Elico digital spectrophotometer, model SL–171, with 1 cm quartz cells was used for the absorbance measurements. pH Measurements were carried out using an Elico digital pH meter, model LI–120. A constant temperature water bath MIC-66 A (±0.1 °C) (Modern Scientific Instrument Company, Mumbai) was used for the temperature controlled studies.

Reagents

A standard stock solution of thallium(I) was prepared by dissolving 1.303 g of thallium(I) nitrate (Across) in 25 ml 1.0 M nitric acid and diluting to 1000 ml with distilled water. It was then standardized complexometrically[34] after oxidation to the thallium(III) state with saturated bromine water. The solution contained 1.0 mg ml^{-1} of thallium(I).

A standard solution of thorium nitrate (0.01 M) was prepared by dissolving 5.881 g thorium nitrate (AR) and diluting to 1.0 l with distilled water. This solution was standardized against standard zinc(II) solution.[35]

A standard solution of EDTA (disodium salt) (0.01 M) was prepared by dissolving 3.722 g of the disodium salt of EDTA in 1.0 l of distilled water.

An acetate buffer solution (pH 4.63) was prepared by mixing equal volumes of 0.2 M sodium acetate trihydrate and 0.2 M of glacial acetic acid.[35]

A 0.025 M solution of 2-octylaminopyridine (2-OAP) was prepared by dissolving in chloroform.[36]

Other standard solutions of the different metals used to study the effect of diverse ions were prepared by dissolving weighed quantities of their salts in distilled water or dilute hydrochloric acid. Solutions of anions were prepared by dissolving the respective alkali metal salts in water. All the employed chemicals were of A. R. grade and double distilled water was used through out.

General extraction and determination procedure for thallium(III)

To an aliquot of solution containing 1.0 mg of thallium(I), few drops of bromine water were added to oxidize the thallium(I) to thallium(III). The solution was then evaporated carefully to remove the excess bromine water. To this, a sufficient quantity of sodium succinate was added to give a final concentration 0.0075 M in a total volume of 25 ml of solution. The pH of the solution was adjusted to 3.0 using dilute hydrochloric acid and sodium hydroxide solutions. The aqueous solution was shaken with 10 ml of 0.025 M 2-OAP in chloroform for 2 min. After phase separation, the organic phase was stripped with three 15 ml portions of acetate buffer. The extracts were evaporated to moist dryness and the residue was dissolved in distilled water. To this, an excess of EDTA solution (10 ml 0.001 M EDTA) was added and the pH of the solution was adjusted to 3.5. The solution was titrated with a standard solution of 0.001 M thorium nitrate using xylenol orange as the indicator. The end point was yellow to red to red violet.[34]

RESULTS AND DISCUSSION

Extraction as a function of pH

The effect of pH on the percent thallium(III) extracted with 2-OAP in chloroform was studied in the pH range 1.0–10.0 in the presence of sodium succinate (0.0075 M). It was observed that the extraction of thallium(III) was quantitative in the pH range 2.0 to 6.0 (Fig. 1). In the proposed method, all the extractions were performed at a fixed pH of 3.0. At pH values, above 6.0, there exists the possibility of hydrolysis, which results in a lowering of the distribution ratio. This indirectly promotes an equilibrium competing with the formation of the ion pair complex, resulting in a decrease in extraction with increasing pH.

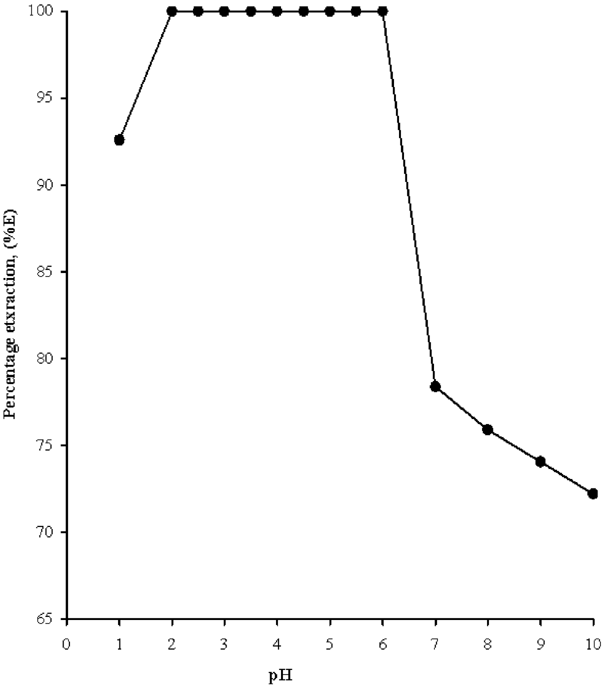

Fig. 1. Extraction behaviour of thallium(III) as a function of pH.

Extraction of thallium(III) as a function of the 2-OAP concentration

The effect of varying the 2-OAP concentration (0.0005–0.5 M) on the distribution of thallium(III) (1.0 mg) was investigated at pH 3.0 in an aqueous solution of ionic strength 0.0075 M sodium succinate. The optimum concentration of 2-OAP required for the quantitative extraction of thallium(III) was found to be 0.005 M. In the recommended procedure 10 ml of 0.025 M 2-OAP was used in order to ensure the complete extraction of thallium(III). However, at higher reagent concentration (> 0.1 M), there was decrease in the extraction of thallium(III). This was probably due to an increase in the concentration of the dimer with increasing concentration of 2-OAP and hence the distribution coefficient decreased due to reduced concentration of monomer.[37]

Extraction as a function of weak organic acid concentration

The extraction of thallium(III) was performed at pH 3.0 with 0.025 M 2-OAP in chloroform in the presence of varying concentrations (0–0.2 M) of sodium succinate, sodium salicylate, sodium malonate and sodium oxalate, as weak acid media (Table I). The extraction of the ion pair complex of thallium(III) was found to be quantitative in the range 0.004 to 0.08 M sodium succinate and at 0.006 M sodium salicylate. With increasing concentration of sodium succinate above this value, the extraction of thallium(III) decreased. The decrease in the extraction at high acid concentration was presumably due to the preferential formation of the succinate of 2-OAP. Therefore, 0.0075 M sodium succinate was used throughout this work. Sodium salicylate was not employed because of its narrow concentration range for extraction and high cost as compared to sodium succinate. The extraction of thallium(III) was found to be incomplete in sodium malonate and sodium oxalate media.

TABLE I. Extraction behaviour of thallium(III) as a function of the concentration of the weak organic acids; *m*(Tl(III)) = 1.0 mg, pH 3.0, 10 ml of 0.025 M solution of 2-OAP in chloroform, aqueous:organic ratio = 2.5:1, equilibrium time = 2 min, strippant = acetate buffer pH 4.63 (3×15 ml)

Acid concentration mol dm^{-3}	Sodium succinate[a]		Sodium malonate		Sodium salicylate		Sodium oxalate	
	% E	D	% E	D	% E	D	% E	D
0	35.85	1.39	35.85	1.39	35.85	1.39	35.85	1.39
0.0020	88.68	19.58	94.34	41.66	84.91	14.06	39.62	1.64
0.0040	100	∞	98.11	130.0	96.23	63.75	43.39	1.91
0.0060	100	∞	98.11	130.0	100.0	∞	18.86	0.58
0.0075	100[a]	∞	81.13	10.75	98.11	130.0	7.54	0.20
0.0080	100	∞	64.15	4.47	98.11	130.0	7.54	0.20
0.0100	100	∞	58.49	3.52	88.68	19.58	0.0	0.0
0.0200	100	∞	54.72	3.02	86.79	16.42	0.0	0.0
0.0400	100	∞	54.72	3.02	83.01	12.22	0.0	0.0
0.0600	100	∞	33.96	1.28	71.42	6.24	0.0	0.0
0.0800	100	∞	11.32	0.31	67.92	5.29	0.0	0.0
0.1000	92.45	30.61	5.62	0.15	49.05	2.40	0.0	0.0
0.2000	75.45	7.68	0.0	0.0	37.73	1.51	0.0	0.0

[a]Recommended for the general extraction procedure

Extraction with various diluents

Ten systems containing identical amounts (1.0 mg) of thallium(III) were prepared and extracted with 10 ml of 0.025 M 2-OAP in each of various solvents (Table II). The following percentage extractions were obtained. 1,2-dichloroethane (55.10) < kerosene (59.18) < *n*-butanol (63.26) < pentanol = pentyl acetate

(67.34) < toluene (73.46) < carbon tetrachloride (93.87) < benzene = xylene = = chloroform (100). No correlation between dielectric constant and percent extraction was observed. 2-Butanone did not extract thallium(III) into the organic phase. In the case of chloroform, a quicker phase separation was observed and this was used as the diluent for all subsequent studies.

TABLE II. Extraction behaviour of thallium(III) as a function of the diluent; m(Tl(III)) = 1.0 mg, pH 3.0, 10 ml of 0.025 M solution of 2-OAP in chloroform, aqueous:organic ratio = 2.5:1, equilibrium time = 2 min, strippant = acetate buffer pH 4.63 (3×15 ml)

Diluent	Dielectric constant, ε	Percentage extraction, % E	Distribution ratio, D
1,2-Dichloroethane	10.50	55.10	3.06
Kerosene	1.80	59.18	3.62
n-Butanol	17.80	63.26	4.30
Pentanol	13.90	67.34	5.15
Pentyl acetate	4.80	67.34	5.15
Toluene	2.38	73.46	6.91
Carbon tetrachloride	2.24	93.87	38.28
Benzene	2.28	100	∞
Xylene	2.30	100	∞
Chloroform[a]	4.40	100	∞

[a] Recommended for the general extraction procedure

Nature of extracted species

The stoichiometry of the extracted species was determined from the experimental studies using the slope analysis method. The plots of log $D_{[\mathrm{Tl(III)}]}$ *vs.* log $c_{[\text{2-OAP}]}$ at a fixed sodium succinate concentration (0.0075 M) were found to be linear with slopes of 1.25 and 0.93 at pH 7.0 and 10.0, respectively (Fig. 2). This indicates that the metal:extractant ratio was 1:1. In addition, plots of log $D_{[\mathrm{Tl(III)}]}$ *vs.* log $c_{[\text{succinate}]}$ at a fixed 2-OAP concentration (0.025 M) were linear with slope values of 1.92 and 1.73 at pH 7.0 and 10.0, respectively (Fig. 3). This indicates two ions of succinate participate in the formation of the anionic species. Thus, the probable composition of the extracted species was 1:2:1 (metal:acid:extractant). The possible mechanism of extracted species appears to involve protonated 2-OAP, which forms cationic species, such as $\mathrm{RR'NH_2^+}$, while the succinate combines with thallium(III) to form anionic species, such as $[\mathrm{Tl(succinate)_2}]^-$, both of which associate to form an ion pair of the type $[\mathrm{RR'NH_2^+Tl(succinate)_2^-}]_{(org)}$, which, being neutral, constitutes the extractable species.

The mechanism of formation of the ion pair complex is:

$$\mathrm{RR'NH_{(org)} + H^+_{(aq)} \rightleftharpoons RR'NH_2{}^+{}_{(org)}}$$

$$\mathrm{Tl^{3+}_{(aq)} + 2\ Succinate^{2-}_{(aq)} \rightleftharpoons [Tl(Succinate)_2]^-_{(aq)}}$$

$$\mathrm{RR'NH_2{}^+{}_{(org)} + [Tl(Succinate)_2]^-_{(aq)} \rightleftharpoons [RR'NH_2{}^+Tl(Succinate)_2{}^-]_{(org)}}$$

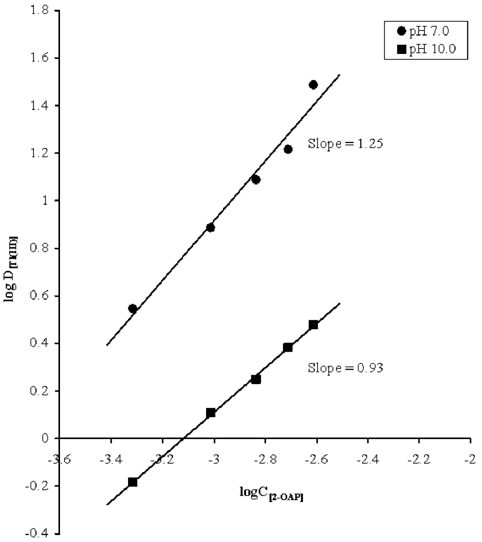

Fig. 2. Log–log plot of log $D_{[\mathrm{Tl(III)}]}$ *vs.* log $c_{[\mathrm{2\text{-}OAP}]}$ at a fixed succinate concentration (0.0075 M).

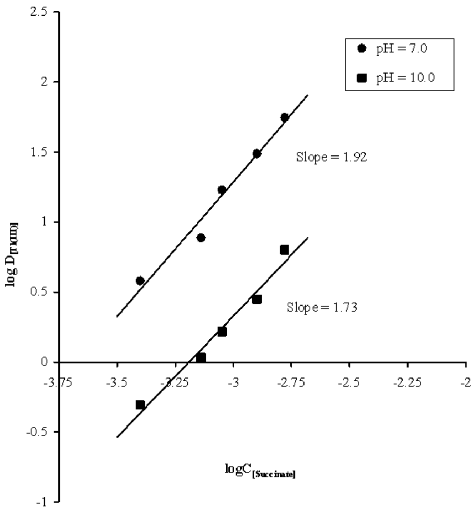

Fig. 3. Log–log plot of log $D_{[\mathrm{Tl(III)}]}$ *vs.* log $c_{[\mathrm{Succinate}]}$ at a fixed 2-OAP concentration (0.025 M).

Effect of equilibrium time

The experiments to investigate the influence of contact time on the extraction of thallium(III) were carried out by shaking an aqueous solution of 1.0 mg thallium(III) containing 0.0075 M succinate with an organic solution of 0.025 M 2-OAP in chloroform at an A/O ratio of 2.5 for various lengths of time at 25±3 °C. The obtained results showed that equilibrium was achieved within 30 s of contact. In the actual work, a two-minute equilibrium time was recommended in order to ensure the complete extraction of thallium(III). However, prolonged shaking above 20 min decreased the percentage extraction of thallium(III).

Extraction behaviour of thallium(III) as a function of metal loading capacity

The amount of thallium(III) was varied to determine the loading capacity of 2-OAP. The loading capacity of 10 ml 0.025 M 2-OAP was found to be 3 mg of thallium(III).

Effect of aqueous to organic volume ratio

Thallium(III) was extracted from 10 to 250 ml of 0.0075 M aqueous sodium succinate medium with 10 ml 0.025 M 2-OAP in chloroform. Thallium(III) was stripped with acetate buffer and estimated as in the recommended procedure. It was found that the extraction of thallium(III) was quantitative when the aqueous to organic volume ratio was 2 to 15, while it decreased when the ratio was in the range 20–25. Hence, the recommended aqueous to organic volume ratio in the procedure is 2.5, in order to minimize the consumption of sodium succinate.

Effect of stripping agents

Stripping of the metal loaded organic phase containing thallium(III) was attempted with hydrochloric acid, nitric acid, sulphuric acid, perchloric acid, acetic acid, ammonia, acetate buffer, ammonia buffer and water as various stripping agents (3×15 ml). The results are shown in Table III. It is clear that of all the examined solutions, only perchloric acid (7–10 M) and acetate buffer (pH 4.63) were effective in stripping thallium(III) from the organic layer. However, acetate buffer (pH 4.63) is recommended because removal of the acetate buffer by evaporation is easier than the removal of perchloric acid and causes less pollution.

TABLE III. Extraction behaviour of thallium(III) as a function of the employed strippant; *m*(Tl(III)) = 1.0 mg, pH 3.0, 10 ml of 0.025 M solution of 2-OAP in chloroform, aqueous:organic ratio = 2.5:1, equilibrium time = 2 min

c mol dm^{-3}	HCl recovery, %	HNO_3 recovery, %	H_2SO_4 recovery, %	$HClO_4$ recovery, %	CH_3COOH recovery, %	NH_3 recovery, %
0.1	18.0	0.0	20.0	18.0	10.63	0.0
0.5	18.0	0.0	34.0	24.0	10.63	0.0
1.0	18.0	24.0	10.0	54.0	10.63	2.12
2.0	22.0	24.0	40.0	54.0	12.76	10.63
3.0	42.0	28.0	42.0	54.0	19.14	10.63
4.0	66.0	42.0	42.0	62.0	19.14	10.63
5.0	84.0	68.0	42.0	70.0	21.27	10.63
6.0	90.0	70.0	52.0	76.0	21.27	10.63
7.0	46.0	70.0	60.0	100.0	21.27	0.0
8.0	42.0	74.0	64.0	100.0	23.40	0.0
9.0	36.0	74.0	68.0	100.0	23.40	0.0
10.0	24.0	74.0	74.0	100.0	27.65	0.0

TABLE IIIA. Recoveries for various stripping agents

Strippant	Recovery, %
Acetate buffer (pH 4.63)	100.0[a]
Ammonia buffer (pH 10.0)	69.79
Water	0.0

[a] Recommended for the general extraction procedure

Effect of temperature on the extraction of thallium(III)

The results of the extraction of thallium(III) from a pH 7.0 succinate solution by 0.025 M 2-OAP in chloroform at temperatures varying from 298 to 310 K are given in Table IV. It was found that the distribution ratio increased with increasing temperature in the extraction of thallium(III) by 2-OAP in chloroform.

The change of the extraction equilibrium constant (K_{ex}) with temperature is expressed by the van’t Hoff Equation:

$$\frac{\mathrm{d}(\log K_{ex})}{\mathrm{d}(1/T)} = \frac{-\Delta H}{2.303R} \tag{1}$$

TABLE IV. Effect of temperature on the extraction of thallium(III) with 2-OAP in chloroform; m(Tl(III)) = 1.0 mg, pH 3.0, 10 ml of 0.025 M solution of 2-OAP in chloroform, aqueous:organic ratio = 2.5:1, equilibrium time = 2 min, strippant = acetate buffer pH 4.63 (3×15 ml)

T / K	Log D	Log K_{ex}	ΔG / kJ mol^{-1}	ΔS / J K mol^{-1}	ΔH / kJ mol^{-1}
298	0.77	4.64	–26.51	329.28	–
301	0.86	4.73	–27.04	327.75	–
304	1.02	4.9	–27.96	327.53	71.61
307	1.15	5.03	–28.71	326.77	–
310	1.23	5.10	–29.15	325.04	–

The plot of log K_{ex} *vs.* 1000/T is linear with a slope of –3.74 (Fig. 4) and the enthalpy change of the extraction performed at constant pH 7.0 was evaluated as ΔH = 71.61 kJ mol^{-1}, which means it is an endothermic process. The free energy ΔG and entropy ΔS were calculated from Eqs. (2) and (3):

$$\Delta G = -2.303RT \log K_{ex} \tag{2}$$

$$\Delta S = \frac{\Delta H - \Delta G}{T} \tag{3}$$

The negative values of free energies imply that the reaction is spontaneous. The positive enthalpy value indicates that the extraction of thallium(III) with 2-OAP in chloroform is favoured by increasing temperature.

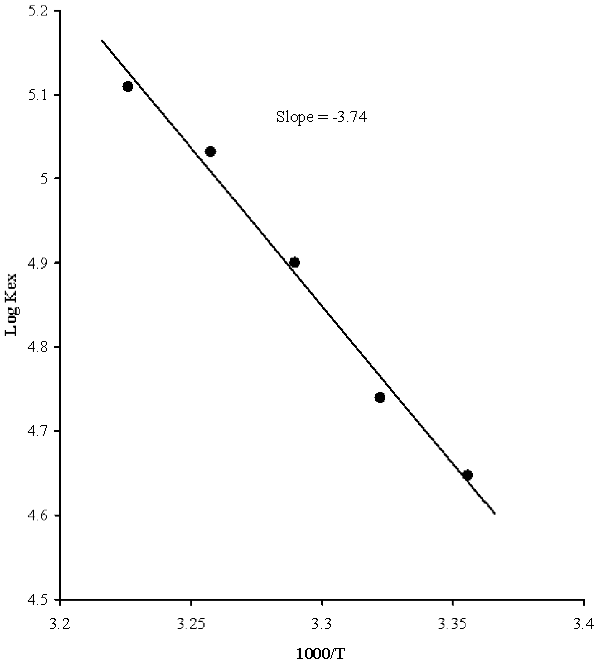

Fig. 4. Extraction behaviour of thallium(III) as a function of temperature.

Effect of diverse ions

The effect of various foreign ions commonly associated with thallium(III) was studied by the recommended procedure. The tolerance limits for the test ions are given in Table V. When the interference was found to be intensive, the tests were repeated with successively smaller amounts of foreign ion until a concentration giving an error less than ±2 % in the recovery of thallium(III) was attained. It was observed that the method is free from interference from a large number of transition and non-transition metal ions and anions. The interference due to Al(III) and Te(IV), Ga(III) and Fe(III) was eliminated by masking each metal ion with 1.0 mg citrate, 1.0 mg fluoride and 1.0 mg oxalate, respectively. Vanadium(V) and Sn(IV) interfered in the extraction procedure of thallium(III).

TABLE V. Effect of foreign ions on extraction behaviour of thallium(III); *m*(Tl(III)) = 1.0 mg, pH 3.0, 10 ml of 0.025 M solution of 2-OAP in chloroform, aqueous:organic ratio = 2.5:1, equilibrium time = 2 min

Ions	Added as	Tolerance limit, mg	Ions	Added as	Tolerance limit, mg
Acetate	Sodium acetate	100.0	Mn(VII)	$KMnO_4$	5.0
Nitrate	Sodium nitrate	100.0	Mo(VI)	$(NH_4)_6Mo_7O_{24}\cdot 6H_2O$	2.0
Nitrite	Sodium nitrite	100.0	Sr(II)[a]	$Sr(NO_3)_2$	2.0
Salicylate	Sodium salicylate	100.0	Ni(II)	$NiCl_2\cdot 6H_2O$	1.0
Bromide	Potassium bromide	25.0	Cr(VI)	$K_2Cr_2O_7$	1.0
Phosphate	Disodium hydrogen orthophosphate	25.0	Sn(II)	$SnCl_2$	1.0
			Tl(I)	$TlNO_3$	1.0
			Co(II)	$CoCl_2\cdot 2H_2O$	1.0
Malonate	Sodium malonate	2.0	Ba(II)	$BaCl_2\cdot 2H_2O$	1.0
Tartarate	Tartaric acid	2.0	Se(IV)	SeO_2	1.0
Fluoride	Sodium fluoride	2.0	Mg(II)	$MgCl_2\cdot 6H_2O$	1.0
Citrate	Citric acid	2.0	Bi(III)	$Bi(NO_3)_3\cdot 5H_2O$	1.0
Oxalate	Oxalic acid	2.0	Te(IV)[b]	Tellurium metal	1.0
Iodide	Potassium iodide	2.0	Cr(III)	$CrCl_3$	1.0
Cd(II)	$Cd(NO_3)_2\cdot 4H_2O$	25.0	W(VI)	$Na_2WO_4\cdot 2H_2O$	1.0
Mn(II)	$MnCl_2\cdot 6H_2O$	25.0	Fe(II)	$FeSO_4\cdot 7H_2O$	1.0
Zn(II)	$ZnSO_4\cdot 7H_2O$	25.0	In(III)	$InCl_3\cdot 4H_2O$	1.0
Hg(II)	$HgCl_2$	10.0	Ga(III)[a]	$GaCl_3$	1.0
Pb(II)	$Pb(NO_3)_2$	10.0	Al(III)[b]	$AlCl_3\cdot 6H_2O$	1.0
Ca(II)	$CaCl_2$	5.0	Fe(III)[c]	$NH_4\ Fe(SO_4)_2\cdot 12H_2O$	1.0
Cu(II)	$CuSO_4\cdot 5H_2O$	5.0	Sb(III)	Sb_2O_3	0.5
			V(V)	V_2O_5	0.0
			Sn(IV)	$SnCl_4$	0.0

[a]Masked by 1 mg fluoride; [b]masked by 1 mg citrate; [c]masked by 1 mg oxalate

APPLICATIONS

Separation and determination of thallium(III) from binary mixture

The suitability of the developed method was examined by applying it to the separation and determination of thallium(III) in a variety of binary mixtures containing commonly associated elements (Table VI).

TABLE VI. Binary separation of thallium(III) from associated elements

Metal ions	Amount taken, mg	Recovery[a] of Tl(III), %	Metal ion remained[a] in the aqueous phase or stripped from the organic phase, %	Separation factor (α)	Estimation procedure for the metal ion in the aqueous phase
Tl(III)	1.0	99.95 Tl(III)	–	∞	–
Zn(II)	1.0	–	100.0 Zn(II)	–	EDTA[35]
Tl(III)	1.0	99.97 Tl(III)	–	3.14×10^5	–
Cd(II)	1.0	–	98.95 Cd(II)	–	EDTA[35]
Tl(III)	1.0	99.61 Tl(III)	–	0.31×10^5	–
Hg(II)	1.0	–	99.2 Hg(II)	–	EDTA[35]
Tl(III)	1.0	98.97 Tl(III)	–	0.10×10^5	–
Pb(II)	1.0	–	99.1 Pb(II)	–	EDTA[35]
Tl(III)	1.0	99.95 Tl(III)	–	3.20×10^5	–
Bi(III)[b]	1.0	–	99.38 Bi(III)	–	EDTA[35]
Tl(III)	1.0	99.0 Tl(III)	–	1.09×10^5	–
Ga(III)[c]	0.5	–	99.91 Ga(III)	–	EDTA[34]
Tl(III)	1.0	98.97 Tl(III)	–	0.10×10^5	–
Al(III)[d]	1.0	–	99.05 Al(III)	–	EDTA[35]
Tl(III)	1.0	99.95 Tl(III)	–	3.36×10^5	–
In(III)[e]	1.0	–	99.41 In(III)	–	EDTA[34]
Tl(III)	1.0	99.47 Tl(III)	–	1.87×10^5	–
Tl(I)[f]	1.0	–	99.9 Tl(I)	–	EDTA[34]
Tl(III)	1.0	99.07 Tl(III)	–	0.10×10^5	–
Se(IV)	1.0	–	99.0 Se(IV)	–	Selenium sol[38]
Tl(III)	1.0	99.43 Tl(III)	–	0.30×10^5	–
Sb(III)	1.0	–	99.43 Sb(III)	–	Potassium iodide[38]
Tl(III)	1.0	99.66 Tl(III)	–	0.85×10^5	–
Te(IV)[d]	0.5	–	99.66 Te(IV)	–	Tellurium sol[38]
Tl(III)	1.0	99.13 Tl(III)	–	0.12×10^5	–
Fe(III)[g]	0.5	–	99.13 Fe(III)	–	Thiocyanate[38]

[a]Average of five determinations; [b]stripped from organic phase with 3×10 ml 0.5 M nitric acid; [c]masked by 1 mg fluoride; [d]masked by 1 mg citrate; [e]Separation at pH 2.0, [f]separation at pH 6.0; [g]masked by 1 mg oxalate

Separation of thallium(III) from Zn(II), Pb(II), Cd(II), Hg(II), Se(IV), Sb(III)

It was found that Zn(II), Pb(II), Cd(II), Hg(II), Se(IV) and Sb(III) remained unextracted under the acidic conditions employed for the extraction of thallium(III) from a 0.0075 M sodium succinate solution by 0.025 M 2-OAP in chloroform. The pregnant organic phase was stripped with acetate buffer (3×15 ml) and thallium(III) was determined by the recommended procedure. The raffinate containing added metal ions was estimated by the standard procedure.[35,38]

Separation of thallium(III) from Ga(III), Al(III), Te(IV) and Fe(III)

The proposed method was extended for the separation of thallium(III) from Ga(III) by masking with 1 mg fluoride, from Al(III) and Te(IV) by masking with 1 mg citrate and from iron(III) by masking with 1 mg oxalate. The masked metal ions remained in the aqueous phase while thallium(III) was selectively extracted from a 0.0075 M sodium succinate solution into the organic phase with 0.025 M 2-OAP in chloroform at pH 3.0. Thallium was stripped from the organic phase with acetate buffer and estimated as per the recommended procedure. The aqueous phases containing the added metal ions was demasked with 2 ml concentrated hydrochloric acid and, after reducing the volume of the aqueous phase, estimated by standard procedures.[34,38]

Separation of thallium(III) from Bi(III)

The separation of thallium(III) from Bi(III) was based on the use of different stripping agents. Bismuth(III) was co-extracted with 0.025 M 2-OAP in chloroform from a 0.0075 M sodium succinate media at pH 3.0. It was found that there was a quantitative recovery of bismuth(III) with 0.5 M nitric acid while thallium(III) remained quantitatively in the organic phase. The thallium(III) was stripped from organic phase by contacting the organic phase with 3×15 ml acetate buffer (pH 4.63). The stripped phases containing thallium(III) and Bi(III) were evaporated to moist dryness and the residues were dissolved in distilled water with heating. Thallium(III) and Bi(III) were estimated by the standard procedure.[34]

Separation of thallium(III) from In(III) and Tl(I)

The separation of thallium(III) from In(III) was based on the use of different pH values. Thallium(III) was extracted quantitatively with 2-OAP (0.025 M) in chloroform at pH 2.0 from 0.0075 M sodium succinate media. It was found that there was zero extraction of In(III) at pH 2.0. Hence, thallium(III) can be extracted quantitatively with In(III) remaining quantitatively in the aqueous phase. Thallium(III) was then estimated after its re-extraction in the aqueous phase, while In(III) was estimated by a complexometric method.[34]

Separation of Tl(I) from Tl(III)

It was found that 10 ml 0.025 M 2-OAP in chloroform transferred about 15 % of Tl(I) into the organic phase from an aqueous 0.0075 M sodium succinate of pH 3.0. However, there was no extraction of Tl(I) at pH 6.0. Hence the extraction of thallium(III) was performed at pH 6.0, at which pH value only thallium(III) is extracted into organic phase, whereas Tl(I) remains in the aqueous phase. The extracted thallium(III) was stripped from the organic phase with acetate buffer and estimated by the recommended method, while Tl(I) from the aqueous phase was estimated by the EDTA method[34] after converting of Tl(I) to Tl(III) with a dilute solution of bromine water.

Analysis of synthetic mixtures

The proposed method was applied to the extraction and determination of thallium(III) from 0.0075 M sodium succinate from various synthetic mixtures. The results are given in Table VII.

TABLE VII. Analysis of synthetic mixtures

Composition of synthetic mixture, mg	Amount of thallium(III) found, mg	Recovery[a], %	R. S. D., %
Tl(III), 1.0	0.995		
Zn(II), 1.0	0.995		
Cd(II), 1.0	0.994	99.4	0.6
	0.997		
	0.992		
Tl(III), 1.0	1.0		
Ga(III)[b], 1.0	0.993		
In(III), 1.0	0.991	99.6	0.4
	1.0		
	1.0		
Tl(III), 1.0	1.0		
Zn(II), 1.0	0.995		
Fe(III)[c], 1.0	0.990	99.2	0.8
	0.980		
	0.997		
Tl(III), 1.0	0.994		
Pb(II), 1.0	0.989		
In(III), 1.0	0.996	99.4	0.6
	0.998		
	0.997		
Tl(III), 1.0	1.0		
Pb(II), 1.0	0.996		
Hg(II), 1.0	0.995	99.8	0.2
Sb(III), 1.0	1.0		
	1.0		

[a]Average of five determinations; [b]masked by 1 mg fluoride; [c]masked by 1 mg oxalate

Analysis of alloys

Since standard alloy samples containing thallium(III) were not available at this working place, a non-ferrous alloy (brass) and a type metal alloy (the Bureau of Analyzed Samples Ltd., UK) to which a known amount of thallium(III) was added. Thallium(III) was recorded from the succinate media by the proposed method (Table VIII). The procedure is given below.

A known weight (0.100 g) of alloy was dissolved in a mixture of 10 ml concentrated nitric acid and 50 ml of distilled water. After the initial reaction was over, the solution was heated with 5 ml portion of 1:1 nitric acid, boiled to dissolve the soluble matter and filtered to remove the silica or metastannic acid. The filtrate was diluted to 100 ml with distilled water. An aliquot of 1.0 ml of filtrate was taken; to this solution 1.0 ml of 1.0 mg ml^{-1} thallium(III) was added and the general procedure for the extraction and determination of thallium(III) was followed.

TABLE VIII. Analysis of alloys

Alloy sample	Composition, %	Thallium(III) taken, mg	Recovery[a], %	R.S.D., %
Non ferrous alloy (Brass)	Pb 2.0 Cu 65.0 Zn 30.0 Sn 1.0	1.0	99.5	0.5
Type metal alloy	Pb 80.0 Sn 17.0 Sb 3.0	1.0	99.2	0.8

[a]Average of five determinations

CONCLUSIONS

The method described herein brings forth the potential of 2-OAP for the separation and recovery of thallium(III). The quantitative extraction of the metal ion can be achieved at pH 3.0 from 0.0075 M sodium succinate using 0.025 M 2-OAP. The extraction proceeds *via* ion pair formation. The partition of thallium(III) in the organic phase is selective in the presence of a number of commonly associated elements. The selectivity of the method can be increased by the use of suitable masking agents and different pH values. The extractant possess a reasonable loading capacity. A very low reagent concentration (0.025 M) is required for the quantitative recovery of thallium(III). The time required for the extraction separation is very short (30 s). It is very simple, selective, reproducible and rapid and can be applied for the analysis of thallium(III) from synthetic mixtures and alloy samples.

Acknowledgements. The financial support to the work by the University Grants Commission (UGC), New Delhi, is gratefully acknowledged. One of the author (SVM) is thankful to the UGC for the award of a fellowship.

ИЗВОД

БРЗА ЕКСТРАКЦИЈА ТЕЧНО–ТЕЧНО ТАЛИЈУМА(III) ИЗ СУКЦИНАТНИХ РАСТВОРА ПОМОЋУ ЕКСТРАКТАНТА 2-ОКТИЛАМИНОПИРИДИНА У ХЛРОФОРМУ

SANDIP V. MAHAMUNI, PRAKASH P. WADGAONKAR[1] и MANSING A. ANUSE

Analytical Chemistry Laboratory, Department of Chemistry, Shivaji University, Kolhapur – 416 004 и
[1]Polymer Science and Engineering Division, National Chemical Laboratory,
Dr. Homi Bhabha Road, Pune – 411 008, India

Изведено је једноставно испитивање екстракције из раствора талијума(III). Селективна и квантитативна екстракција талијума(III) изведена је помоћу 2-октиламинопиридина (2-OAP) у хлороформу из воденог раствора натријум-сукцината (0,0075 M) при pH 3,0. Талијум(III) је повратно екстрахован помоћу ацетатног пуфера (pH 4,63). Испитивани су ефекат концентрације сукцината и 2-OAP, улога разних разблаживача, стрипинг агенаса, ефикасност 2-OAP, равнотежно време и однос запремина водене и органске фазе на екстракцију талијума(III). Стехиометрија екстрахованих врста, одређена на основу методе анализе нагиба, износила је

1:2:1 (метал:киселина:екстрактант). Такође је испитивана и температурна зависност константе равноже екстракције да би се процениле термодинамичке функције ΔH, ΔG и ΔS за процес екстракције. Тачност методе не зависи од присуства разних катјона и анјона. Метода је коришћена за селектривну екстракцију талијума(III) из бинарних смеша са Zn(II), Cd(II), Hg(II), Bi(III), Pb(II), Se(IV), Te(IV), Sb(III), Ga(III), In(III), Al(III), Tl(I) и Fe(III). Предложена метода је примењена на синтетичке смеше и легуре. Метода је једноставна, селективна, брза и чиста.

(Примљено 28. маја 2007)

REFERENCES

1. E. Marian, *Metals and Their Compounds in the Environment*, VCH, Wenham, 1991
2. M. J. Sienko, R. A. Plane, *Chemical Principles*, McGraw – Hill, London, 1974
3. P. N. Gabby, *U. S. Geological Survey*, Mineral Commodity summaries, Reston, VA, 2006, p. 172
4. J. E. Fergusson, *The Heavy Elements: Chemistry, Environmental Impact and Health Effects*, Pergamon Press, Oxford, 1990
5. I. C. Smith, B. L. Carson, *Trace Metals in the Environment, Thallium*, Ann Arbor Science Publishers, Michigan, 1977
6. X. Zhang, G. Yin, Z. Hu, *Talanta* **59** (2003) 905
7. B. Y. Mishra, M. D. Rokade, P. M. Dhadke, *Chem. Environ. Res.* **10** (2001) 27
8. S. D. Pawar, P. M. Dhadke, *J. Serb. Chem. Soc.* **68** (2003) 581
9. J. N. Iyer, P. M. Dhadke, *Sep. Sci. Tech.* **36** (2001) 2773
10. T. Sato, K. Sato, Y. Noguchi, I. Ishikawa, *Shigen to Sozai* **113** (1997) 185
11. X.–Z. Liu, D.–W. Fang, J. Li, J.–Z. Yang, S.–L. Zang, *J. Phase Equilib. Diffusion* **26** (2005) 342
12. X.–Z. Liu, D.–W. Fang, Y.–H. Kang, J. Li, S.–L. Zang, *Chin. J. Chem*. **23** (2005) 567
13. S. M. Khopkar, C. Malkhede, *Indian J. Chem.* **42A** (2003) 2945
14. A. R. Ghiasvand, F. Moradi, S. Shadabi, H. Sharghi, A. R. Hasaninejad, *Asian J. Chem.* **18** (2006) 2016
15. P. N. Bongroo, R. C. Saxena, H. C. Arora, *Indian J. Chem.* **38A** (1999) 89
16. Y. S. Kim, Y. S. Choi, W. Loo, *Bull. Korean Chem. Soc.* **23** (2002) 1381
17. S. V. Vartak, V. M. Shinde, *Talanta* **45** (1998) 925
18. K. Watanabe, H. Isomura, M. Itagaki, *Bunseki Kagaku* **49** (2000) 691
19. J. Narbutt, J. Krejzler, *Radiochim. Acta* **9–10** (2005) 627
20. D. Zendelovska, T. Stifilov, *Anal. Sci.* **17** (2001) 425
21. J. Gao, Q. Deng, B. Peng, X. Guo, *Rare Metals* **22** (2003) 86
22. T. M. Trtić-Petrović, G. T. Vladisavljević, S. C. Archimandritis, A. Varvarigou, J. J. Comor, *J. Sep. Sci.* **24** (2001) 519
23. T. M. Trtić, G. T. Vladisavljević, J. J. Comor, *Sep. Sci. Technol.* **36** (2001) 295
24. T. M. Trtić, G. T. Vladisavljević, J. J. Comor, *Sep. Sci. Technol.* **35** (2000) 1587
25. T. M. Trtić, G. T. Vladisavljević, M. Tesić, K. Kumrić, J. J. Comor, *Desalination* **148** (2002) 241
26. Y. Nagaosa, K. Horita, *Microchim. Acta* **108** (1992) 151
27. N. H. Chung, J. Nishimoto, O. Kato, M. Tabata, *Anal. Chim. Acta* **477** (2003) 234
28. K. Yamamoto, M. Endo, *Anal. Sci.* **12** (1996) 739
29. I. Nukatsuka, H. Seitoh, K. Ohzeki, *Microchim. Acta* **148** (2004) 177
30. M. A. Taher, *Bull. Kor. Chem. Soc.* **24** (2003) 1177

31. P. K. Saha, U. S. Roy, *J. Indian Chem. Soc.* **75** (1998) 330
32. N. Rajesh, M. S. Subramanian, *J. Hazardous Mater.* **135** (2006) 74
33. T. N. Shilimkar, M. A. Anuse, *Ann. de Chim.* **92** (2004) 717
34. F. J. Welcher, *The Analytical Uses of Ethylenediamine Tetraacetic Acid*, D. Van Nostrand Company Inc., New York, London, 1958, p.p. 176, 178, 182
35. A. I. Vogel, *A Textbook of Quantitative Inorganic Analysis*, ELBS, London, 1961, p.p. 442, 444
36. N. A. Borshch, O. M. Petrukhin, *Zh. Anal. Khim.* **33** (1978) 1805
37. Y. Marcus, A. S. Kertes, *Ion Exchange and Solvent Extraction of Metal Complexes*, Wiley-Interscience, New York, 1969
38. Z. Marckzenko, *Spectrophotometric Determination of Elements*, Ellis Horwood Ltd., Chichester, 1976, p.p. 125, 307, 475, 522, 549.

www.shd.org.yu

Journal of the Serbian Chemical Society
Version Electronic

JSCS@tmf.bg.ac.yu • www.shd.org.yu/JSCS

J. Serb. Chem. Soc. 73 (4) 453–461 (2008)
JSCS–3727

UDC 550.4:543+546.47+546.815+
546.65:597+631.442.4'2
Original scientific paper

Cretaceous – Paleogene boundary Fish Clay at Højerup (Stevns Klint, Denmark): Zn, Pb and REE in kerogen

PAVLE I. PREMOVIĆ[1]*, MAJA N. STANKOVIĆ[1], MIRJANA S. PAVLOVIĆ[2#]
and MILOŠ G. DJORDJEVIĆ[1]

[1]*Laboratory for Geochemistry, Cosmochemistry and Astrochemistry, University of Niš,*
P. O. Box 224, 18000 Niš and [2]*Institute of Nuclear Sciences Vinča,*
P. O. Box 522, 11001 Belgrade, Serbia

(Received 28 May, revised 29 June 2007)

Abstract: Geochemical analyses of Zn, Pb and rare earth elements (La, Ce, Nd, Sm, Eu, Tb, Yb and Lu) in the kerogen of the black marl at the Cretaceous – – Paleogene boundary Fish Clay at Højerup were performed. Substantial proportions of the Zn, Pb and rare earths were probably contained in terrestrial humic substances (the kerogen precursor) arriving at the marine sedimentary site. This is in accord with a previous hypothesis that kerogen is mainly derived from humic acids of an oxic soil in of the adjacent coastal areas of eastern Denmark. It is also suggested that humics enriched in Zn, Pb and rare earth elements were transported mainly through fluvial transport into the deposition site of the Fish Clay. Local weathering/leaching of the impact–eject fallout on the land surface and local terrestrial rocks by impact-induced? acid surface waters perhaps played an important role in providing Zn, Pb and rare earths to these humic substances. Apparently, chondritic and non-chondritic Zn originated from the impact fallout; Pb and rare earth elements were most likely sourced by exposed rocks in the coastal areas of eastern Denmark.

Keywords: geochemistry; Cretaceous – Paleogene boundary; zink; lead; rare earth elements; kerogen.

INTRODUCTION

Fish Clay is a thin grey-to-black marl marking the Cretaceous – Paleogene boundary (KPB) at Stevns Klint in eastern Denmark, Fig. 1A. A detailed lithology of the Fish Clay at Højerup was described by Premović *et al.*[1] The authors differentiated three distinct layers across the boundary section: the bottom layer III (black marl), the middle layer IV (grey to black marl) and the top layer V (light-grey marl). Layer III is underlain by late Maastrichtian chalk. Layer V is

---

[*] Corresponding author. E-mail: asteroid.pavle@yahoo.com

[#] Serbian Chemical Society member.

doi: 10.2298/JSC0804453P

overlain by Danian Cerithium Limestone (VI). Elliott [2] subdivided layer III into a red layer IIIA (0.2–0.5 cm) overlain by a black marl layer IIIB (2–5 cm), Fig. 1B. Layer IIIB shows high contents of Ir[3,4] and the kerogen is enriched in Cu^{2+}-porphyrins.[5] Layer IIIB also contains minute macroscopic pyrite (FeS$_2$), probably of postdiagenetic origin.[6] Layers IIIB/IV are considered here to constitute the main part of the KPB section.

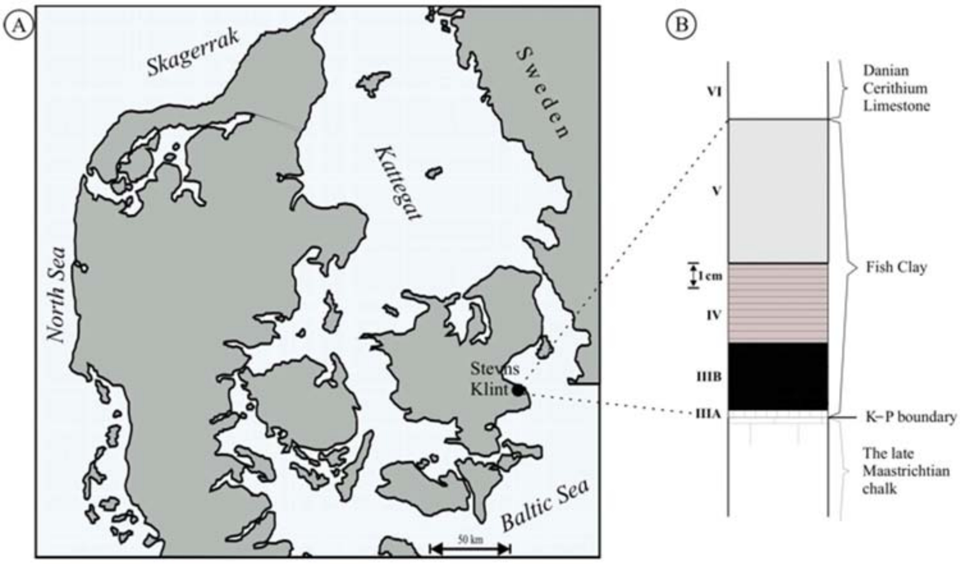

Fig. 1. A) Geographic location map of the sample from the Danish K–P boundary section. B) Lithological profile of the internal layering of the Fish Clay.

Alvarez *et al.*[7] reported an anomalously high Ir concentration in layer IIIB. To explain this enhanced Ir concentration, they proposed a late Cretaceous asteroid impact on the Earth.[8] In addition to Ir, layer IIIB is also enriched in other trace metals, such as: meteoritic or partly meteoritic Ni, Co, Au and some non-meteoritic terrestrial metals.[9]

The late Cretaceous impact is thought by most researchers to have occurred at the Chicxulub location (Yucatan Peninsula, Mexico). Shukolyukov and Lugmair[10] analyzed Cr in layers IIIA and IIIB employing high precision mass spectrometry and found that their Cr isotopic compositions strongly suggest that the impactor comprised C1 carbonaceous chondrite-type material. Very recently, Trinquier *et al.*[11] showed that the Cr isotopic signature of layer IIIB exhibits an isotopic ratio which would represent a mixture of a carbonaceous chondrite of CM2 type with terrestrial material in the ratio 3.8–6.8 % and that a single impactor may account for this signature.

Geochemical analyses of layer IIIB revealed that it contains up to *ca*. 3 % kerogen.[5,12,13] The kerogen content of the Fish Clay increased abruptly with an accumulation of the basal part of layer IIIB and declined gradually towards the top of layer IIIB and across IV.[3] Layer IV also contains kerogen but much less abundant than in layer IIIB. The underlying late Maastrichtian chalk and layer IIIA, and the overlying layer V contain no kerogen. Layer IIIB and, probably, layer IV were deposited under continuous anoxic bottom-water conditions[5,13] which prevailed 65 Ma after its formation.[6]

In many previous studies of Fish Clay, most attention was focused on the trace metals present in smectite, but much less attention was paid to trace metals associated with the IIIB kerogen. Very recently, Premović *et al.*[14] reported a geochemical study of Ni in the kerogen of layer IIIB. In the present study, Zn and Pb in the IIIB kerogen were determined. These elements were chosen primarily because of their relatively simple chemistry in natural waters and sediments. Zn and Pb show a similar geochemical behavior in natural oxic or anoxic waters. La, Ce, Nd, Sm, Eu, Tb, Yb and Lu, which belong to the rare earth elements (REE), were also analyzed. REE comprise a highly coherent geochemical group and are characterized by a large and unique similarity in their geochemical properties. The present study is complementary to earlier studies[1,5,13] and may be important for the understanding of the geochemical and paleoecological events that occurred during the deposition of the KPB section.

EXPERIMENTAL

The experimental techniques and methods were described in a previous paper.[14]

RESULTS

Zn, Pb and REE of the IIIB kerogen

Geochemical analysis showed that layer IIIB contains 1.8 % of kerogen, made up mainly (> 95 %) of organic matter, Table I. The IIIB kerogen contains high organic S (*ca.* 1.6 %) and low S (< 0.2 %), ascribed to finely disseminated FeS_2 embedded into the kerogen skeleton; this material contains no or very little non-pyritic sulfate S.[14] The contents of Zn, Pb and REE (La, Ce, Nd, Sm, Eu, Tb, Yb and Lu) in the IIIB kerogen were determined and the analytical results are given in Table I. The blank levels were more than an order of magnitude lower than the given numbers. The concentrations of Zn, Pb and REE are likely to represent the lower limits of their actual levels due to loss of a fraction of these elements which are labile and loosely bound to the IIIB kerogen during the acid demineralization. The distribution pattern of Zn, Pb and REE associated with the IIIB kerogen is also presented in Table I. Of note, the acid demineralization steps remove almost completely Zn.

DISCUSSION AND INTERPRETATION

Zn and Pb: Anoxic vs. *oxic environment*

As sedimentary FeS_2 is generally an unimportant sink for Zn and Pb and because ZnS and PbS are completely soluble in cold HCl, it is very likely that these two metals are bound to the IIIB kerogen. Humics (mainly humic acids) in coastal soil can be regarded as the progenitor of the IIIB kerogen.[1,5,14] It is possible that incorporation of Zn and Pb into the humics occurred under the anoxic sedimentary environment of layer IIIB (*in-situ* model). However, under these conditions, most of the Zn and Pb would precipitate as insoluble solid sulfides.[15] In this way, an anoxic environment would act as a sink for these metals. Strong anoxic conditions of layer IIIB would be adverse for the incorporation of Zn and Pb into the humics. It can thus be concluded that the enriched association of Zn and Pb in the IIIB kerogen does not reflect anoxic but oxic conditions. Indeed, the excess of these two metals in the IIIB kerogen is a strong indication of their rather high concentrations as free ions and/or soluble complexes. Indeed, high soluble Zn is only present under well-oxygenated conditions of sedimentation.[16] Consequently, the Zn and Pb of the IIIB kerogen were probably incorporated into humic structures during the early diagenesis of the humics in the oxic milieu of coastal soil. The fact that the humics were enriched in Zn implies that the solution of the coastal soil was of relatively low pH because this metal is not very soluble at pH > 5.[17] Moreover, if the incorporation of Zn and Pb into the humics occurred under acidic and oxidizing conditions of coastal soil then predominantly free Zn^{2+} and Pb^{2+} ions would be almost solely present in the soil solution.[18]

TABLE I. INAA/ICP-OES Data for the abundances of Zn, Pb and REE in the IIIB kerogen and in C1 chondrite

Metal		Whole-rock	Kerogen[a]	Content, %[b]	C1 Chondrite
Zn	ppm	340	25.0	< 0.5	312
Pb	ppm	na[c]	12.5	–	2.47
La	ppb	na	34.8	–	234.7
Ce	ppb	na	61.0	–	603.2
Nd	ppb	na	< 5.0	–	452.4
Sm	ppb	na	4.5	–	147.1
Eu	ppb	na	1.6	–	56.0
Tb	ppb	na	1.0	–	36.3
Yb	ppb	na	8.6	–	162.5
Lu	ppb	na	1.3	–	24.3

[a] Percentage of kerogen of the whole-rock sample is 1.8 %. the IIIB kerogen is composed of > 95 % organic matter with *ca.* 4.7 % of S (determined by INAA); [b] percentage of total metal remaining in the IIIB kerogen; [c] not analyzed

Zn and Pb in the IIIB kerogen: chondritic vs. *terrestrial origin*

An enigmatic finding in the IIIB kerogen is a marked Zn enrichment (340 ppm), which is comparable with the average Zn (312 ppm) in C1 chondrites. This suggests that the Zn in the IIIB kerogen could be augmented by chondritic volatiles of the impactor. Strong *et al.*[19] suggested that the Zn in the KPB deposit at the Flaxbourne River was derived from crustal rocks. Here, it is suggested that the high Zn in the IIIB kerogen was probably primarily sourced by chondritic and non-chondritic materials of the impact fallout.

The concentration of Pb in the IIIB kerogen is almost 6 times higher than its mean abundance in C1 chondrites, Table I. If the Pb originated from the chondritic component of the impact fallout, it would necessitate rather drastic concentrations of the metal during the weathering/leaching of the impact fallout and it seems likely that the Pb arose from a terrestrial source. Indeed, geochemical studies of this metal in layer IIIB strongly indicate that it is probably of terrestrial origin.[20,21] Here, it is suggested that the Pb originated from the rock(s) exposed in the coastal areas; its predominant species in coastal soil could, therefore, be complexes of Pb^{2+} ions with humics.

REE of the IIIB kerogen

REE have been used as proxy indicators for reconstructing the Eh and pH conditions of ancient sedimentary environments.[22] Except for Ce, REE in natural waters commonly occur in the 3+ oxidation state and exhibit very similar geochemical properties.[18] Layers IIIB and IV contain relatively high concentrations of REE and the bulk (> 90 %) of the total rare earths resides in the apatite phase.[12] These authors concluded that most of these elements precipitated from seawater at Stevns Klint.

The REE of the IIIB kerogen are largely incorporated into its structure because they do not form sulfides. The REE signature of the IIIB kerogen is approximately comparable to the REE signature of North American Shale Composite (NASC[23]) but highly enriched in REE relative to C1 chondrites, (Table I; Fig. 2). It seems improbable, therefore, that a C1 chondritic source could have made an important contribution to the REE in the IIIB kerogen.

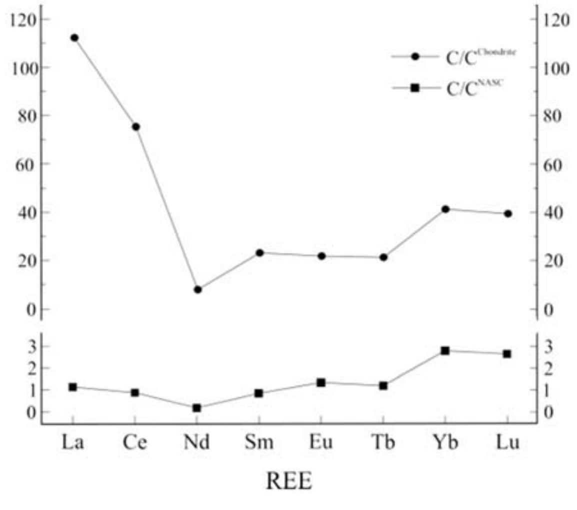

Fig. 2. Distribution of REE in IIIB kerogen normalized relative to REE in the NASC (■)[23] and chondrite (●).[36]

A prominent feature of various ancient and modern marine sedimentary environments and the associated waters is the strongly negative Ce and Eu anomalies and, less commonly, zero and positive anomalies.[24–29] In addition, the REE pattern of the authigenic component of marine sediment is, in general, the mirror image of the most common non-flat pattern for seawater. In contrast, marine waters show both a flat shale type pattern[27] and an absence of a Ce anomaly.[30]

The IIIB kerogen displays a flat pattern with no Ce and Eu anomalies (Table I; Fig. 2), indicating that its REE, probably, did not originate from seawater. It is rather likely, therefore, that this kerogen (*i.e.*, humics in the coastal soil) must have inherited the rare earths from the surface waters. The REE patterns of the surface waters with the exception of the negative Ce anomaly usually reflect the REE compositions of the lithologies along their flow paths.[31] Thus, it is suggested that ultimately the REE of the IIIB kerogen were perhaps sourced by rocks exposed on the adjacent land.

The mobility of REE in natural (oxic and anoxic) waters is mainly controlled by their ability to form complexes with organic and inorganic ligands. Several studies have indicated extensive association of REE with terrigenous humics[32–35] and that these types of complexes dominate in acid surface waters enriched in humics.[29] It is, thus, rather likely that the REE were initially complexed with humics in the coastal soil.

We offer a model as a first approximation to the geochemical processes involved, Fig. 3. It is thus suggested that chondritic and non-chondritic Zn was leached from impact-ejecta fallout on land probably by impact-induced? acid surface waters. Pb and REE were most likely removed by the same waters from the rocks in the coastal areas of eastern Denmark. Zn, Pb and REE were then chelated by the humics of coastal soil and this uptake occurred rapidly during early diagenesis. Local conditions, such as topography (*e.g.* highlands *vs.* lowlands) were perhaps favorable for an efficient and concentrated accumulation of these metals and REE in the humics-rich coastal soil. These humics were then fluvially transferred to the sea and further to the area where the Fish Clay was deposited, Fig. 3.

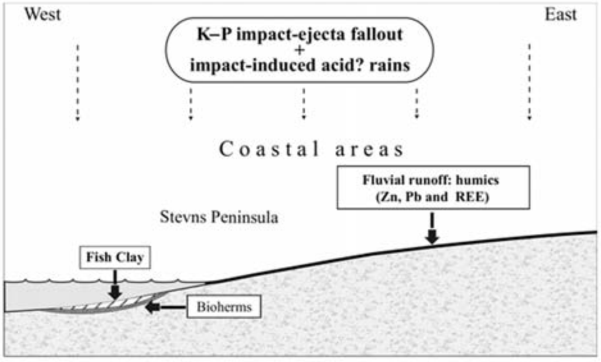

Fig. 3. Proposed model for the geochemical relations between the impact-ejecta fallout, humics in the coastal soil and Fish Clay at Stevns Klint.

CONCLUSIONS

In summary, the IIIB kerogen enriched in Zn and Pb were probably derived from the humics (mostly humic acids) enriched in these metals. These humics in the coastal soil were fluvially transported to the site of deposition of the Fish Clay, Fig. 3. This must also be true for the IV kerogen. This interpretation is in accordance with a previous *ex-situ* scenario for the IIIB kerogen enriched in Cu and Cu^{2+}-porphyrins.[5]

From the geochemistry of Zn, Pb and REE associated with the IIIB kerogen, it may be deduced that most of these metals and REE were originally bound with these humics in an acidic ($pH < 5$) and oxic soil of the adjacent coastal areas in eastern Denmark. Apparently, chondritic and non-chondritic Zn was most likely augmented by the impact-ejecta fallout through the leaching by the impact-induced? acid surface waters. Pb and REE were also leached by the same waters from the rocks on the adjacent land. Humics having functional carboxyl and phenolic groups were able to chelate Zn, Pb and REE before they were deposited in the Fish Clay; this chelation can account for their high content in the IIIB kerogen. The most plausible scenario is that humics and associated Zn, Pb and REE were fluvially transferred onto the Fish Clay site at the KPB.

Acknowledgements. Dr. Helle Schummel (the Højerup sample), to whom our thanks go, collected the Fish Clay samples at Stevns Klint used in this work. The Institut de Minéralogie et de Physique des Milieux Condensés (IMPMC) without whose help, patience and understanding this paper would not have appeared. We are also indebted to IMPMC for the use of their laboratory and instrumental facilities. Funding support from le Ministere Francais de l`Education National, de l`Enseignement Superieur et de la Recherche to P. I. P. for his stay at IMPMC, Université Pierre et Marie Curie (Paris) is gratefully acknowledged. The Ministry of Science of Serbia financially supported in part this work (project 142069).

ИЗВОД

КРЕДА – ПАЛЕОГЕН ГРАНИЧНИ СЛОЈ FISH CLAY СА HØJERUP-А (STEVNS KLINT, ДАНСКА): Zn, Pb И REE У КЕРОГЕНУ

ПАВЛЕ И. ПРЕМОВИЋ[1], МАЈА Н. СТАНКОВИЋ[1], МИРЈАНА С. ПАВЛОВИЋ[2] и МИЛОШ Г. ЂОРЂЕВИЋ[1]

[1]*Лабораторија за геохемију, космохемију и астрохемију, Природно–математички факултет, Универзитет у Нишу, п. пр. 224, 18000 Ниш и* [2]*Институт за нуклеарне науке "Винча", п. пр. 522, 11000 Београд*

Урађене су геохемијске анализе Zn, Pb и елемената ретких земаља (La, Ce, Nd, Sm, Eu, Tb, Yb и Lu) у керогену црног лапорца из креда – палеоген граничног слоја Fish Clay са Højerup локације. Знатан део Zn, Pb и елемената ретких земаља, вероватно, је био садржан у копненим хумичним супстанцама (претечи керогена) при дотоку на место морске седиментације. Ово је у складу са претходним претпоставкама да кероген, углавном, потиче од хумичних киселина из земљишта околне приобалне области источне Данске. Такође, претпоставља се да су хумичне супстанце обогаћене Zn, Pb и елементима ретких земаља пренете површинским водама, углавном, до места седиментације Fish Clay-а. Спирање киселим површинским водама астероидне падавине на околном земљишту и стенама, вероватно, је играло значајну улогу у обогаћивању наведених хумичних супстанца цинком, оловом и елементима

ретких земаља. Изгледа да хондритски и не-хондритски Zn потиче од астероидне падавине; Pb и ретке земље, највероватније, потичу од околних стена у приобалној области источне Данске.

(Примљено 28. маја, ревидирано 29. јуна 2007)

REFERENCES

1. P. I. Premović, B. Ž. Todorović, M. N. Stanković, *Geol. Acta,* in press
2. W. C. Elliott, *Clays Clay Miner.* **41** (1993) 442
3. B. Schmitz, *Geology* **16** (1988) 1068
4. G. Graup, H. Palme, B. Spettle, *Lunar Planet. Sci.* **23** (1992) 445
5. P. I. Premović, N. D. Nikolić, I. R. Tonsa, M. S. Pavlović, M. P. Premović, D. T. Dulanović, *Earth. Planet. Sci. Lett.* **177** (2000) 105
6. B. Schmitz, *Geochim. Cosmochim. Acta* **49** (1985) 2361
7. L. W. Alvarez, W. Alvarez, F. Asaro, H. V. Michel, *Science* **208** (1980) 1095
8. M. Kastner, F. Asaro, H. V. Michel, W. Alvarez, L. W. Alvarez, *Science* **226** (1984) 137
9. L. Christensen, S. Fregerslev, A. Simonsen, J. Thiede, *Bull. Geol. Soc. Denmark* **22** (1973) 193
10. A. Shukolyukov, G. W. Lugmair, *Science* **282** (1998) 927
11. A. Trinquier, J.-L. Birck, C. J. Alle'gre, *Earth Planet. Sci. Lett.* **241** (2006) 780
12. B. Schmitz, P. Andersson, J. Dahl, *Geochim. Cosmochim. Acta* **52** (1988) 229
13. P. I. Premović, N. Z. Pavlović, M. S. Pavlović, N. D. Nikolić, *Geochim. Cosmochim. Acta* **57** (1993) 1433
14. P. I. Premović, M. M. Krsmanović, B. Z. Todorović, M. S. Pavlović, N. D. Nikolić, D. M. Djordjević, *J. Serb. Chem. Soc.* **71** (2006) 793
15. M. A. Huerta-Diaz, J. W. Morse, *Mar. Chem.* **29** (1990) 119
16. R. P. Gambrell, J. B. Wiesepape, Jr. W. H. Patrick, M. C. Duff, *Water Air Soil Poll.* **57–58** (1991) 359
17. D. J. Swaine, in *Nickel in the environment*, J. O. Nriagu, Ed., Wiley, New York, 1980, p. 67
18. D. G. Brookins, *Eh-pH Diagrams for Geochemistry*. Springer-Verlag, Berlin, 1988, p. 176
19. C. P. Strong, R. R. Brooks, S. M. Wilson, R. D. Reeves, C. J. Orth, X.-Y. Mao, L. R. Quintana, E. Anders, *Geochim. Cosmochim. Acta* **51** (1987) 2769
20. A. Dia, G. Manhès, B. Dupré, C. J. Allégre, *Chem. Geol.* **75** (1989) 291
21. R. Frei, K. M. Frei, *Earth Planet. Sc. Lett.* **203** (2002) 691
22. Y. G. Lui, M. R. U. Miah, R. A. Schmitt, *Geochim. Cosmochim. Acta* **52** (1988) 1361
23. L. P. Gromet, R. F. Dymek, L. A. Haskin, R. L. Korotev, *Geochim. Cosmochim. Acta* **48** (1984) 2469
24. H. Elderfield, C. J. Hawkesworth, M. J. Greaves, S. E. Calvert, *Geochim. Cosmochim. Acta* **45** (1981) 513
25. H. Elderfield, M. J. Greaves, *Nature* **296** (1982) 214
26. H. J. W. de Baar, M. P. Bacon, P. G. Brewer, *Nature* **301** (1983) 324
27. H. J. W. de Baar, M. P. Bacon, P. G. Brewer, *Geochim. Cosmochim. Acta* **49** (1985) 1943
28. E. R. Sholkovitz, W. M. Landing, B. L. Lewis, *Geochim. Cosmochim. Acta* **58** (1994) 1556
29. A. V. Dubinin, *Lithol. Miner. Resour.* **39** (2004) 289
30. D. Turner, M. Whitfield, A. G. Dickson, *Geochim. Cosmochim. Acta* **51** (1981) 597
31. P. L. Verplanck, D. K. Nordstrom, H. E. Taylor, *U.S. Geol. Surv. Water-Resour. Invest. Rep.* **4018A** (1999) 83
32. J. Hoyle, H. Elderfield, A. Gledhill, M. Greaves, *Geochim. Cosmochim. Acta* **48** (1984) 143

33. S. J. Goldstein, S. B. Jacobsen, *Earth Planet. Sci. Lett.* **89** (1988) 35
34. E. R. Sholkovitz, T. J. Shaw, D. L. Schneider, *Geochim. Cosmochim. Acta* **56** (1992) 3389
35. J. Tang, K. H. Johannesson, *Geochim. Cosmochim. Acta* **67** (2003) 2321
36. E. Anders, N. Grevesse, *Geochim. Cosmochim. Acta* **53** (1989) 197.

Journal of the Serbian Chemical Society
JSCS@tmf.bg.ac.yu • www.shd.org.yu/JSCS
J. Serb. Chem. Soc. *73* (4) 463–478 (2008)
JSCS–3728
UDC 546.717–36+542.92:662.67:678.094.3
Original scientific paper

Characterization of type III kerogen from Tyrolean shale (Hahntennjoch, Austria) based on its oxidation products

S. BAJC[1*#], O. CVETKOVIĆ[1#], A. AMBLÈS[2] and D. VITOROVIĆ[1#]

[1]Center of Chemistry, Institute of Chemistry, Technology and Metallurgy, Njegoševa 12, 11000 Belgrade, Serbia and [2]Department of Chemistry, Faculty of Science, University of Poitiers, 40, Av. du Recteur Pineau, 86022 Poitiers, France

(Received 15 October, revised 19 November 2007)

Abstract: A 29-step alkaline permanganate degradation of type III kerogen from Tyrolean (Hahntennjoch, Austria) oil shale was performed. A high yield of oxidation products was obtained (93.7 % relative to the original kerogen): 0.5 % neutrals and bases, 19.5 % ether-soluble acids and 58.9 % of precipitated (PA). A substantial amount of kerogen carbon (14.8 %) was oxidized into carbon dioxide. The organic residue remaining after the final oxidation step was 6.9 %. The PA components were further oxidized and the total yields relative to original PA were 1.0 % neutrals and bases and 59.0 % ether-soluble acids, the non-degraded residue being 29.3 %. Detailed quantitative and qualitative analysis of all oxidation products suggested the Tyrolean shale kerogen to be a heterogeneous macromolecular substance consisting of three types of structures differing in composition and susceptibility towards alkaline permanganate: the first, resistant, presumably composed of aromatic structures linked by resorcinol ethereal bonds; the second, combined in nature, the aliphatic part comprising methyl-substituents and short cross-links, both easily oxidized into CO_2, water and low molecular weight acids and aromatic structures yielding aromatic di- and tri-carboxylic acids as oxidation products; finally the third, composed of aliphatic cross-links and substituents, alicyclic (and/or heterocyclic) and some aromatic structures, bound into units moderately resistant towards oxidation. The overall yields of kerogen and PA oxidation products lead towards a balance between aromatic, alkane mono- and dicarboxylic and alkanepolycarboxylic acids, suggesting a shift of the structure of Tyrolean shale kerogen from typical aromatic reference type III towards a heterogeneous aromatic-aliphatic-alicyclic type structure.

Keywords: Tyrolean shale; type III kerogen; structural characterization; alkaline permanganate degradation; oxidation products.

---

[*] Corresponding author. E-mail: sbajc@chem.bg.ac.yu

[#] Serbian Chemical society member.

doi: 10.2298/JSC0804463B

INTRODUCTION

Structural elucidation of kerogen, the most abundant form of organic matter in the crust of the Earth, is of continuing organic geochemical interest.[1] A graph of atomic H/C *vs.* O/C ratios, named van Krevelen diagram, for long served for the classification of kerogens into three principal reference types (I, II and III) based on their similar structural evolution paths.[2] Yet, it was shown that controlled oxidative degradation offered a more precise structural differentiation and structural interpretation of the kerogens. Namely, very high yields of identifiable kerogen oxidation products with retained precursor structural characteristics, obtained by an optimized multi-step oxidative degradation method, clearly demonstrated remarkable differences between kerogens which, according to their atomic H/C and O/C ratios, appeared to be similar.[3–7] Thus, the position in the van Krevelen diagram, determined by the overall nature of the elemental analysis, was shown to be insufficient to fully characterize a kerogen.

Consequently, the proportions of various kinds of acidic oxidation products observed in several oxidation studies were used as a basis for an advantageous characterization and classification of kerogens, materialized in the form of an aliphatic/aromatic/alkane-polycarboxylic + cycloalkanoic acids triangular diagram, these types of acids being the main oxidation products of kerogen aliphatic, aromatic and alicyclic/heterocyclic structures, respectively.

Parallel studies of twelve samples of type I (4), type II (4), intermediate type I-II (3), and type III (1) kerogens from shales of various geographic origin, using a similar or identical standard optimized alkaline permanganate method, have so far been carried out. These oxidative degradation studies neglected type III kerogens. Namely, as shown, only one sample of type III kerogen, *i.e.*, kerogen originating from the Mannville shale, Canada,[8] was examined until now, and that was even before the method was completely optimized. In order to supplement data on structural characteristics of type III kerogens and thus provide a basis for comparison of their structures, a type III kerogen from a Tyrolean (Austria) "Hauptdolomit" Triassic sediment was studied using the optimized alkaline permanganate degradation method and the results reported in this paper.

EXPERIMENTAL

Sample preparation

The investigated oil shale sample (No. H124C) originated from a Tyrolean (Austria) "Hauptdolomit" Triassic sediment. It was taken at 48.4 m from an outcrop located by the road to Hahntennjoch, *ca*. 3 km west of Imst. The vitrinite reflectance of this sample was found to be 1.38 % Ro.

The powdered sample contained 0.2 % moisture, 1.0 % bitumen, and 3.7 % kerogen. The kerogen concentrate was prepared by the method described by Vitorović *et al*.[9] Most of the sample (85.8 %) was soluble in dilute (1:4) hydrochloric acid. The resulting HCl concentrate was treated with a mixture of hydrochloric and hydrofluoric acids. The yield of HCl/HF concentrate was 4.3 % relative to original, dry sample. Its bitumen was eliminated by extraction with a mixture of benzene and methanol. The final HCl/HF kerogen concentrate contained 84.6 % kerogen, composed of 80.78 % C, 5.11 % H, 0.80 % N and 13.31 % O + S_{org} (by difference). The atomic H/C and O/C ratios, calculated on the basis of the elemental analysis, were 0.76 and 0.125, respectively, corresponding to the reference type III kerogen.[10]

Oxidative degradation

The HCl/HF kerogen concentrate (2.95 g, containing 2.5 g kerogen) was oxidized in 29 steps at 75 °C with 0.5 g $KMnO_4$ in 10 cm^3 water and 100 cm^3 1.0 % KOH per step, according to standard degradation scheme described by Vitorović *et al.*[3] The same ratio of oxidant *vs.* substrate was used in all previous kerogen structural studies by the authors. The end of reaction in each step was established by the disappearance of the violet and green colors. The alkaline solution containing the oxidation products was removed by centrifugation and thorough washing of the remaining solids.

Following every five steps, the accumulated MnO_2 was removed by treatment with an excess of 5.0 % oxalic acid solution (50 cm^3 plus 10 cm^3 2M H_2SO_4) and thorough rinsing with distilled water. The final oxidation mixture was treated in a similar way. The solid residue was dried at 80 °C and analyzed for organic matter.

The reduction periods gradually increased during the oxidation procedure as shown in Fig. 1. The occasional shorter reduction periods (6th , 11th, 16th, and 21st steps) followed the removal of MnO_2. Hence, the shorter reduction periods were probably a result of the increased reactivity of the "purified" kerogen concentrate.

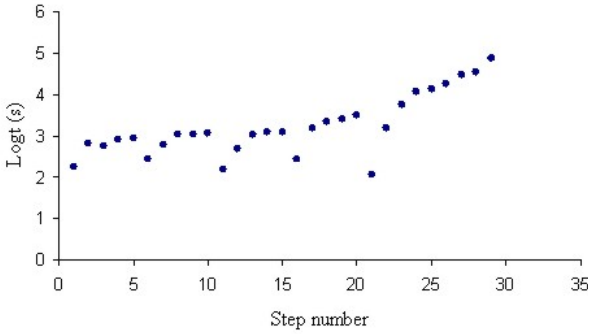

Fig. 1. Duration of successive degradation steps.

The last, 29th portion of permanganate was not fully reduced after 23 h. The 29th step was, therefore, taken as the final degradation step.

The products from each five steps, as well as the products of the last four steps, were combined (6 fractions in total) and worked up separately according to the procedure described by Amblès *et al.*[11] A 100 cm^3 aliquot was separated from each fraction, aimed at determining the amount of carbon dioxide produced by oxidation of the kerogen. A modified Partridge and Schroeder method was used for this purpose.[12,13]

Three types of products were isolated from the six fractions: neutrals and bases, ether-soluble acids and precipitated acids. The remaining aqueous solutions were made alkaline, evaporated to a small volume, acidified with HCl and finally diluted to standard 100 cm^3. The soluble acids were then extracted with ether.[14] Consequently, five types of products were obtained from each fraction: neutrals and bases (not examined), ether-soluble acids [marked Ty 1(1) to Ty 6(1)], precipitated (ether-insoluble) acids, acids from aqueous solutions [Ty 1(2) to Ty 6(2)], and kerogen carbon oxidized to carbon dioxide.

Further degradation of precipitated acids

The precipitated acids from all six fractions were combined (1.48 g) and homogenized by redissolving in 1.0 % KOH and co-precipitation with 1:1 HCl. An aliquot of 0.88 g was further oxidized in 8 steps with small amounts of $KMnO_4$ (0.45 g per step in 8 cm^3 water and 88 cm^3 1.0 % KOH). Prior to the addition of each new portion of permanganate, the acids were dissolved in KOH solution and heated to the standard reaction temperature of 75 °C. After the reduction of each portion of reagent, the reaction mixture was treated in the same way as the kerogen degradation products. The thus obtained precipitated acids were each time further oxidized in the next step with a new portion of permanganate. The produced MnO_2 was reduced after the fifth step. The products from the 1st–5th and 6th–8th step were combined into two fractions. The portion of permanganate in the last, the 8th, step was not fully reduced after more than 30 h. The precipitated acids obtained in the 8th step were washed with distilled water and dried at 100 °C. For further investigation, the ether-soluble acids were combined into two fractions [marked Ty P1 (1) and Ty P2 (1)]. Acids from the corresponding aqueous solutions were also isolated [marked Ty P1 (2) and Ty P2 (2)].

Investigation of soluble acids

All the soluble acids were methylated with ethereal diazomethane. The esters were analyzed by GC and identified by GC–MS. The GC separations were carried out in a Packard Model 427 gas chromatograph, using a 25 m fused silica WCOT CP Sil 5 (0.16 μm) capillary column, coupled to an integrator-calculator Spectra Physics System 1. The temperature of the column was programmed from 70 °C (10 min isothermally) to 300 °C, at 2 °C min^{-1}. Nitrogen was used as the carrier gas.

The GC–MS analyses were performed with a system consisting of a gas chromatograph Perkin-Elmer Sigma 3 coupled to a mass spectrometer Kratos MS 25. The column temperature was also programmed from 70 to 300 °C at 2 °C min^{-1}. The mass spectra were recorded for all the significant separated peaks.

Identification of the individual components was accomplished by comparison with the mass spectra of available authentic compounds, literature data and the available spectral data bank.

Efficient capillary GC separations, combined with the integrator-calculator service, enabled the quantitative evaluation of the proportions of the various kinds of ether-soluble acids obtained from: (a) oxidation of the kerogen concentrate, (b) oxidation of the precipitated acids and (c) aqueous solutions produced in both of these oxidations.

RESULTS

Oxidative degradation of kerogen concentrate

Twenty-nine steps were necessary for the degradation of the kerogen and a total amount of 14.5 g $KMnO_4$ was consumed (5.8 g $KMnO_4$ per g of kerogen). Approximately 66 h were required for the 29 steps. As already indicated, in the 29th step, which lasted 23 h, the $KMnO_4$ had not been fully reduced.

The yields of products in the six oxidation stages are shown in Fig. 2. The yields of neutrals and bases, total ether-soluble acids (0.27 g of ether soluble acids and 0.21 g of acids isolated from aqueous solutions), and precipitated acids (1.48 g) were 0.5, 19.5 and 58.9 %, respectively, relative to the original kerogen, the total yield being 78.9 %. Hence, the participation of neutrals and bases, total ether-soluble acids, and precipitated acids, in the total degradation product was

0.69, 26.76 and 74.64 %, respectively. The ratio of insoluble *vs*. soluble acids was 3.02.

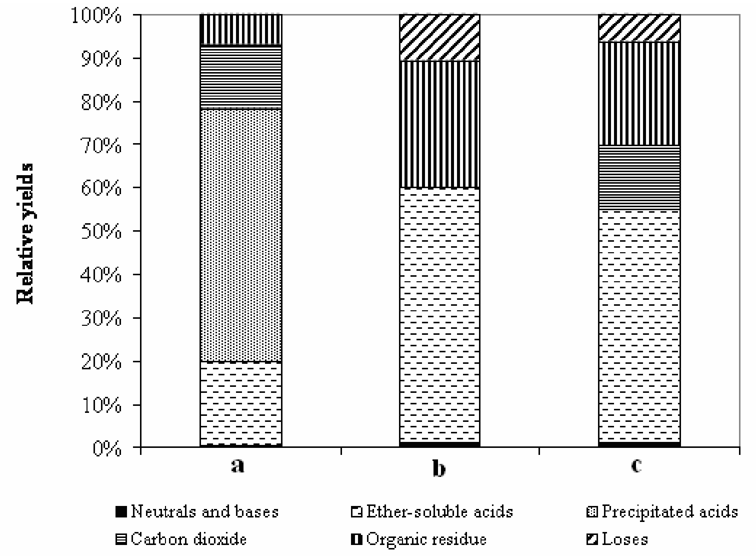

Fig. 2. Yield of products obtained by oxidative degradation of kerogen concentrate (a), precipitated acids (b) and total yield obtained by oxidative degradation of kerogen concentrate and precipitated acids (c).

Analysis of the aliquots of the six fractions of the aqueous solutions containing soluble kerogen oxidation products by a modified Partridge–Schroeder method[13] showed a substantial amount of kerogen carbon, 0.37 g, had been oxidized into carbon dioxide (14.8 % relative to the original kerogen).

The solid residue in the final step (0.20 g) contained 0.17 g organic matter (6.9 % relative to the original kerogen).

Ether-soluble acids

One of the gas chromatograms of the ether-soluble acids in the form of their methyl esters is given as an example in Fig. 3.

The GC–MS analysis of the various fractions revealed the presence of different aromatic mono-, di-, tri- and tetra-carboxylic acids, minor amounts of saturated normal monocarboxylic and α,ω-dicarboxylic acids, as well as aromatic acids, anhydrides and several unidentified compounds. Similar types of products were isolated from the corresponding aqueous solutions, *i.e.*, different aromatic mono-, di-, tri- and tetracarboxylic acids as major constituents, with minor amounts of aliphatic mono- and dicarboxylic acids, aromatic acids, anhydrides, saturated hydrocarbons and several unidentified compounds. All the identified ether-soluble oxidation products are listed in Table I.

Further oxidation of the precipitated acids

Eight steps were carried out in the degradation of an aliquot of 0.88 g of precipitated acids. A total amount of 3.6 g of $KMnO_4$ was consumed (4.1 g per g of acids).

The yields of products obtained in the degradation of precipitated acids are shown in Fig. 2. The total yields of neutrals and bases and ether-soluble acids (including the acids isolated from aqueous solutions) *i.e.,* 0.48 of ether-soluble acids and 0.04 g of acids from aqueous solutions were 1.0 % and 59.0 %, respectively, relative to original precipitated acids. A gas chromatogram of one of the fractions of these ether-soluble acids is shown as an example in Fig. 4. The yield of precipitated acids in the eight steps (non-degraded precipitated acids) was 0.26 g (29.3 %).

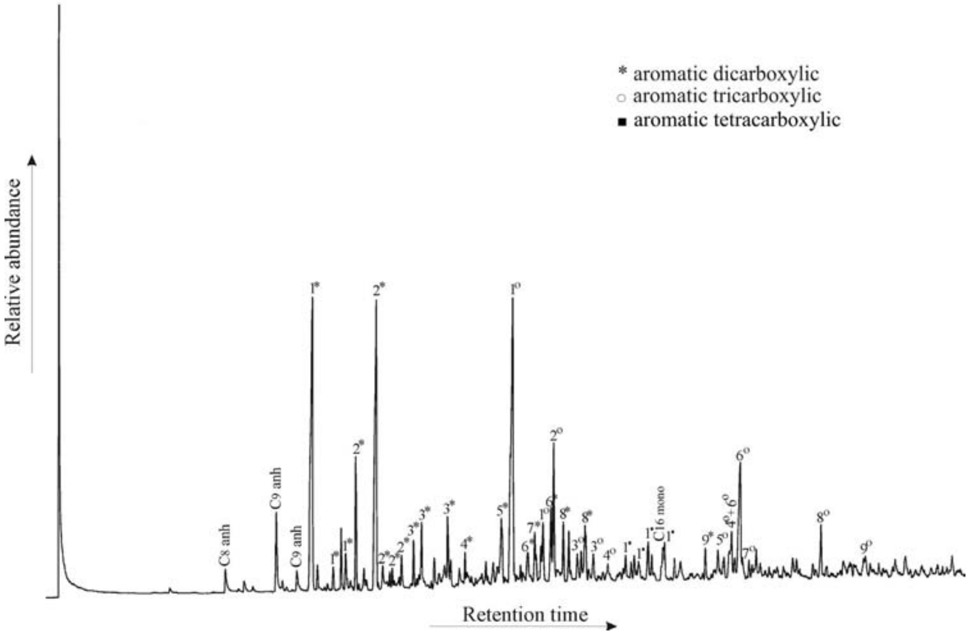

Fig. 3. Gas chromatogram of the ether-soluble acids Ty 4 (1), in the form of methyl esters. See Appendix.

The GC–MS analysis of the two fractions of ether-soluble acids (including the acids isolated from the corresponding aqueous solutions) revealed the presence of different saturated normal and branched mono- and dicarboxylic and alkane tri- and tetracarboxylic acids as the major constituents, different aromatic mono-, di-, tri- and tetracarboxylic acids, as well as minor amounts of saturated hydrocarbons and DHA. The acids identified as oxidation products of the precipitated acids are listed in Table II.

TABLE I. Ether-soluble acids and related compounds obtained by oxidation of kerogen (including acids isolated from the corresponding aqueous solutions)

Compund		From kerogen[a] Ty 1–6 (1)	From aqueous solutions[a] Ty 1–6 (2)
Aromatic acids[b]	mono-	C_8H_9-; $C_{12}H_{17}$-; $C_{10}H_7$-[b]; $C_{11}H_9$-[b]; $C_{12}H_{11}$-[b]; $C_{13}H_{13}$-[b]; $C_{16}H_{19}$-[b]; $C_{24}H_{35}$-[b]	$C_{11}H_{15}$-; $C_{12}H_{17}$-; $C_{22}H_{37}$-; $C_{11}H_9$-[b]; $C_{21}H_{29}$-[b]; $C_{23}H_{33}$-[b]; $C_{24}H_{35}$-[b]
	di-	$C_6H_4=$; $C_7H_6=$; $C_8H_8=$; $C_9H_{10}=$; $C_{10}H_{12}=$; $C_{11}H_{14}=$; $C_{10}H_6=$[b]; $C_{11}H_8=$[b]; $C_{12}H_{10}=$[b]; $C_{14}H_{14}$[b]; $C_{16}H_{18}=$[b]	$C_6H_4=$; $C_7H_6=$;$C_8H_8=$; $C_9H_{10}=$; $C_{11}H_{14}=$; $C_{11}H_8=$[b]; $C_{12}H_{10}=$[b]; $C_{23}H_{32}=$[b]
	tri-	$C_6H_3\equiv$; $C_7H_5\equiv$; $C_8H_7\equiv$; $C_9H_9\equiv$; $C_{10}H_{11}\equiv$; $C_{11}H_{13}\equiv$; $C_{16}H_{23}\equiv$; $C_{10}H_5\equiv$[b]; $C_{11}H_7\equiv$[b]; $C_{14}H_{13}\equiv$[b]; $C_{16}H_{17}\equiv$[b];$C_{17}H_{19}\equiv$[b]	$C_6H_3\equiv$; $C_7H_5\equiv$; $C_8H_7\equiv$; $C_{10}H_{11}\equiv$; $C_{16}H_{23}\equiv$; $C_{10}H_5\equiv$[b]; $C_{11}H_7\equiv$[b]; $C_{12}H_9\equiv$[b]; $C_{16}H_{17}\equiv$[b]
	tetra-	$=C_6H_2=$; $=C_{10}H_{10}=$; $=C_{16}H_{22}=$	$=C_6H_2=$; $=C_7H_4=$; $=C_{10}H_{10}=$; $C_{16}H_{22}=$
Aliphatic acids	mono-	nC_{16}; nC_{18}	nC_{16}; nC_{18}; nC_{24}; C_{17}br
	di-	–	nC_5; nC_7; nC_8; C_5*br*; C_6br
Anhydrides		C_8; C_9	C_8; C_9
Saturated hydrocarbons		–	C_{21}-C_{32}

[a]The individual isomers of the various oxidation products were not identified. Hence, the proposed R groups are tentative. They may represent any other possible combination of R groups. Free valences indicate carboxylic groups; [b]naphthalene-carboxylic acids

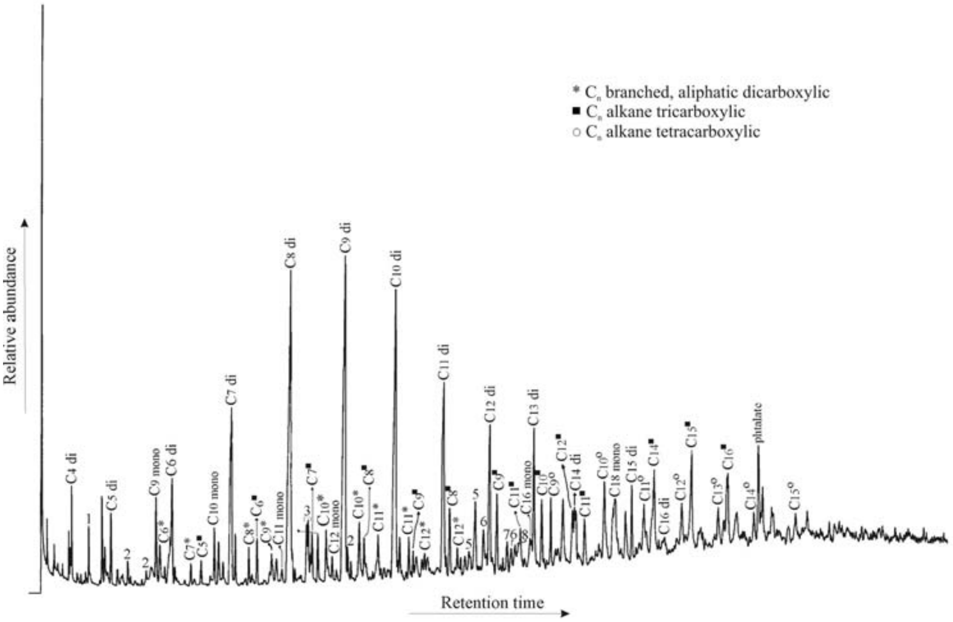

Fig. 4. Gas chromatogram of the ether-soluble acids Ty P 1 (1), in the form of methyl esters. See Appendix.

DISCUSSION

A detailed structural study of a type III kerogen originating from a Tyrolean (Austria) "Hauptdolomit" Triassic sediment was carried out, aimed at obtaining evidence on the relationship between a type III kerogen and the yields and chemical nature of the degradation products produced using an optimized alkaline permanganate oxidation method. The results served as a basis for the reconstruction of the kerogen structure. They are also expected to be a basis for comparison with the structure of other type III kerogens, in particular with the structure of the type III Mannville shale kerogen, the single type III kerogen hitherto studied under similar experimental conditions.[8]

TABLE II. Ether-soluble acids and related compundsobtained by oxidation of precipitated acids (including acids isolated from the corresponding aqueous solutions)

Compond		From precipitated acids[a] Ty P 1–2 (1+2)
Aromatic acids	mono-	C_6H_5-; C_7H_7-; $C_{11}H_9$-[b]; $C_{14}H_{15}$-[b]
	di-	C_6H_4=; C_7H_6=; $C_{10}H_{12}$=; $C_{10}H_6$=[b]; $C_{11}H_8$=[b]; $C_{12}H_{10}$=[b]
	tri-	$C_6H_3\equiv$; $C_7H_5\equiv$; $C_9H_9\equiv$; $C_{11}H_7\equiv$[b]
	tetra-	$=C_6H_2=$
Aliphatic acids	mono-	nC_9-C_{12}; nC_{14}-C_{18}; nC_{22}-C_{24}; nC_{26}; C_{17}br; C_{19}br
	di-	nC_4-C_{17}; C_5-C_{12}*br*
Alkane-poly-carboxylic acids	tri-	C_3-C_{12}; C_{14}-C_{19}
	tetra-	C_5-C_{15}
Saturated hydrocarbons		C_{21}-C_{24}; C_{26}-C_{29}
Diterpenoids		DHA

[a] The individual isomers of the various oxidation products were not identified. Hence, the proposed R groups are tentative. They may represent any other possible combination of R groups. Free valences indicate carboxylic groups; [b] naphthalene-carboxylic acids

The twenty-nine step alkaline permanganate degradation of Tyrolean shale kerogen resulted in a very high total yield of oxidation products, 93.7 % based on the original kerogen, comprising neutrals and bases (0.5 %), ether-soluble acids (11.0 %), acids isolated from the corresponding aqueous solutions (8.5 %), precipitated acids (58.9 %), and 14.8 % of kerogen carbon in the form of carbon dioxide, an oxidation product quantified by a modified method of Partridge and Schroeder.[12,13] The amount of residual organic matter remaining after the last oxidation step was 6.9 %, making the total material balance 100.6 %, which included the permanganate oxygen incorporated into the oxidation products.

The observed high yields of the recovered oxidation products suggested that the material losses during the complex experimental procedure were rather low. However, material losses cannot be completely excluded.

The solubility of the oxidation products in diethyl ether was found to be relatively low, the ratio of precipitated (ether-insoluble) *vs*. ether-soluble acids (PA/ESA) being quite high, 3.02.

The qualitative and quantitative compositions of the oxidation products obtained by degradation of Tyrolean shale kerogen are shown in Tables I and III.

The composition of the ether-soluble acids was surprising: 0.8 % C_{16} and C_{18} alkane-monocarboxylic acids, no alkane-dicarboxylic acids, and practically 99 % aromatic acids (Tables I and II), with almost 60 % of the dominating aromatic dicarboxylic acids. The acids isolated from the concentrated aqueous solutions had a somewhat different composition: *ca.* 1.2 % of alkane-mono- and dicarboxylic acids of narrow range and simple distribution, the rest representing aromatic acids, the composition of which differed from the corresponding composition of the ether-soluble aromatic acids, due to the higher solubility of polycarboxylic aromatic acids (Tables I and II).

TABLE III. Composition of oxidation products obtained by degradation of Tyrolean oil shale kerogen

Acids	Content relative to identified acids, %						Total I + II
	Oxidation of kerogen			Oxidation of precipitated acids			
	Ether soluble acids	Acids from aqueous solutions	Total I	Ether soluble acids	Acids from aqueous solutions	Total II	
Alkane carboxylic acids							40.7
n-Mono-acids	0.83	0.41	0.66	4.28	9.24	4.69	3.2
n-Br-mono-	–	–	–	–	1.63	0.13	0.1
n-Di-	–	0.63	0.22	52.14	37.76	50.95	32.8
br-Di-acids	–	0.17	0.06	7.68	1.75	7.19	4.6
Alkane polycarboxylic acids							16.3
Tricarboxylic	–	–	–	16.32	15.06	16.22	10.4
Tetracarboxylic	–	–	–	9.20	9.79	9.25	5.9
Aromatic acids							43.0
Monocarboxylic	2.53	6.24	3.77	3.15	3.16	3.15	3.3
Dicarboxylic	59.19	24.05	47.82	4.61	11.73	5.20	20.0
Tricarboxylic	32.31	42.16	35.04	2.32	8.60	2.84	14.0
Tetracarboxylic	5.15	26.34	12.43	0.30	1.27	0.38	4.6
Anhydride of alkyl phthalic acid	–						1.1

Histograms illustrating the ranges and distributions of the total alkane-mono- and dicarboxylic acids observed after kerogen degradation are shown in Figs. 5a and 6a.

Alkane-mono-carboxylic acids were isolated in very low yields. They were composed exclusively of C_{16} and C_{18} members. Hence, they were most probably linked to the kerogen matrix by ester-type bonds.

The major aromatic components in the ether-soluble acids, including those isolated from the corresponding aqueous solutions, were different substituted benzene- and naphthalene-mono-, di- and tricarboxylic acids, as well as benzene-

-tetracarboxylic acids (Table I). Low amounts of phthalic acid anhydride and saturated hydrocarbons (contamination) were also identified. The most abundant were benzene-dicarboxylic acids (from $C_6H_4=$ up to $H_{11}C_5{\cdot}C_6H_3=$), naphthalene-dicarboxylic acids (from $C_{10}H_6=$ up to $H_{27}C_{13}{\cdot}C_{10}H_5=$), benzene-tricarboxylic acids (from $C_6H_3\equiv$ up to $H_{21}C_{10}{\cdot}C_6H_2\equiv$) and naphthalene-tricarboxylic acids (from $C_{10}H_5\equiv$ up to $H_{15}C_7{\cdot}C_{10}H_4\equiv$).

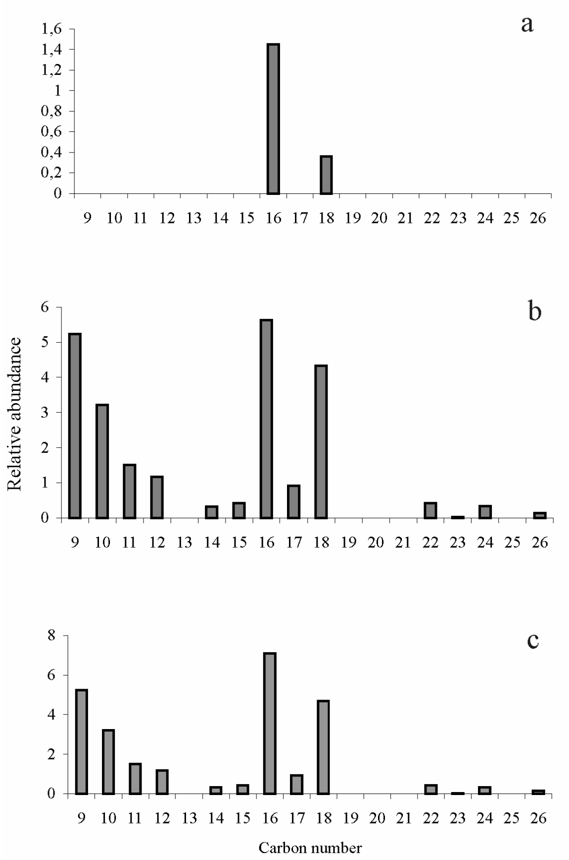

Fig. 5. Relative abundance and distribution of *n*-monocarboxylic acids obtained by oxidative degradation of kerogen (a) and precipitated acids (b), and their total abundance and distribution (c).

Reconstruction of the original macromolecular structure of the Tyrolean shale kerogen based exclusively on the composition of its ether-soluble acidic oxidation products obtained in a moderate yield, *i.e.*, 19.5 % relative to kerogen, can only be tentative. Nevertheless, taking into consideration, in addition to the composition of ether-soluble acids, the amount of kerogen carbon oxidized into CO_2 (14.8 %), the degradation products of at least one part of the kerogen suggest cross-linking and substitution in its structure by very short alkyl chains as well as slight aryl-substitution, resulting in a low yield of aromatic monocarboxylic acids. The proportion of aromatic tetracarboxylic acids indicates a limited amount of condensed aromatic structural elements in this part of the kerogen. On the other hand, the high proportions of aromatic tricarboxylic and particularly dicarboxylic acids indicate precursor aromatic structures cross-linked by short *n*- or eventually branched aliphatic or alicyclic hetero-functional chains, and characterized by methyl-substitution.

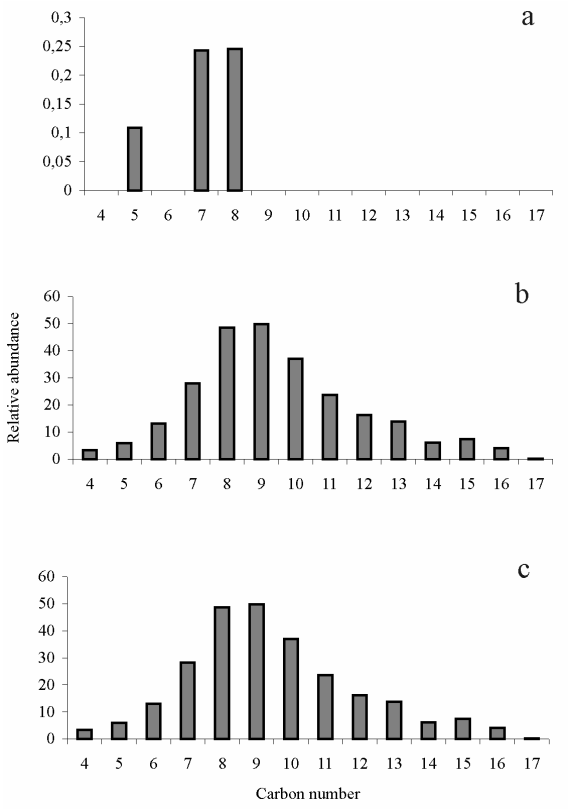

Fig. 6. Relative abundance and distribution of α,ω-dicarboxylic acids obtained by oxidative degradation of kerogen (a) and precipitated acids (b), and their total abundance and distribution (c).

Heterocyclic structures probably are not constituents of this part of kerogen, since alkane-polycarboxylic acids were not observed in the oxidation products. On the other hand, the degradation residue, being relatively high, 6.9 %, suggests that Tyrolean shale kerogen contains structures resistant towards alkaline permanganate.

The degradation of kerogen and the observed PA/ESA ratio indicates structural non-homogeneity of the kerogen matrix, *i.e.*, the existence of at least two structural entities, one abundant in cross-links sensitive to oxidative cleavage and the other consisting of bulky units with cross-links less sensitive towards oxidative degradation.

However, as mentioned, the final structural interpretation of the kerogen depended on the investigation of the degradation products of the precipitated, ether-insoluble acids, which were the main kerogen degradation product.

Qualitative and quantitative data observed in the further degradation of the precipitated acids gave a completely different image of the kerogen structure (Tables II and III). Ether-soluble acids were obtained in *ca*. 59.0 % yield relative to the precipitated acids. On the other hand, 29.3 % of the total precipitated acids (17.3 % relative to kerogen) remained after the eighth oxidation step in the form of a non-degraded residue, *i.e.*, they were resistant towards the oxidant.

The ratio of aliphatic *vs.* aromatic acids differed substantially from the corresponding ratio observed in the degradation of the kerogen (Table III). Surprisingly, aliphatic *n*-mono- and particularly *n*- and branched α,ω-dicarboxylic, as well as alkane-tri- and tetracarboxylic acids were the major oxidation products of the precipitated acids (63.0 %). Aromatic mono- to tetracarboxylic acids represented minor oxidation products, 11.6 %. Long-chain acids dominated among the aliphatic acids, 50.9 % of these being C_4–C_{17} *n*-alkane-dicarboxylic acids, with a maximum at C_9 (a histogram is shown in Fig. 6b) and 7.2 % were branched alkane-dicarboxylic acids. Monocarboxylic acids were obtained in lower yield. Their range (C_9–C_{26}) and distribution is illustrated by the histogram shown in Fig. 5b. The alkane-di-/alkane-monocarboxylic acids ratio was high, 10.9. The observed data give a different picture of the proportion and type of alkyl-substituents and the proportion, structure and length of the aliphatic cross-links in the precipitated acids from Tyrolean shale kerogen. The degradation loss was 10.6 % relative to the initial precipitated acids.

The ranges of the aromatic di- and tricarboxylic acids were simpler compared to the aromatic acids identified in the ether-soluble oxidation products of the kerogen (Tables II and III).

Hence, the data obtained from the further degradation of the precipitated acids corroborated the presumption concerning the heterogeneity of the Tyrolean shale kerogen.

Finally, the amount of residual precipitated acids resistant towards further stepwise oxidative degradation, as mentioned, was rather high, 17.3 % relative to kerogen. Consequently, in total, approximately 24 % of the kerogen (6.9 % in kerogen degradation plus 17.3 % in degradation of the precipitated acids) was found to be resistant towards alkaline permanganate. On the other hand, the material loss (CO_2 plus low molecular weight acids remaining in the aqueous solutions) during the further degradation of the precipitated acids was 6.3 %. Together with the 14.8 % loss (quantified as CO_2) observed in the degradation of kerogen, the total loss was 21 %, originating mainly from C_1–C_3 alkyl substituents and/or short aliphatic chain cross-links.

Since the yields of aliphatic, alkane-polycarboxylic and aromatic acids, as the main oxidation products of the aliphatic, alicyclic and/or heterocyclic and aromatic components of the kerogen matrix, were proposed as a basis for the classification of kerogens,[9] the corresponding values observed in the degradation of the Tyrolean shale kerogen (Table III) were introduced into a triangular diagram shown in Fig. 7. The diagram includes corresponding positions of several other kerogens hitherto examined by the same degradation method.

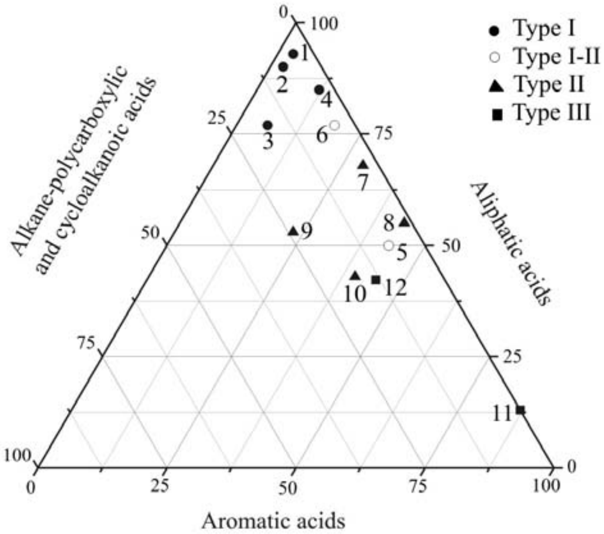

1 – Pumpherston
2 – Colorado
3 – Aleksinac
4 – Irati
5 – Timahdit
6 – Pyongan
7 – Toarcian, Paris basin
8 – Whitby
9 – Messel
10 – Xin Jang
11 – Mannville
12 – Tyrolean

Fig. 7. Composition of the oxidation products obtained by degradation of Tyrolean shale kerogen and of several other kerogens.

Combining the yields of the oxidation products of Tyrolean shale kerogen and precipitated acids, both calculated relative to the original kerogen, one comes to a balance between the aromatic, alkane mono- and dicarboxylic and alkane-polycarboxylic acidic oxidation products which suggests a shift of the structure of Tyrolean shale kerogen from the expected typical aromatic type III kerogen towards a heterogeneous aromatic-aliphatic-alicyclic type structure, *i.e.*, towards some kind of intermediate type III-II kerogen.

The estimated structure of the Tyrolean shale kerogen based on oxidative degradation products shown in the triangular diagram (Fig. 7) obviously differs substantially from the estimated structure of type III Mannville shale kerogen, based also on multistage alkaline permanganate degradation. This difference, however, may be explained by the fact that methods used for the oxidative degradation of these two type III kerogens were different. Namely, the Mannville shale kerogen was studied[8] before the alkaline permanganate degradation method had been optimized by the addition of the isolation and identification of acids from aqueous solutions and the determination of the amount of kerogen carbon oxidized into carbon dioxide.[13] Thus, in the degradation procedure of Mannville shale kerogen at that time, a part of its structure, yielding acids highly soluble in water, and methyl or short aliphatic chain substituents and cross-links, yielding CO_2 on oxidation with alkaline permanganate, were neglected. Therefore, the estimation of the structure of Mannville shale kerogen based on alkaline permanganate oxidative degradation must be reappraised before comparison of its structure with the estimated structure of Tyrolean shale kerogen.

Likewise, neither the so-called kerogen nor the precipitated acid residues resistant to degradation should be neglected, particularly when their proportion is shown to be as high as in the degradation of Tyrolean shale kerogen. Namely, the H/C ratio of the latter (0.76) indicated an overall aromaticity which, however, was not confirmed through the yield of aromatic acids obtained as its oxidation products. Consequently, the Tyrolean shale kerogen and precipitated acids residues, observed in a total yield of 24 % relative to kerogen, are suggested to be in the form of resorcinol units linked by ether bonds. Such a presumption is based on chemical and geochemical evidence. On the one hand, resorcinol structures are known to be resistant towards alkaline permanganate. On the other hand, continental (terrestrial) flora residues consisting of lignin (generally resorcinol) structures, diagenetically resistant dominant biostructures, are often type III precursors.

CONCLUSIONS

Experimental data observed by stepwise oxidative degradation of Tyrolean oil shale type III kerogen, and further degradation of the resulting insoluble (precipitated) acids, as well as the results of detailed qualitative and quantitative analyses of the obtained acidic oxidation products suggest the following conclusions.

Tyrolean oil shale kerogen is a heterogeneous macromolecular substance consisting of three types of structures, differing in composition and susceptibility towards alkaline permanganate as an oxidant.

One type is composed of quite resistant structures, presumably consisting of aromatic units cross-linked by resorcinol ethereal bonds, its estimated proportion in the kerogen matrix being *ca.* 24 %.

The second type of structure is, on the one hand, aliphatic in nature, comprising abundant methyl-substituents and shorter chain cross-links, both easily oxidized into "non-isolated" products such as CO_2, water, and low molecular weight acids. Their proportion in the kerogen matrix is estimated to be *ca.* 21 %. These cross-links consolidate the aromatic components which, upon oxidation, are converted into high yields of aromatic di- and tricarboxylic acids.

The third type, moderately resistant towards oxidation, is composed of aliphatic-alicyclic (and/or heterocyclic) structures, mutually bound into units containing low proportion of aromatic structures.

Although classified as type III kerogen and characterized by a significantly high vitrinite reflectance (Ro = 1.38), its oxidative degradation produced a high total yield of alkane-mono- and dicarboxylic acids. They were of unusually simple ranges, particularly the identified *n*-alkane-monocarboxylic acids, and simple distributions, which were also uncommon, indicating the existence of precursor aliphatic structural elements of relatively homogenous composition and structure.

The rather high proportion of acidic oxidation products (4.6 %) consisting for the most part of branched alkane-dicarboxylic acids, with just a small proportion of branched alkane-monocarboxylic acids, obviously originated from the corresponding branched structural elements in the kerogen matrix. Such a high proportion of these structures in kerogen oxidation products seems to be a specificity of type III kerogens inherited from a terrestrial precursor biomass.

A high yield of alkane-polycarboxylic (tri- and tetracarboxylic) acids (16.3 %) originates from a similar high proportion of precursor alicyclic/heterocyclic structures in the kerogen matrix, which probably also may be considered as unexpected for a type III kerogen.

APPENDIX

Appendix to Fig. 3

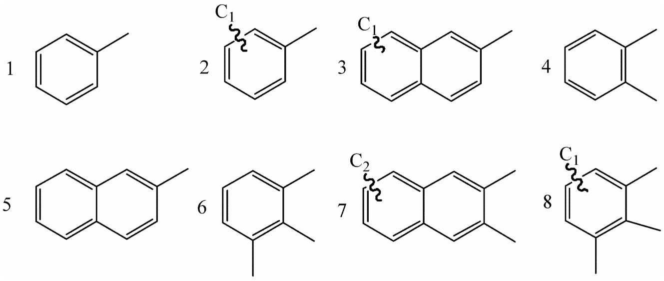

Appendix to Fig. 4

■ – Aromatic tetracarboxylic

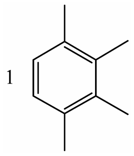

∗ – Aromatic dicarboxylic

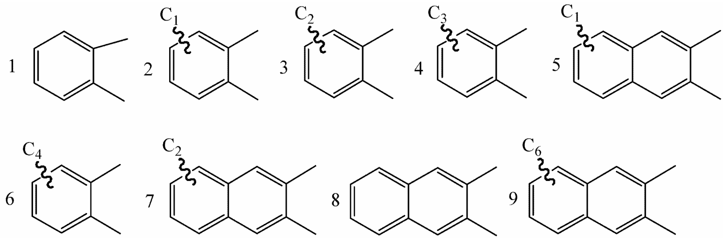

○ – Aromatic tricarboxylic

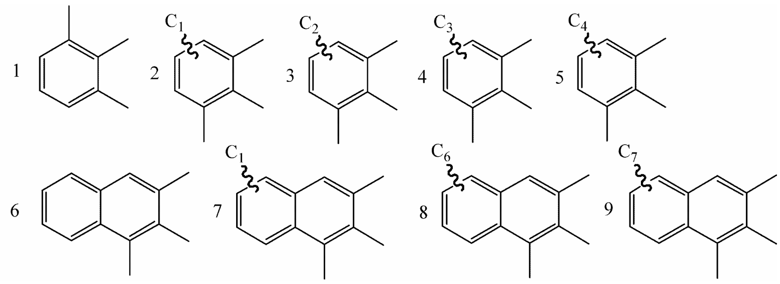

И З В О Д

КАРАКТЕРИЗАЦИЈА КЕРОГЕНА ТИПА III ТИРОЛСКОГ ШКРИЉЦА (HAHNTENNJOCH, АУСТРИЈА) ЗАСНОВАНА НА ЊЕГОВИМ ОКСИДАЦИОНИМ ПРОИЗВОДИМА

С. БАЈЦ[1], О. ЦВЕТКОВИЋ[1], A. AMBLÈS[2] и Д. ВИТОРОВИЋ[1]

[1]*Центар за хемију, ИХТМ, Његошева 12, 11000 Београд и* [2]*Department of Chemistry, Faculty of Science, University of Poitiers, 40, Av. du Recteur Pineau, 86022 Poitiers, France*

Ступњевитом деградацијом керогена тиролског шкриљца помоћу алкалног перманганата добијени су високи приноси оксидационих производа. Добијене нерастворне киселине накнадно су деградоване у 8 ступњева. Детаљна GC–MS анализа киселина растворних у етру, добијених деградацијом керогена, потом интермедијарних нерастворних киселина, показала је да је кероген тиролског шкриљца хетерогена макромолекуларна супстанца и да се састоји из три типа структуре, различитог састава и различите осетљивости на примењено оксидационо средство. Први тип је ароматичне природе са резорцинолним етарским умрежењем, отпоран према алкалном перманганату. Други се врло лако оксидује, а састоји се од ароматичних структура умрежених кратким алифатичним низовима и са већим уделом метил-супституената. Овај тип структуре је при оксидацији дао висок принос CO_2, алифатичне киселине малих молекулских маса и ароматичне ди- и трикарбоксилне киселине у високом приносу. Трећи тип структуре је средње осетљивости на перманганат, а састоји се од алицикличних и/или хетероцикличних и ароматичних језгара повезаних алифатичним низовима средњих дужина. Квантитативан однос алифатичних, ароматичних и алкан-поликарбоксилних киселина у оксидационим производима показао је да структура керогена тиролског шкриљца одступа од типских, доминантно ароматичних структура типа III, којима припада по свом H/C–O/C атомском односу, и да је померена ка хетерогеним, ароматично-алифатично-алицикличним структурама типа II.

(Примљено 15. октобра, ревидирано 19. новембра 2007)

REFERENCES

1. M. Vandenbroucke, C. Largeau, *Org. Geochem.* **38** (2007) 719
2. B. P. Tissot, D. H. Welte, *Petroleum Formation and Occurrence*, Springer Verlag, Berlin, 1978
3. D. Vitorović, A. Amblès, S. Bajc, O. Cvetković, M. Djordjević, *J. Serb. Chem. Soc.* **53** (1988) 175
4. D. Vitorović, A. Amblès, S. Bajc, O. Cvetković, P. Polić, *J. Serb. Chem. Soc.* **59** (1994) 75
5. D. Vitorović, A. Amblès, S. Bajc, O. Cvetković, P. Polić, *J. Serb. Chem. Soc.* **61** (1996) 137
6. D. Vitorović, A. Amblès, S. Bajc, O. Cvetković, P. Polić, *J. Serb. Chem. Soc.* **63** (1998) 419
7. S. Bajc, A. Amblès, C. Largeau, S. Derenne, D. Vitorović, *Org. Geochem.* **32** (2001) 773, and references therein
8. A. Amblès, M. Djordjević, D. Vitorović, *Chem. Geol.* **48** (1985) 305
9. D. Vitorović, A. Amblès, M. Djordjević, *Org. Geochem.* **6** (1984) 333
10. B. Durand, J. C. Monin, in *Kerogen, Insoluble Organic Matter from Sedimentary Rocks*, B. Durand, Ed., Editions Technip, Paris, 1980, pp. 113–142
11. A. Amblès, M. V. Djuričić, D. Vitorović, *Bull. Soc. Chim. Beograd* **46** (1981) 275
12. E. P. Partridge, W. C. Schroeder, *Ind. Eng. Chem. Anal. Ed.* **4** (1932) 271
13. S. Bajc, A. Amblès, D. Vitorović, *J. Serb. Chem. Soc.* **60** (1995) 553
14. D. Vitorović, A. Amblès, M. Djordjević, *Org. Geochem.* **10** (1986) 1119.

www.shd.org.yu

Journal of the Serbian Chemical Society
version electronic

JSCS@tmf.bg.ac.yu • www.shd.org.yu/JSCS

J. Serb. Chem. Soc. *73* (4) 479–486 (2008)
JSCS–3729

UDC 546.654.027*123+544.773.42:
:542.913.004.12:621.315
Original scientific paper

Synthesis and characterization of Ln-123 superconductors

ARTURAS ZALGA[1], REMIGIJUS JUSKENAS[2], ALGIRDAS SELSKIS[2],
DARIUS JASAITIS[1] and AIVARAS KAREIVA[1]*

[1]*Faculty of Chemistry, Vilnius University, Naugarduko 24, LT-03225 Vilnius and* [2]*Institute of Chemistry, A. Gostauto 9, LT-01108 Vilnius, Lithuania*

(Received 10 January, revised 12 November 2007)

Abstract: A sol–gel method was applied to prepare precursors for $NdBa_2Cu_3O_{7-x}$ (Nd-123) and $SmBa_2Cu_3O_{7-x}$ (Sm-123) superconducting compounds. The sintered products were examined by X-ray diffraction analysis (XRD) and scanning electron microscopy (SEM). The powders sintered at 950 and 1000 °C showed the formation of monophasic Nd-123 and Sm-123 superconductors. The formation of Nd-123 and Sm-123 phases from the sol-gel derived precursors at higher temperatures (1050 and 1100 °C), however, did not proceed due to the melting process. The correlation between the T_C for different lanthanides (Ln – Ho, Nd and Sm) in the Ln-123 compound and orthorhombicity and oxygen stoichiometry were also estimated.

Keywords: 123 superconductors; substitution effects; lanthanides; sol–gel synthesis.

INTRODUCTION

Practical application of high-temperature superconductors requires long length and complex shapes of the textured ceramic materials.[1,2] An important step in the fabrication of such superconducting architectures is the development of joining technologies between individual superconducting components.[3] Two melt-textured $YBa_2Cu_3O_{7-x}$ superconducting blocks can be successfully welded with $LnBa_2Cu_3O_{7-x}$ (Ln – rare earth element) solders.[4] For almost all practical applications – large and small scale – the superconducting ceramics must carry sufficiently large electrical currents, typically > 10^6 A cm^{-2} and operate in strong magnetic fields. It is a consequence of poor reproducibility of the critical transport current density in bulk ceramic high-temperature superconductors that enormous interest in the development of new synthetic methods for their preparation continues.

The critical transport current density in bulk ceramic high-temperature super–conductors, such as $LnBa_2Cu_3O_{7-x}$, is highly dependent on the microstructure.[5–8]

---

* Corresponding author. E-mail: aivaras.kareiva@chf.vu.lt

doi: 10.2298/JSC0804479Z

For most of the multimetallic oxides, an unusual combination of physical and chemical properties depends largely on the compositional homogeneity, phase purity, surface morphology and microstructure. These features crucial for the preparation of electronic, optic and catalytic materials are dependent on the method of synthesis.[2]

Obviously the variation of homogeneity region, as well as the structural and superconducting properties in $LnBa_2Cu_3O_{7-x}$ superconductors should also be very dependent on the employed preparation technique.[6,9] Recently, a simple *chimie douce* synthetic approach was developed to obtain a high-purity crystalline $HoBa_2Cu_3O_{7-x}$ superconducting phase by heat treatment of mixed-metal gels at different temperatures.[10] The powders sintered at 950 and 1000 °C showed the formation of monophasic Ho-123 superconductors. The formation of the Ho-123 phase from sol–gel derived precursors at higher temperatures (1050 and 1100 °C) was, however, strongly controlled by the peritectic reaction Ho-211 + + L $\rightleftarrows$ Ho-123. Also, the effect of holmium substitution on the structural and surface morphological properties of Y-123 superconductors synthesized by sol–gel technique was studied.

Clearly, the difference in the ionic radius of the Ln ion has an effect on the superconductivity of Ln-123.[9,11,12] In the present study, the Ho^{3+} ion (r = 1.07 Å) in Ho-123 was replaced by the larger Nd^{3+} (r = 1.16 Å) and Sm^{3+} ion (r = 1.32 Å) and the effect of the lanthanide substitution on the oxygen stoichiometry, superconducting properties and the orthorhombicity of the unit cell of the resulting Ln-123 (Ln – Ho, Nd, Sm) was studied.

EXPERIMENTAL

$LnBa_2Cu_3O_{7-x}$ (Ln – Nd, Sm) were synthesized by a two-step method in which a precursor was first synthesized using the sol–gel technique and then calcined at different temperatures. In the sol–gel process, stoichiometric amounts of Nd_2O_3, Sm_2O_3, $Cu(CH_3COO)_2\cdot H_2O$ and $Ba(CH_3COO)_2$ (all of analytical grade) were used as the starting compounds. The Nd_2O_3 or Sm_2O_3 was first dissolved in 0.20 M acetic acid at 55–60 °C. Next, $Ba(CH_3COO)_2$ and $Cu(CH_3COO)_2\cdot H_2O$, dissolved in a small amount of distilled water, were added with intermediate stirring during several hours at the same temperature. A solution of tartaric acid in water was added to adjust the pH to 5.6, thus preventing crystallization of copper acetate during gelation. The obtained solutions were concentrated during about 8 hours at 60–65 °C in an open beaker. Under continuous stirring, the transparent blue Nd–Ba–Cu–O and Sm–Ba–Cu–O precursor gels formed. After further drying in an oven at 80 °C, fine-grained blue powders were obtained. The precursor powders were placed in an alumina crucible and calcined for 10 h at 850 °C in an oxygen atmosphere, reground in an agate mortar and pelletized. The pellets were again placed in an alumina crucible and, starting from room temperature, annealed in an ordinary tube furnace for 5 h at different temperatures (950, 1000, 1050 and 1100 °C). The heating and cooling rate was 5 °C min^{-1}. At the end of the growth experiment, the crystals were cooled in the furnace to 200 °C and crucible was raised from the furnace. Finally, the crystals obtained at different temperatures were annealed for 10 h at 500 °C in oxygen to be converted into the orthorhombic superconducting form.[13]

The X-ray powder diffraction (XRD) studies were performed on a STOE diffractometer operating with CuKα_1 radiation. The lattice parameters of the synthesized samples were obtained from the diffraction spectra by fitting the peaks of the identified reflections using a least-squares procedure.[6,14,15] A scanning electron microscope (SEM) JXA-50A JEOL was used to study the morphology and microstructure of the ceramic samples. T_C values of the superconducting compounds were obtained from magnetic susceptibility measurements performed in gelatine capsules with a SQUID magnetometer (Quantum Design, MPMS) in the temperature region between 5 and 120 K. The oxygen content in the superconducting samples was determined by the well-known iodometric titration method.[16-18]

RESULTS AND DISCUSSION

As was already previously reported, the sintering of a Ho–Ba–Cu–O precursor gel at 950 or 1000 °C produced a fully crystalline single-phase $HoBa_2Cu_3O_{7-x}$ superconducting oxide.[10] Further heating to 1050–1100 °C, however, resulted in XRD patterns indicating the definite presence of different phases. The following Equations describe the equilibria in the investigated system at 1050 and 1100 °C, respectively:

$$2HoBa_2Cu_3O_{7-x} \rightleftarrows Ho_2BaCuO_5 + 1.5Ba_2Cu_3O_{5+x} + \\ + 0.5CuO + (0.5 - 1{,}75x)O_2 \qquad (1)$$

$$2HoBa_2Cu_3O_{7-x} \rightleftarrows Ho_2BaCuO_5 + 3BaCuO_2 + 2CuO + (0.5 - x)O_2 \qquad (2)$$

The Nd–Ba–Cu–O and Sm–Ba–Cu–O gel powders sintered at 950 and 1000 °C also showed the formation of single phase Nd-123 and Sm-123 superconductors, respectively. However, contrary to the case of holmium, the heating of neodymium and samarium starting materials at higher temperatures (1050 and 1100 °C) gave fully melted synthesis products, the compositions of which were not analyzed.

The textural properties of the calcined Nd–Ba–Cu–O precursor gels at different temperatures (950, 1000, 1050, and 1100 °C) are shown in Fig. 1.

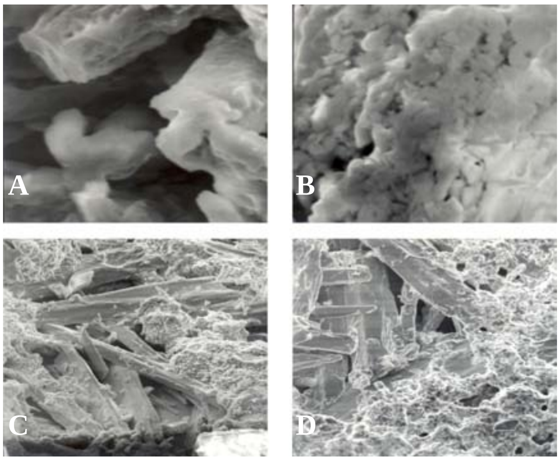

Fig. 1. Scanning electron micrographs of the Nd–Ba–Cu–O precursor gels annealed at 950 °C (C), 1000 °C (D), 1050 °C (A) and 1100 °C (B). Magnification 170×.

The microstructure of the $NdBa_2Cu_3O_{7-x}$ ceramic sample obtained at 950 °C was composed of a number of elongated grains. The SEM micrograph of the powders calcined at 1000 °C shows that the individual particles seem to be also stick-like crystals. A progressive change in the morphology was evident with increasing calcination temperature. The micrograph of the specimen sintered at 1050 °C shows a lack of grain growth and an undeveloped microstructure due to the partial melting of the specimen at this temperature. The microstructure of the sample obtained at 1100 °C consisted of a clustered matrix, which is typical for a melted ceramic product. The surface features of the Sm–Ba–Cu–O precursor gels calcined at the same temperatures (950, 1000, 1050, and 1100 °C) are shown in Fig. 2.

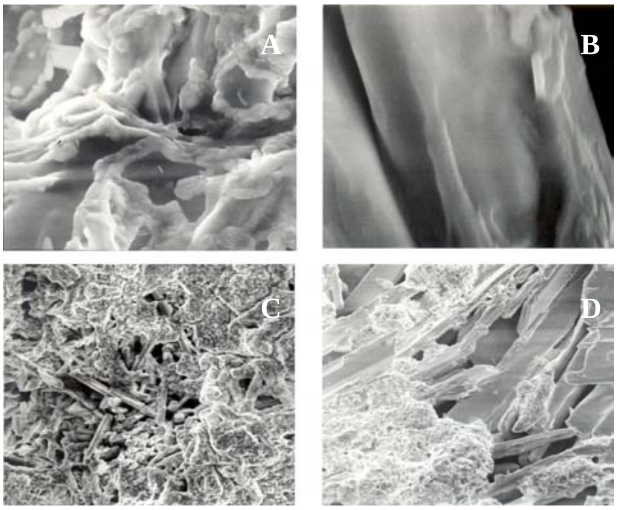

Fig. 2. Scanning electron micrographs of the Sm–Ba–Cu–O precursor gels annealed at 1050 °C (A), 1100 °C (B), 950 °C (C) and 1000 °C (D). Magnification 170×.

Evidently, the ceramic samples obtained by sintering the Sm–Ba–Cu–O precursor gels at 950, 1000, 1050 and 1100 °C had a similar microstructure to those of the Nd-based samples.

The lattice parameters and orthorhombicity of the $LnBa_2Cu_3O_{7-x}$ superconducting cuprates synthesized at 950 °C and 1000 °C are given in Table I.

TABLE I. Lattice parameters and orthorhombicity, $2(b - a)/(a + b)$, of $LnBa_2Cu_3O_{7-x}$

Sample	Temperature °C	a / Å	b / Å	c / Å	V / Å^3	Orthorhombicity
$HoBa_2Cu_3O_{7-x}$	950	3.855	3.907	11.684	176.0	0.0133
	1000	3.857	3.907	11.680	176.0	0.0129
$NdBa_2Cu_3O_{7-x}$	950	3.868	3.914	11.749	177.9	0.0117
	1000	3.867	3.915	11.753	177.9	0.0122
$SmBa_2Cu_3O_{7-x}$	950	3.889	3.924	11.763	179.5	0.0090
	1000	3.890	3.926	11.761	179.6	0.0092

As can be seen, all the samples crystallized into the orthorhombic Ln-123 phase, indicating that the systems did not tend towards tetragonality on changing the lanthanide ion. Moreover, the lattice parameters and orthorhombicity obtained for the samples containing the same lanthanide ion but synthesized at different temperatures were very similar. Figures 3 and 4 show that the mean values of all lattice parameters of $LnBa_2Cu_3O_{7-x}$ oxides synthesized at 950 and 1000 °C slightly increased with increasing ionic radius of the rare earth element.

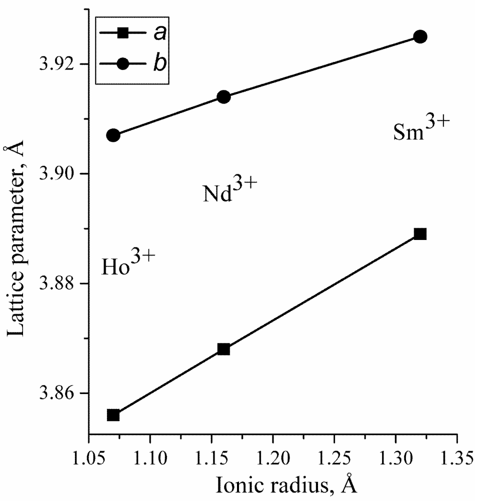

Fig. 3. Lattice parameters (*a* and *b*) as a function of ionic radius.

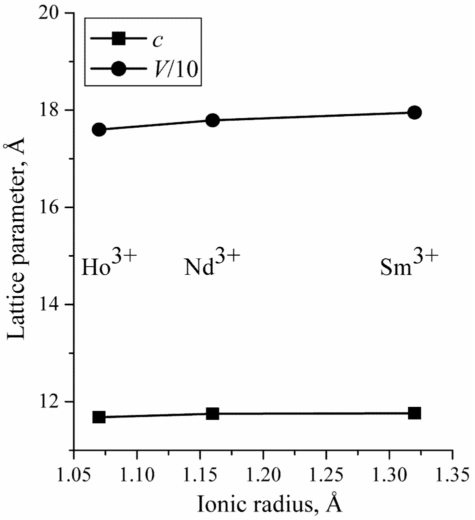

Fig. 4. Lattice parameters (*c* and *V*) as a function of ionic radius.

Figure 5 shows that the orthorhombicity decreased almost linearly with increasing ionic radius of the Ln^{3+} ion.

The orthorhombicity, $2(b - a)/(a + b)$, is a measure of the length difference between the *b*- and *a*-axis, which is related to the occupancy of the oxygen atom sites at O(4) and O(5) in the basal plane, respectively.[9] Therefore, the oxygen content in the superconducting $LnBa_2Cu_3O_{7-x}$ samples was also determined. The results of the determination of the oxygen stoichiometery, x, were used for the calculation of the hole concentration (n_h) in the Cu–O chains. According to the literature,[6] the chain hole concentration is $(7 - x) - 6.5$. The oxygen stoichiometry, hole concentration and T_C values of the $LnBa_2Cu_3O_{7-x}$ superconductors are listed in Table II.

As can be seen, the specimens found to be superconducting had a T_C (onset) of 89, 91 and 93.5 K for $HoBa_2Cu_3O_{7-x}$, $NdBa_2Cu_3O_{7-x}$ and $SmBa_2Cu_3O_{7-x}$, respectively. In addition, it is evident that the obtained parameters (x, n_h, T_C (onset), T_C (zero)) did not depend on the preparation temperature.

Figure 6 shows the T_C (onset) decreased monotonically with decreasing oxygen content in the $LnBa_2Cu_3O_{7-x}$ samples.

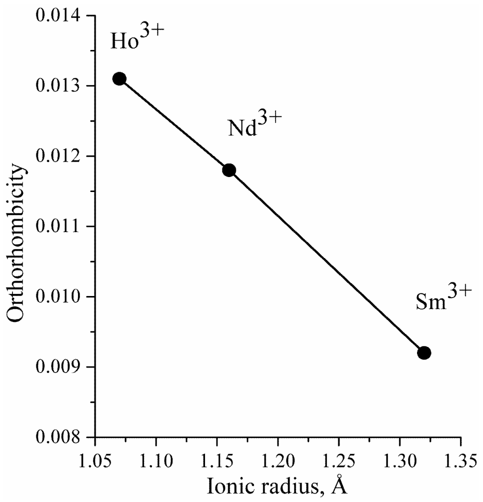

Fig. 5. Correlation between orthorhombicity and ionic radius.

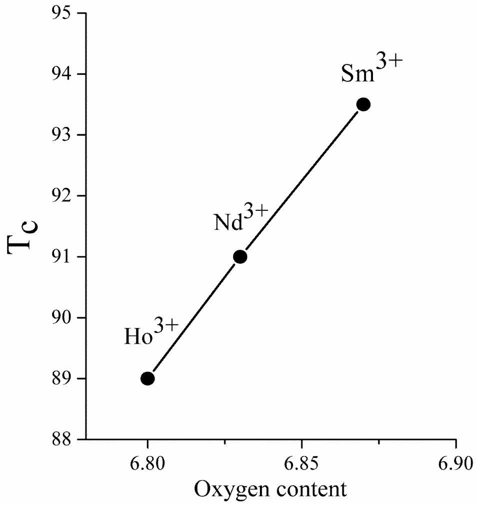

Fig. 6. T_C *vs.* oxygen content for $LnBa_2Cu_3O_{7-x}$ superconducting cuprates.

Similarly, Fig. 7 shows that the correlation between T_C (onset) and the hole concentration in the Cu–O chains had the same trend. T_C (onset) increased from 89 to 93.5 K on increasing n_h from 0.315 to 0.375.

Hence, it can be concluded that the hole carrier density in the sol–gel derived $LnBa_2Cu_3O_{7-x}$ samples corresponded to their optimal values.[19,20] Thus, these results indicate that no underdoping or overdoping effects can be observed in the Ln-123 phases.

The relationship between T_C (onset) and orthorhombicity is plotted in Fig. 8, from which it can be seen T_C decreased with increasing orthorhombicity.

The decrease in T_C with increasing orthorhombicity could be related to electronic transfer from the Cu–O linear chains to the CuO_2 planes.[9,21,22] Therefore, from the obtained results, it can be concluded that in the series of Sm-, Nd- and Ho-substituted Ln-123 samples, the occupancy of the oxygen atom sites at O(4) relatively decreases. On the contrary, the occupancy of oxygen atom at O(5) increased in the range from Sm^{3+} to Ho^{3+}. Only in this case, does the relative difference between the *b* and *a* parameters decrease, resulting in a decrease in the orthorhombicity.

Finally, the T_C (onset) correlated very well with the values of the ionic radius of the lanthanide ions (Fig. 9).

As can be seen from Fig. 9, the T_C value increased linearly with increasing ionic radius, probably indicating the highest hole concentration to be in the $SmBa_2Cu_3O_{7-x}$ sample.

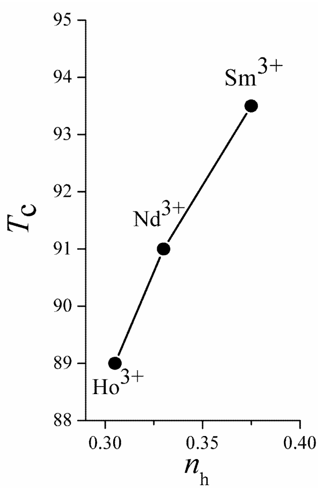

Fig. 7. T_C *vs*. hole concentration for $LnBa_2Cu_3O_{7-x}$ superconducting cuprates.

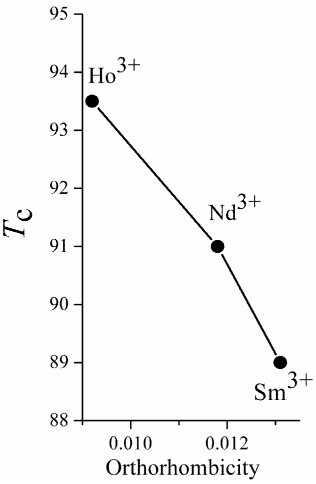

Fig. 8. T_C *vs*. orthorhombicity for $LnBa_2Cu_3O_{7-x}$ superconducting cuprates.

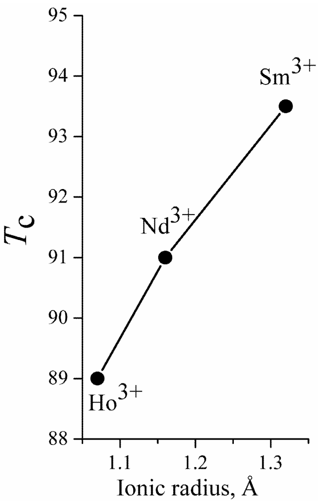

Fig. 9. T_C *vs*. ionic radius of the lanthanide ion for $LnBa_2Cu_3O_{7-x}$ superconducting cuprates.

CONCLUSIONS

The present study demonstrated the versatility of the sol–gel method to yield superconducting $LnBa_2Cu_3O_{7-x}$ (Ln-123) samples. The correlation between the T_C values for different lanthanides (Ln–Ho, Nd and Sm) in the Ln-123 compound and different parameters, such oxygen stoichiometry, hole concentration, orthorhombicity and ionic radius, were investigated. The T_C values of the $LnBa_2Cu_3O_{7-x}$ oxides increased progressively with increasing oxygen content, hole concentration and ionic radius of the lanthanide ion. However, the T_C decreased with increasing orthorhombicity of the Ln-123 phase.

ИЗВОД

СИНТЕЗА И КАРАКТЕРИЗАЦИЈА Ln–123 СУПЕРПРОВОДНИКА

ARTURAS ZALGA[1], REMIGIJUS JUSKENAS[2], ALGIRDAS SELSKIS[2],
DARIUS JASAITIS[1] и AIVARAS KAREIVA[1]

[1]*Faculty of Chemistry, Vilnius University, Naugarduko 24, LT-03225 Vilnius и*
[2]*Institute of Chemistry, A. Gostauto 9, LT-01108 Vilnius, Lithuania*

Сол–гел метода је примењена за припрему полазних једињења при добијању $NdBa_2Cu_3O_{7-x}$ (Nd-123) и $SmBa_2Cu_3O_{7-x}$ (Sm-123) суперпроводних једињења. Синтеровани производи испитивани су анализом дифракције X-зрака (XRD) скенирајућом електронском микроскопијом (SEM). У праховима који су синтеровани на 950 и 1000 °C формирани су монофазни Nd-123 и Sm-123 суперпроводници. Међутим, формирање Nd-123 и Sm-123 фаза из полазних једињења добијених сол–гел поступком на вишим температурама (1050 и 1100 °C) није се одиграло због процеса топљења. Такође је процењен и однос између T_C различитих лантанида (Ln–Ho, Nd и Sm) у једињењу Ln-123 и степена орторомбичности, односно стехиометрије кисеоника.

(Примљено 10. јануара, ревидирано 12. новембра 2007)

REFERENCES

1. O. F. Schilling, *Supercond. Sci. Technol.* **17** (2004) L17
2. L. C. Pathak, S. K. Mishra, *Supercond. Sci. Technol.* **18** (2005) R67
3. J. G. Noudem, E. S. Reddy, M. Tarka, M. Noe, G. J. Schmitz, *Supercond. Sci. Technol.* **14** (2001) 363
4. K. Iida, J. Yoshioka, N. Sakai, M. Murakami, *Physica C* **370** (2002) 53
5. M. Andersson, O. Rapp, Z. Hegedus, T. L. Wen, M. Nygren, *Physica C* **190** (1992) 255
6. R. Nagarajan, C. N. R. Rao, *J. Mater. Chem.* **3** (1993) 969
7. K. Ogasawara, N. Sakai, M. Murakami, *J. Cryst. Growth* **229** (2001) 358
8. E. S. Reddy, G. J. Schmitz, *Supercond. Sci. Technol.* **15** (2002) 727
9. C. H. Chin, H.-C. I. Kao, C. M. Wang, *Mater. Chem. Phys.* **89** (2005)143
10. A. Zalga, E. Matulionis, D. Jasaitis, R. Juskenas, A. Selskis, A. Kareiva, *Env. Chem. Phys.* **25** (2003) 43
11. M. Karppinen, L. Niinisto, H. Yamauchi, *J. Therm. Anal.* **48** (1997) 1123
12. P. Benzi, E. Bottizzo, N. Rizzi, *J. Cryst. Growth* **269** (2004) 625
13. A. N. Christensen, *Acta Chem. Scand.* **46** (1992) 909
14. J. Linden, M. Lippmaa, J. Miettinen, I. Tittonen, T. Katila, A. Kareiva, M. Karppinen, L. Niinistö, J. Valo, M. Leskelä, *Phys. Rev. B* **50** (1994) 4154
15. L. Vilciauskas, A. Beganskiene, A. Kareiva, K. Gibson, P. Ziegler, H.-J. Meyer, *J. Mater. Sci. Lett.* **41** (2006) 579
16. D. C. Harris, T. A. Hewston, *J. Solid State Chem.* **69** (1987) 182
17. P. Lanza, G. Rossi, *Anal. Chim. Acta* **244** (1991) 253
18. A. Kareiva, S. Tautkus, *Chemija* **4** (1997) 58
19. G. Nenartaviciene, A. Beganskiene, S. Tautkus, D. Jasaitis, A. Kareiva, *Chem. Phys.* **332** (2007) 225
20. A. Biju, R. P. Aloysius, U. Syamaprasad, *Mater. Lett.* **61** (2006) 648
21. X. S. Wu, J. Gao, *Physica C* **313** (1999) 79
22. Y. Yasukawa, T. Nakane, M. Karppinen, H. Yamauchi, *Physica C* **357–360** (2001) 230.

Journal of
the Serbian
Chemical Society

JSCS@tmf.bg.ac.yu • www.shd.org.yu/JSCS

J. Serb. Chem. Soc. 73 (4) 487–497 (2008)
JSCS–3730

UDC 66.011+519.22:54–32:546.46–31:66.061
Original scientific paper

Process improvement approach to the acid activation of smectite using factorial and orthogonal central composite design methods

LJILJANA ROŽIĆ*#, TATJANA NOVAKOVIĆ# and SRĐAN PETROVIĆ#

ICTM – Department of Catalysis and Chemical Engineering, Njegoševa 12, Belgrade, Serbia

(Received 4 September, revised 23 November 2007)

Abstract: The purpose of this study was to determine the effective operating parameters and the optimum operating conditions of an acid activation process within the framework of improvement of the process. Full two-level factorial and orthogonal central composite design methods were used successively. The examined parameters were the main and interaction effects of temperature, leaching time, acid normality, solid-to-liquid ratio and stirring rate. The selected process response was the leaching yield of the MgO content because Mg is the element most readily removed from the octahedral sheet, which affects the tendency for activation. Statistical regression analysis and analysis of variance were applied to the experimental data to develop a predictive model, which revealed that temperature, leaching time and acid normality exert the strongest influence on the specific surface area of smectite, whilst the solid-to-liquid ratio and the stirring rate have a secondary effect. Furthermore, the highest leaching yield of MgO was found to be 41.86 %, which is responsible for the increase in the specific surface area of up to 221 $m^2 g^{-1}$.

Keywords: statistical modeling; acid activated smectite; leaching of MgO; specific surface area.

INTRODUCTION

The major clay minerals in bentonites are smectites, such as montmorillonite, beidellite, saponite, nontronite and hectorite.[1]. Bentonites may also contain other clay minerals and non-clay minerals.[2] Bentonite consists predominately of smectite 2:1, a clay mineral containing an octahedral sheet between two tetrahedral sheets. Smectite crystals are negatively charged due to the substitution of the trivalent aluminum ions by ions such as Mg^{2+} and Fe^{3+} and substitution of the tetrahedral Si^{4+} by Al^{3+}.[3]

In the raw state, the clay material generally shows mediocre performance but acid activation improves its textural and adsorptive characteristics. The important

---

* Corresponding author. E-mail: ljrozic@nanosys.ihtm.bg.ac.yu

\# Serbian Chemical Society member.

doi: 10.2298/JSC0804487R

physical changes in acid-activated smectite are the increase of the specific surface area and the average pore volume, depending on the acid strength as well as the time and temperature of treatment.[4,5] Some studies have shown that leaching of octahedral Al^{3+}, Fe^{3+} or Mg^{2+} cations by protons and substitution of exchangeable cations Ca^{2+}, Na^+ or K^+ by the protons of the mineral acid occur and increase with the time of activation of smectite clays.[6,7] Mg is the most readily removed element of the octahedral sheet during activation.[4]

Experiments performed to determine the effect of the independent variables (factors) on the dependent variable (responses) of the process and the relation between them, as illustrated by a regression model obtained utilizing the experimental data. Statistical design of experiments is a well known efficient experimentation technique[8] and has been applied in a wide range of fields, such as the drug and food industry, chemical and biological processes, *etc*., to enable the production of high quality products, to operate the processes more economically and to ensure more stable and reliable processes.

The aim of this study was to determine the highest leaching of MgO from Serbian smectite clay and derive a model for acid activation using a full factorial design.

EXPERIMENTAL

Design of experiments

Factorial design is widely used in statistical planning of experiments to obtain empirical linear models relating process responses to process factors. The 2^n factorial design, where each variable runs at two levels, is often used to obtain first-order models. If the variance analysis indicates that the overall curvature is significant, auxiliary experiments are performed to develop a second-order model. Among the various second-order designs, the orthogonal central composite design is widely used as it only requires $2n$ additional runs.[8,9]

A full factorial design was selected to study the influence of the five relevant factors (n), *i.e.*, temperature, leaching time, acid normality, solid-to-liquid ratio and stirring rate on the leaching yield of MgO from smectite.

The results of the experimental design were studied and interpreted by Design Expert 6.0.6 statistical software to estimate the response of the dependent variable.

Materials

Smectite from Bogovina, Serbia was used as the raw material.

Natural smectite clay (A) with particle sizes of mostly less than 75 μm (200 mesh, ASTM), dried at 383 K, having an average composition, wt. %: SiO_2, 69.12; Al_2O_3, 14.01; Fe_2O_3, 5.43; CaO, 1.62; MgO, 2.57; Na_2O, 1.33; K_2O, 0.66, TiO_2, 0.57; a loss ignition of 4.69 was used as the starting material. The CEC, 78 meq/100 g, was determined by the standard method using 1.0 M NH_4Cl.[10]

Acid activation

The chemical activation was carried out under atmospheric pressure in a jacketed glass reactor equipped with a reflux condenser, a thermometer and a stirrer. A typical run was performed as follows: specified amounts of hydrochloric acid of known concentration and smectite clay were loaded into the glass reactor. The stirring speed was held constant by means of a digitally controlled stirrer. The suspension was cooled in air and filtered off and then washed several times with hot distilled water to remove excess Cl^- and dried to constant weight at 373 K.

Characterization

The contents of the metal cations in the natural clay and the content of major octahedral cations, Mg^{2+}, total Fe and Al^{3+}, in the activated samples were determined by induced coupled plasma (ICP) spectroscopy using a Spectroflame M-Spectro instrument. The percents of the cations removed from the smectite after acid activation are given in Table I.

TABLE I. Quantities of cations removed from smectite by acid treatment, expressed in terms of oxides

Run	Content of oxides, %		
	MgO	Fe_2O_3	Al_2O_3
1	11.98	1.11	2.19
2	17.23	2.58	5.24
3	32.24	16.02	15.87
4	31.95	14.36	17.99
5	13.44	2.39	5.24
6	19.85	6.63	0.07
7	41.86	29.46	24.57
8	29.03	11.42	11.88
9	39.67	18.97	23.77
10	21.89	6.44	6.51
11	6.88	0.37	0.53
12	0.63	0.92	0.80
13	5.87	0.55	0.93
14	37.93	13.44	14.28
15	30.34	18.42	21.31
16	22.04	22.74	26.49
17	25.24	12.34	9.83
18	25.24	12.34	9.83
19	25.24	12.34	9.83
20	17.05	2.72	7.49
21	34.57	13.12	24.30
22	13.01	2.99	7.25
23	15.92	9.99	8.37
24	24.59	9.44	14.18
25	20.29	4.42	9.69
26	24.22	4.65	11.69
27	20.43	3.27	11.69
28	13.51	3.13	5.71
29	36.17	25.60	26.29

X-Ray diffraction patterns of Serbian smectite were obtained using a Philips PW 1710 diffractometer with CuK_α radiation (40 kV, 30 mA, $\lambda = 0.154178$ nm). The diffraction patterns of Serbian smectite before and after activations, for the sample with the highest leaching yield of MgO, are shown in Fig. 1.

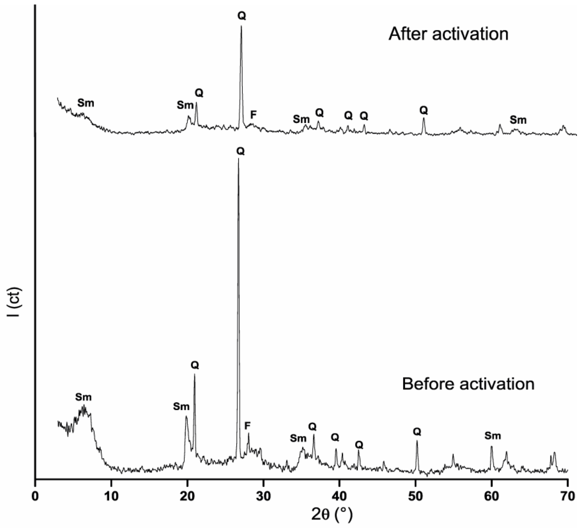

Fig. 1. X-Ray diffraction patterns of natural and acid activated smectite.

Nitrogen adsorption–desorption isotherms were collected on a Sorptomatic 1990 Thermo Finningen surface area and pore size analyzer at 77 K. Prior to adsorption, the samples were outgased overnight at 473 K under a residual pressure of 10^{-2} Pa. The specific surface area was determined by applying the Brunauer–Emmet–Teller (BET) Equation, using 16.3 $Å^2$ for the cross-sectional area of nitrogen.[11] The total pore volumes of the micro pores and meso pores were obtained from the N_2 adsorption at $p/p_0 = 0.98$ expressed in liquid form. The micro-pore volumes were estimated according to the theory of the micro-pore volume filling process and the logarithmic form of the Dubinin–Radushkevich Equation.[12] The pore size distributions were calculated using the Barret–Joyner–Halenda method applied to the parallel pore model.[13] The adsorption branch of the isotherms was taken for the calculation. The desorption branch of the isotherms are not suitable for the determination of the pore size distributions since, during desorption, blocking of nitrogen in the trapped pores occurs.[14]

RESULTS AND DISCUSSION

In order to determine the optimum conditions and derive a model for acid activation of smectite, a full factorial of the type 2^5 was used. The parameters reaction temperature (X_1), hydrochloric acid normality (X_2), stirring speed (X_3), solid-to-liquid ratio (X_4) and reaction time (X_5) were chosen as independent variables and their effect on the leaching yield of MgO from the smectite clay from Serbia was investigated in the light of pre-experiments. The factor levels are shown in Table II.

The matrix for five variables was varied at two levels (+1 and –1). The higher level of variable was designated as "+1" and the lower level as "–1". Initially, a half replicate of the full 2^5 factorial design was used to obtain the first-order model with interaction terms.

As usual, the experiments were performed in random order to avoid systematic error. In addition, three central replicates were added to the experimental plan to calculate the experimental error. The design of the experimental matrix of smectite acid activation and leaching yield of MgO, both the experimental and the predicted values, calculated by Eq. (2), are presented in Table III.

TABLE II. Factor levels used in the experiments

Factor	Physical quantity	Low level (–)	Medium level (0)	High level (+)
X_1	Temperature, K	343	353	363
X_2	HCl concentration, mol dm^{-3}	3.0	4.5	6.0
X_3	Stirring speed, rpm	300	450	600
X_4	Solid/liquid ratio	1:3	1:4	1:6
X_5	Time, h	1	2	3

TABLE III. Experimental design and leaching yields of MgO

Run	X_1	X_2	X_3	X_4	X_5	MgO content, %	
						Experimental	Predicted
1	–1	1	–1	1	1	6.88	7.34
2	–1	–1	1	1	1	11.98	11.28
3	1	1	–1	1	–1	29.03	29.41
4	–1	–1	1	–1	–1	37.93	37.91
5	1	–1	1	1	–1	21.89	21.11
6	1	–1	1	–1	1	30.34	30.55
7	1	1	1	1	1	41.86	41.18
8	–1	1	–1	–1	–1	0.63	1.77
9	1	1	1	–1	–1	31.95	33.20
10	1	1	–1	–1	1	39.67	41.04
11	–1	1	1	–1	1	5.87	6.10
12	–1	1	1	1	–1	19.85	20.35
13	–1	–1	–1	1	–1	20.00	19.33
14	1	–1	–1	1	1	32.24	30.40
15	–1	–1	–1	–1	1	13.44	12.51
16	1	–1	–1	–1	–1	17.23	17.32
17	0	0	0	0	0	25.24	22.97
18	0	0	0	0	0	25.24	22.97
19	0	0	0	0	0	25.24	22.97

The response was expressed as mass % leaching yield of MgO, calculated as $((c_0-c)/c_0)\times 100$ where c_0 is the initial concentration of MgO and c is the final concentration of MgO. Initially, a first order model with interaction terms was chosen to fit the experimental data:

$$y = b_0 + \sum_{i=1}^{5} b_i x_i + \sum_{i=1}^{5} \sum_{j\geq 1}^{5} b_{ij} x_i x_j \tag{1}$$

The first-order model obtained by variance analysis conducted at the 95 % confidence level is:

$$\begin{aligned} y_{\mathrm{MgO}} = {} & 22.55 + 7.98X_1 + 2.66X_3 + 5.68X_1X_2 - 1.68X_1X_3 + 5.27X_1X_5 \\ & + 2.02X_2X_4 + 1.37X_2X_5 - 1.73X_3X_4 - 2.93X_3X_5 \end{aligned} \tag{2}$$

Analysis of the variance detected a curvature effect. Since the analysis of variance revealed that quadratic terms were effective, the orthogonal central composite design was applied to separately estimate the quadratic terms. With $F = 16$ (the number of experimental design), $m_0 = 3$ (the number of central replicates) and $n = 5$ (the number of factors), β was calculated as 1.6644 according to relation:[11]

$$\beta = \left(\frac{QF}{4}\right)^{0.25}; \quad Q = \left(N^{0.5} - F^{0.5}\right)^2; \quad N = 2n + F + m_0 \tag{3}$$

and the new factor levels ($-\beta$,$+\beta$) are given in Table IV, where some variable levels were rounded based on the sensitivity of the equipment employed.

TABLE IV. Auxiliary factor levels used in the central composite design

Factor	Physical quantity	Low level ($-\beta$)	Medium level (0)	High level ($+\beta$)
X_1	Temperature, K	336	353	370
X_2	HCl concentration, mol dm^{-3}	2.0	4.5	7.0
X_3	Stirring speed, rpm	200	450	700
X_4	Solid/liquid ratio	1:2.3	1:4	1:7.3
X_5	Time, h	0.336	2	3.66

The design matrix and the results of the auxiliary experiments carried out to calculate the second order model parameters are given in Table V. The second-order model is defined in its usual form as:

$$y = b_0' + \sum_{i=1}^{5} b_i x_i + \sum_{i=1}^{5} b_{ii} x_i^2 + \sum_{i=1}^{5}\sum_{j>1}^{5} b_{ij} x_i x_j \tag{4}$$

where $b_0' = b_0 - \sum_{i=1}^{5} b_{ij}\bar{x}_i^2$, and $\bar{x}_i^2 = \frac{1}{N}\sum_{i=1}^{n} x_i^2 = \frac{F + 2\beta^2}{N}$.

TABLE V. Experimental design for the second-order model and the leaching yields of MgO

Run	X_1	X_2	X_3	X_4	X_5	MgO content, %.	
						Experimental	Predicted
20	+1.664	0	0	0	0	17.05	14.85
21	–1.664	0	0	0	0	34.57	38.76
22	0	+1.664	0	0	0	13.01	15.96
23	0	–1.664	0	0	0	15.92	14.96
24	0	0	+1.664	0	0	24.59	20.86
25	0	0	–1.664	0	0	20.29	26.01
26	0	0	0	+1.664	0	24.22	23.13
27	0	0	0	–1.644	0	20.43	23.50
28	0	0	0	0	+1.664	13.51	22.79
29	0	0	0	0	–1.664	36.17	28.88

The second-order model tested at the 95 % confidence level is as follows:

$$y_{\mathrm{MgO}} = 23.56 + 7.18X_1 - 0.30X_2 + 1.55X_3 + 0.11X_4 + \\ +1.83X_5 + 1.10X_1^2 - 3.00X_2^2 + 0.75X_5^2 + 5.81X_1X_2 + \\ +5.39X_1X_5 + 1.89X_2X_4 + 1.49X_2X_5 - 1.86X_3X_4 \quad (5)$$

From the statistical analysis, the temperature, stirring rate, liquid/solid ratio and time have positive effects, whereas the HCl concentration has a negative effect on the leaching yield of MgO, as can be seen from Eq. (5). Also, the interaction effects between temperature and HCl concentration, temperature and time, HCl concentration and liquid/solid ratio, HCl concentration and time, stirring rate and liquid/solid ratio, were found to be significant.

Residual analysis is a valuable tool to detect the existence of systematic errors. The normalized residual is defined as:

ε = (experimental value – model value)/standard deviation

For a well-established model, systematic errors are absent and the normalized residuals result from experimental error which exhibit a normal distribution according to a widely accepted statistical convention.[9]

The test graphics are shown in Fig. 2, which supports the reliability of the model, Eq. (5).

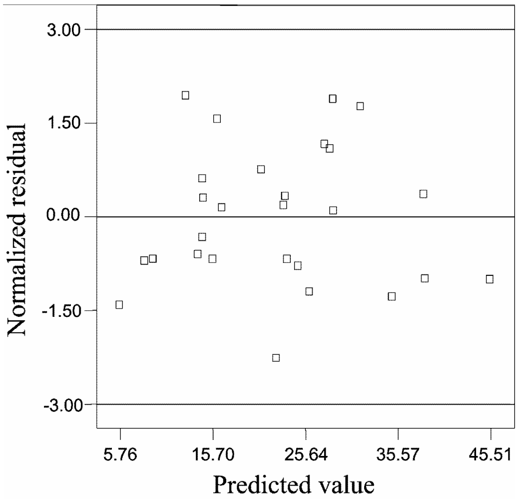

Fig. 2. Test graphics.

Also, the graphs of the residuals *vs.* the individual factors are presented in Fig. 3. The residual plot shows an equal scatter of the residual data above and below the *x*-axis for all the individual factors (temperature, HCl concentration, stirring rate, liquid/solid ratio and time), which indicates that the data are dependent on the model.

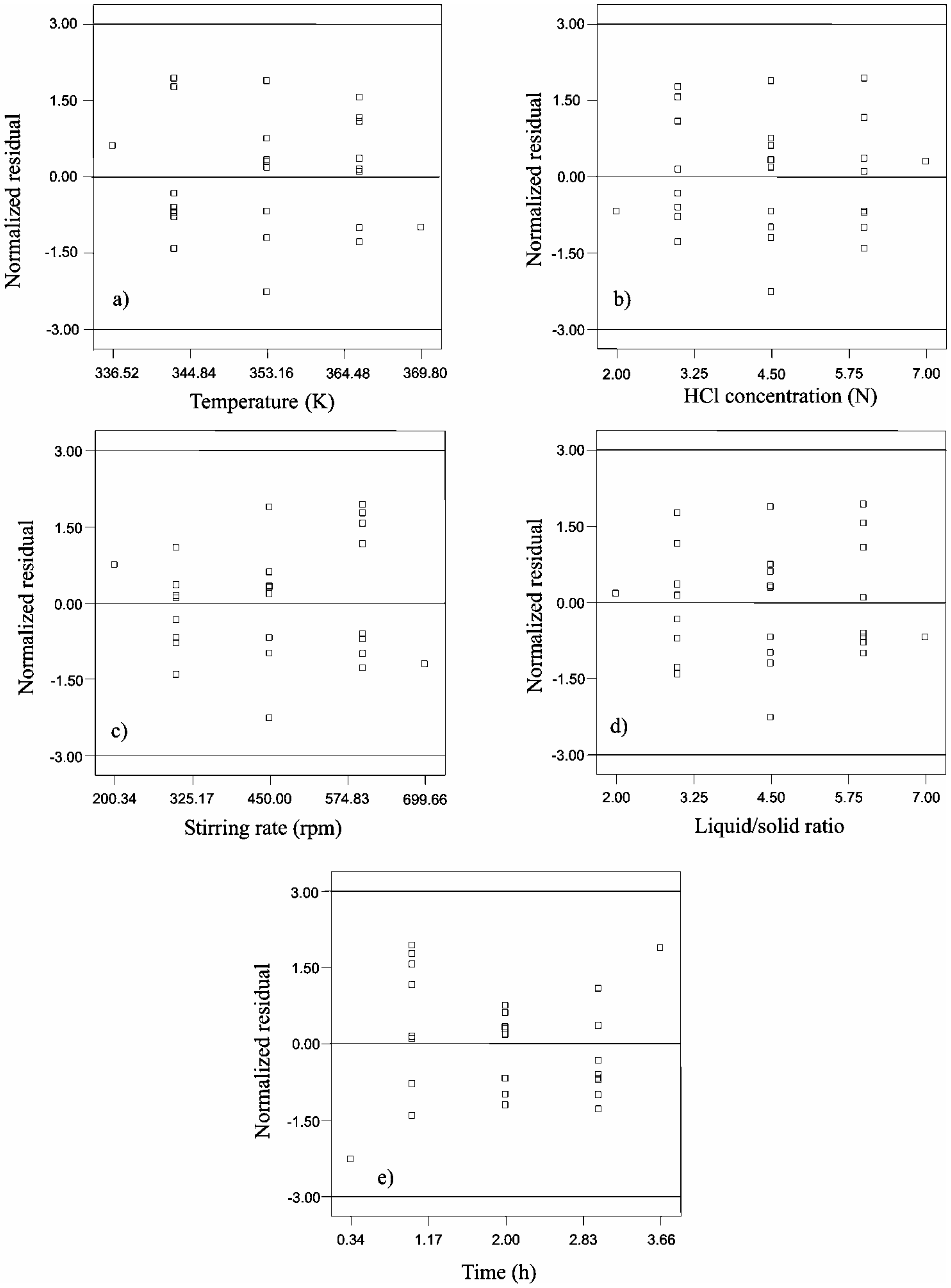

Fig. 3. The graphs of the residuals *vs.* the individual factors.

The highest leaching yield of MgO was obtained at 363 K, 6.0 M HCl, 600 rpm, a solid-to-liquid ratio of 1:6 and a process duration of 3 h. The lowest leaching yield of MgO was obtained at 343 K, 6.0 M HCl, 300 rpm, a solid-to-liquid ratio of 1:3 and a process duration of 1 h. When the second order model, Eq. (5), and the first order model, Eq. (2), are compared, it can be seen that X_2 (acid concentration), X_4 (solid to liquid ratio) and X_5 (time) are significant in the second order model. For the first order model, the low level of acid concentration, the solid to liquid ratio and the reaction time are 3.0 M, 1:3 and 1 h, respectively, while for the second order model, they are 2.0 M, 1:2.3 and 0.336 h, respectively.

It appears that the leaching yield is significantly dependent on the acid concentration of 2.0 M HCl and the reaction time, especially during the first twenty min.

Natural smectite has a relatively underdeveloped micro pore volume, total porosity and specific surface area, as measured by nitrogen adsorption (Table VI).

TABLE VI. Pore structure parameters for natural and acid-activated smectite

Run	S_{BET} / m^2 g^{-1}	$\Sigma V_{0.98}$ / cm^3 g^{-1}	d / nm	V_{mic} / cm^3 g^{-1}
1	138	0.125	3.8	0.061
2	159	0.143	2.4	0.066
3	218	0.255	3.6	0.090
4	154	0.136	2.2	0.066
5	121	0.110	4.0	0.053
6	125	0.128	3.8	0.054
7	222	0.207	3.6	0.096
8	162	0.163	3.8	0.068
9	210	0.272	1.8	0.085
10	113	0.138	1.9	0.055
11	117	0.131	2.0	0.051
12	73	0.092	1.8	0.033
13	110	0.128	3.8	0.052
14	54	0.069	3.8	0.024
15	177	0.212	3.6	0.076
16	62	0.075	3.8	0.029
17	153	0.158	2.3	0.065
18	153	0.158	2.3	0.065
19	153	0.158	2.3	0.065
20	69	0.078	3.9	0.033
21	157	0.182	3.6	0.068
22	87	0.087	3.8	0.042
23	121	0.131	3.7	0.056
24	142	0.133	3.8	0.060
25	127	0.124	3.7	0.054
26	148	0.144	3.7	0.062
27	143	0.136	3.7	0.059
28	104	0.101	3.9	0.048
29	192	0.212	3.6	0.077
Natural smectite	63	0.071	4.1	0.028

Acid treatment of the samples contributed to their adsorption capacity. As can be seen in the Table VI, the specific surface area and the textural properties of the acid activated smectite were strongly affected by the processes parameters.

The specific surface area, total pore volume and micro pore volume attained a maximum for sample 7. This indicates that the observed chemical and structural changes after treatment with 6.0 M HCl, at 363 K during 3 h caused an alteration of the morphology and, consequently, of the adsorption properties of the smectite samples. The pore size analysis showed that the natural clay had a wide pore size distribution with a mean pore diameter of 4.1 nm. The acid-activated samples had a greater increase of the pore volume of the micro- and meso-pores and this resulted in a lower value of the average pore diameter, compared to that of natural clay (Table VI). These changes of the pore structure are a result of removal of exchangeable cations and impurities from the clay by HCl.

CONCLUSIONS

The process improvement approach to the acid activation of smectite clay from Serbia was investigated by means of the full factorial design. The recovery of the Mg content from natural smectite, as a process response, was determined with respect to temperature, leaching time, acid normality, solid-to-liquid ratio and stirring rate. Initially, the 2^5 full factorial design was used to obtain a first-order model with interaction terms. Based on the results of the analysis of the variance, it was necessary to conduct auxiliary experiments using an orthogonal central composite design to obtain a second-order model relating the MgO leaching yield to the experimental variables.

The highest leaching yields of MgO were obtained at 363 K, 6.0 M HCl, 600 rpm, solid-to-liquid ratio 1:6 and a process duration of 3 h.

The specific surface area and the textural properties of acid activated smectite were strongly affected by the processes parameters. Pore size analysis showed that the acid-activated samples had a greater increase of the pore volume of the micro- and meso-pores, which resulted in a lower value of the average pore diameter, compared to that of natural clay. These changes of the pore structure are the result of removal of exchangeable cations and impurities from the clay by HCl.

The obtained results may provide a background for pilot and industrial scale applications.

Acknowledgments. This work was supported by the Ministry of Science of the Republic of Serbia (Projects numbers TR 6712B and ON 142019)

ИЗВОД

ФАКТОРИЈАЛНИ И ОРТОГОНАЛНО ЦЕНТРАЛНО КОМПОЗИТНИ ПЛАН ЕКСПЕРИМЕНТА КИСЕЛИНСКЕ АКТИВАЦИЈЕ СМЕКТИТА

ЉИЉАНА РОЖИЋ, ТАТЈАНА НОВАКОВИЋ и СРЂАН ПЕТРОВИЋ

ИХТМ – Центар за катализу и хемијско инжењерство, Његошева 12, Београд

Сврха овог рада била је одређивање ефективних процесних параметара и оптималних процесних услова киселинске активације смектита из Србије. Успешно су коришћене две методе математичког моделовања: пун факторијални и ортогонални централни композитни план

експеримента. При оптималном планирању експеримента истовремено се мењају сви параметри који утичу на процес, што нам омогућава одређивање њиховог међусобног утицаја и смањење укупног броја експеримената. Током планирања експеримената разматран је утицај следећих релевантних параметара: температуре, времена активације, концентрације киселине, односа течно/чврсто и броја обртаја мешалице, на степен издвајања магнезијум-оксида. Резултати оптимизације параметара киселинске активације смектита, на бази статистичких планова експеримента, показали су да концентрација киселине, температура и време активације имају најјачи утицај на промену специфичне површине смектита, док однос течно/чврсто и број обртаја мешалице имају секундарни ефекат. Максимални степен издвајања магнезијум-оксида од 41,86 % узрокује и највећи пораст специфичне површине до 221 $m^2 g^{-1}$.

(Примљено 4. септембра, ревидирано 23. новембра 2007)

REFERENCES

1. R. E. Grim, G. Güven, *Bentonites: Geology, Minerology, Properties and Uses, Development in Sedimentology Vol. 24*, Elsevier, Amsterdam, 1978
2. D. M. Moore, R. C. Reynolds Jr., *X-ray Diffraction and the Identification and Analysis of Clay Minerals*, Oxford University Press, New York, 1997
3. H. H. Murray, *Clay Miner.* **34** (1999) 39
4. G. E. Christidis, P. W. Scott, A. C. Dunham, *Appl. Clay Sci.* **12** (1997) 329
5. C. N. Rhodes, D. R. Brown, *J. Royal Soc. Chem. Faraday Trans.* **88** (1992) 2269
6. C. K. Lee, K. S. Low, P. Y. Gan, *J. Chem. Technol. Biotechnol.* **69** (1998) 93
7. M. Rossi, M. Gianazza, C. Alamprese, F. Stanga, *Food Chem.* **82** (2003) 291
8. Ž. Lazić, *Design of Experiments in Chemical Engineering*, Wiley-VCH Verlag GmbH & Co. KGaA, Weinheim, 2004, p. 157
9. E. Şayan, M. Bayramoğlu, *Hydrometallurgy* **57** (2000) 181
10. H. D. Chapman, in *Methods of Soil Analysis: Chemical and Microbiological Properties, Part 2*, C. A. Black, Ed., American Society of Agronomy, Madison, WI, 1965, p. 891
11. S. H. Gregg, K. S. Sing, *Adsorption, Surface Area and Porosity*, Academic Press, New York, 1967, p. 124
12. M. M. Dubinin, *Prog. Surf. Membrane Sci.* **9** (1975) 1
13. E. P. Barrett, L. G. Joyner, P. H. Halenda, *J. Am. Chem. Soc.* **73** (1951) 373.

JSCS@tmf.bg.ac.yu • www.shd.org.yu/JSCS

J. Serb. Chem. Soc. 73 (4) 499–506 (2008) UDC 536.7.001.2:546.82'62'711:681.3.06:536.7
JSCS–3731 *Original scientific paper*

Thermodynamic calculations in ternary titanium–aluminium–manganese system

ANA I. KOSTOV[1]* and DRAGANA T. ŽIVKOVIĆ[2]#

[1]*Copper Institute Bor, Zeleni bulevar 35, 19210 Bor and* [2]*University of Belgrade, Technical Faculty Bor, VJ 12, 19210 Bor, Serbia*

(Received 24 May, revised 15 October 2007)

Abstract: Thermodynamic calculations in the ternary Ti–Al–Mn system are shown in this paper. The thermodynamic calculations were performed using the FactSage thermochemical software and database, with the aim of determining thermodynamic properties, such as activities, coefficient of activities, partial and integral values of the enthalpies and Gibbs energies of mixing and excess energies at two different temperatures: 2000 and 2100 K. Bearing in mind that no experimental data for the Ti–Al–Mn ternary system have been obtained or reported. The obtained results represent a good base for further thermodynamic analysis and may be useful as a comparison with some future critical experimental results and thermodynamic optimization of this system.

Keywords: thermodynamic calculations; Ti–Al–Mn ternary system; FactSage thermochemical software and database.

INTRODUCTION

Due to the combination of lightweight and high strength, titanium-based alloys are of practical interest for the aerospace and automotive industries, as well as for various high temperature applications. Alloys with lower contents of aluminium are brittle and provide moderate resistance to oxidation, however alloying with manganese enhance their ductility and strength, as well as their oxidation and corrosion resistance. Nevertheless, a thermodynamic study of the Ti–Al–Mn system has not been completely reported in the literature.

Ti-based alloys were one of the first types of materials to which thermodynamic phase diagram calculation were applied. However, the early limitations in modelling, particularly with respect to the uptake of elements such as oxygen and nitrogen, restricted their use.[1] It is almost 30 years since a detailed presentation of thermodynamic phase diagram calculations for titanium alloys was made

---

* Corresponding author. E-mail: kostov2004@yahoo.com

\# Serbian Chemical Society member.

doi: 10.2298/JSC0804499K

by Kaufman and Nesor[2] at the 2nd World Conference on titanium. They presented a series of computer calculated phase diagrams for Ti-based alloys and even included an early calculation for the Ti–Al system. Since then substantial advances have been made in terms of theoretical models, computer software and hardware and it is now possible to deal with extremely complex materials on a routine basis.[1]

Kaufman and Nesor[2] showed that some binary and ternary phase diagrams of Ti alloys, in particular the beta isomorphous systems, such as Ti–V and Ti–Nb, could be reasonably represented by simple regular and sub-regular models. However, the combination of the chemical affinity of Ti for light elements, such as O, C and N, and their powerful influence on phase equilibria means that even a simple alloy such as Ti–6Al–4V should be considered as a six-component system. Although Kaufman and Clougherty[3] produced a calculated diagram for Ti–O, this work was not generally extended to produce a database which could handle multi-component alloys with the requisite of O, C and N additions.

In studies by Gros, Ansara and Allibert[4] and Lee,[5] CALPHAD methods were employed for predicting phase equilibria in Ti alloys. Gros[4] published a thermodynamic assessment of the phase equilibria between liquid, β-Ti, α-Ti and α2-Ti3Al phases in the Ti-rich region of the diagram. The Gibbs energies of both the ordered α2-Ti3Al and disordered α-Ti phases were described by a unified two-sublattice model. However, the models used in both papers lack the necessary uptake of light elements, which could easily lead to differences between the experimental and observed T^{β} of up to 60–80 °C. Murray[6] also applied the same unified formalism to the Gibbs energy of the three ordered phases, while Ohnuma[7] experimentally studied the phase equilibria between the Ti-rich solid phases, which were determined on specimens with carefully controlled low levels of oxygen contamination.

The roots of the CALPHAD approach lie in the mathematical description of the thermodynamic properties of the phases of interest. If they are stoichiometric compounds, the composition is defined and a mathematical formula is then used to describe fundamental properties, such as enthalpy and entropy. Where phases exist over a wide range of stoichiometries, which is usually the case for metallic materials, other mathematical models were used which take into account the effect of compositional changes on the free energy. Details of the modelling procedures can be found in a review of Ansara.[8] All types of models require the input of coefficients that uniquely describe the properties of the various phases and these coefficients are held in databases, which either are in the open literature or are proprietary.

Kattner and Boettinger[9] attempted one of the first extensions of ternaries to the Ti–Al–Nb system. However, although the form of their diagram is reasonable, they did not take into consideration the effect of the ordering of the β phase on the structure of B2 CsCl, which has been observed in almost all Ti–Al–X systems, where X is one of the refractory metals, such as Nb and V. Work by Saunders[10] on a series of Ti–Al–X ternaries, where X = Cr, Mn, Mo, Nb or V, showed the importance of including this ordering for an accurate representation of the phase equilibria and it is of particular interest to be able to differentiate between the ordered and disordered form when considering mechanical properties. At the end of this survey, we mention the work of Jingqi,[11] concerning a thermodynamic analysis of the Gd–Mn–Ti system by X-ray powder diffraction and differential thermal analysis in the isothermal section at 773 K should be mentioned.

Bearing in mind such problems, it could be anticipated that most of the thermodynamic data of ternary and multi-component systems would come from theoretical calculations rather than from direct experimentation. The main reasons are the experimental difficulties, especially the high investigation temperatures required. It is clear that mostly solid alloys and their thermodynamic behaviour have been researched. For this reason, this paper presents the results of thermodynamic calculations of liquid Ti–Al–Mn alloys using FactSage thermochemical software and database.[12]

CALCULATION PROCEDURE

Thermodynamic calculations and predicting of the ternary Ti–Al–Mn system have been done using FactSage thermochemical software and database.[12]

FactSage was introduced in 2001 and is a fusion of the FACT-Win/F*A*C*T and ChemSage/SOLGASMIX thermochemical packages, which were developed over 25 years ago. The FactSage package consists of a series of information, database, calculation and manipulation modules, which enable access to and manipulation of pure substances and solution databases. With the various modules, a wide variety of thermochemical calculations can be performed and tables, graphs and figures of interest to chemical and physical metallurgists, chemical engineers, inorganic chemists, geochemists, ceramists, electrochemists, environmentalists, *etc*., to be generated.

The FactSage package offers access to the modules of the package, which are grouped into four categories:

1. Info – this includes detailed slide shows of most of the program modules and general information with frequently asked questions on FactSage and its databases.

2. Databases – these program modules enable the user to view, manipulate and edit the pure substances and solution databases, which may be private (read/write) or public (read only).

Calculate – these modules are the central programs of FactSage. They permit the calculation of phase diagrams and thermochemical equilibria in various forms with direct access to the databases.

3. Manipulate – this group offers various graphical and tabular program modules for post-processing the results and manipulating the calculated phase diagrams and other figures.

In this study, the Calculate modules performed all the calculations.

The Calculate modules are the heart of FactSage. One can interact with the software and databases in a variety of ways and calculate thermochemical equilibria in various forms. They consist of a Reaction module, Predom and EpH modules, an Equilib module, Phase diagram and Figure modules.

The Reaction module calculates changes in extensive thermochemical properties (enthalpy, Gibbs energy, entropy, *etc.*) for a single species, a mixture of species or for a chemical reaction. The species may be pure elements, stoichiometric compounds or ions (both plasma and aqueous ions).

With the Predom module, isothermal predominance area diagrams for one-, two- or three--metal systems can be calculated and plotted using data retrieved from the compound databases.

The EpH module is similar to the Predom module and permits the generation of E_h *vs.* pH (Pourbaix) diagrams for one-, two- or three-metal systems using data retrieved from the compound databases, which also include infinitely dilute aqueous data.

The Equilib module is the Gibbs energy minimization workhorse of FactSage. It calculates the concentrations of chemical species when specified elements or compounds react or partially react to reach a state of chemical equilibrium.

The Phase diagram and Figure modules is a generalized module which permits the calculation, plotting and editing of unary, binary, ternary and multi-component phase diagram sections, whereby the axes can be various combinations of temperature, pressure, volume, composition, activity, chemical potential, *etc*. The resulting phase diagram is automatically plotted by the Figure module.

In this study, calculations within the Reaction, Equilib, Phase diagram and Figure modules were performed.

The thermodynamic calculations of the Ti–Al–Mn ternary system were carried out from each corner using 15 cross-sections in total. The compositions of all investigated cross-sections are given in Table I.

TABLE I. Composition of the ternary alloys in the investigated sections

Cross-section	A	B	C	D	E
x_{Al}:x_{Mn}	9:1	7:3	5:5	3:7	1:9
x_{Ti}:x_{Mn}	9:1	7:3	5:5	3:7	1:9
x_{Ti}:x_{Al}	9:1	7:3	5:5	3:7	1:9

RESULTS AND DISCUSSION

The thermodynamic properties of the ternary system Ti–Al–Mn were calculated using FactSage at 2000 and 2100 K. The phase diagrams of Al–Mn and Ti–Mn binary systems, as constitutive binaries of the ternary systems Ti–Al–Mn, were calculated by FactSage and are shown in Figs. 1 and 2, respectively.

Activity values in the investigated Ti–Al–Mn ternary system from titanium, aluminium and manganese at 2000 and 2100 K are shown in Figs. 3–8, respectively.

The binaries Ti–Al and Al–Mn have negative values for the integral excess Gibbs energy, while the Ti–Mn system has positive values, considering that Al was selected as the symmetrical component by some others and different models for thermodynamic prediction.

The enthalpies of mixing values indicate that the strongest chemical interaction between the components in the investigated Ti–Al–Mn ternary system exist between aluminium and manganese and the weakest between titanium and manganese.

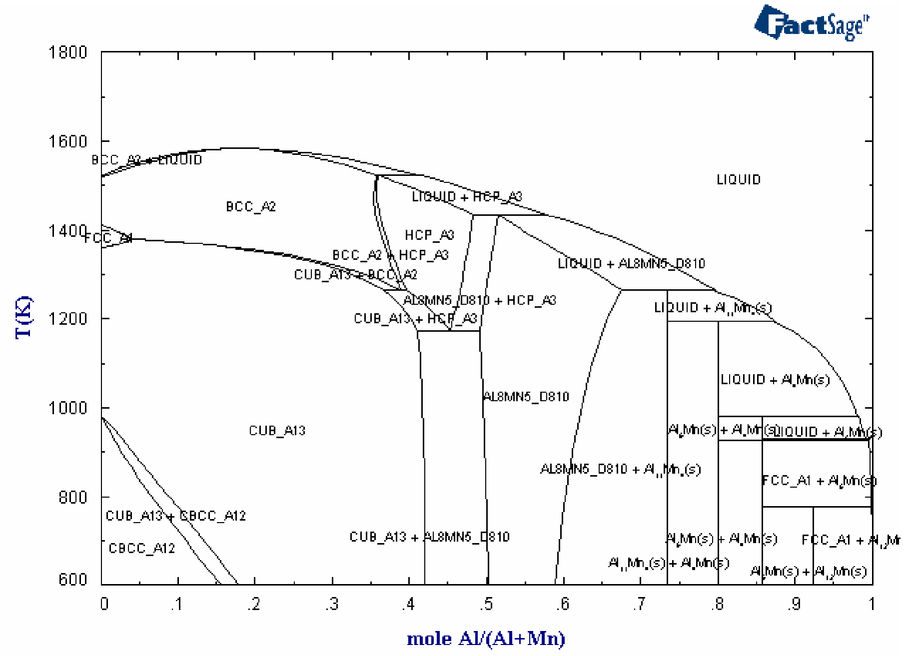

Fig. 1.Al–Mn phase diagram.

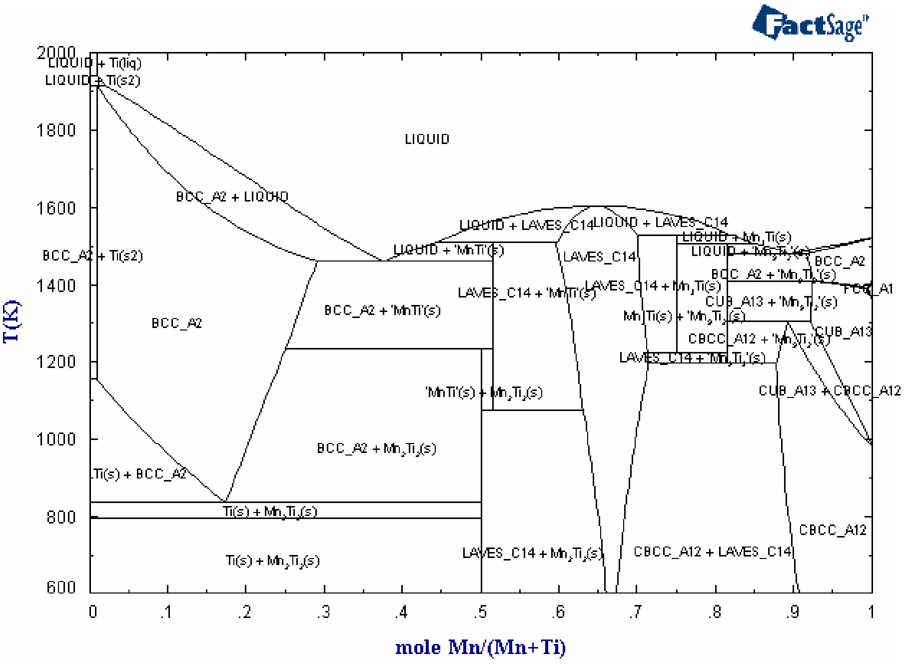

Fig. 2. Mn–Ti phase diagram.

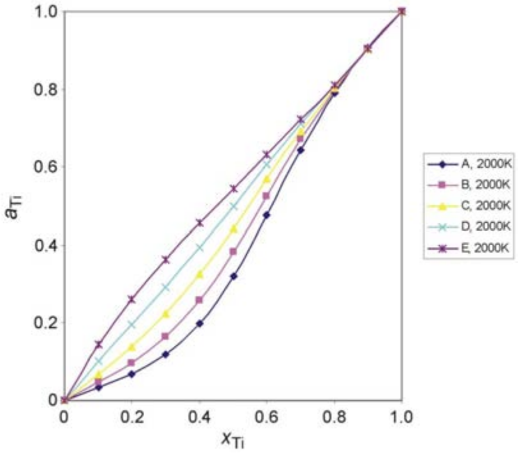

Fig. 3. Activity of titanium in Ti–Al–Mn at 2000 K.

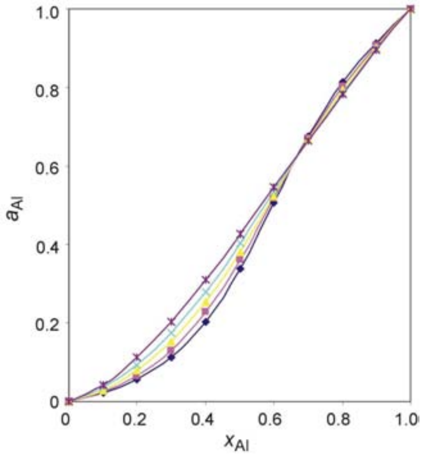

Fig. 4. Activity of aluminium in Ti–Al–Mn at 2000 K.

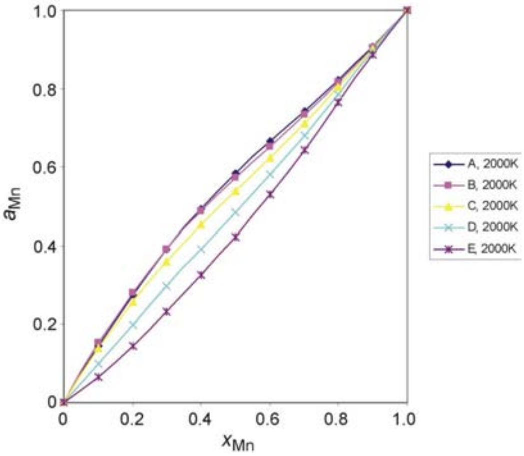

Fig. 5. Activity of manganese in Ti–Al–Mn at 2000 K.

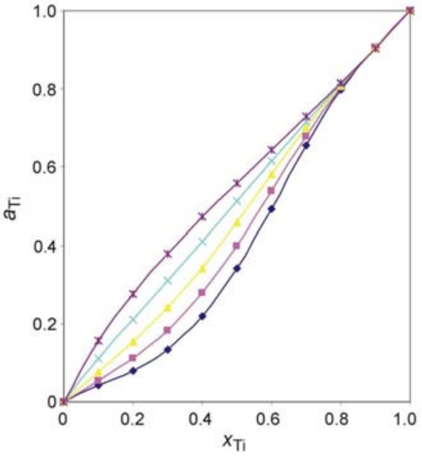

Fig. 6. Activity of titanium in Ti–Al–Mn at 2100 K.

In the case of the investigated sections from the aluminium corner, the enthalpy of mixing values are strongly affected by the Ti–Mn binary system. The activity values of titanium decrease and the activity values of manganese increase proportionally in the Ti–Al and Al–Mn systems, while those of aluminium decrease with increasing titanium content and increase with increasing manganese content, as would be expected for behaviour according to the Raoult law.

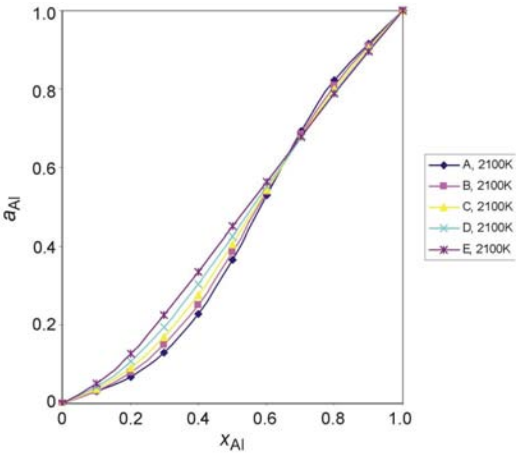

Fig. 7. Activity of aluminium in Ti–Al–Mn at 2100 K.

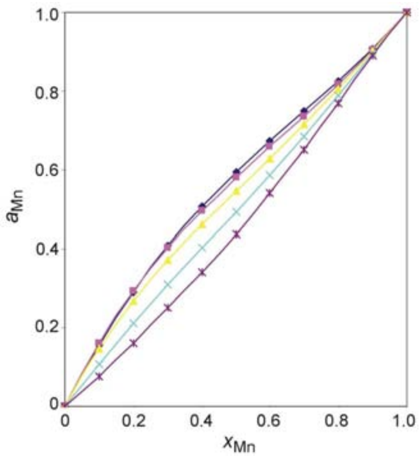

Fig. 8. Activity of manganese in Ti–Al–Mn at 2100 K.

CONCLUSIONS

The thermodynamic properties of the ternary system Ti–Al–Mn at 2000 and 2100 K were calculated using FactSage thermochemical software and databases.

Bearing in mind that no experimental data for the Ti–Al–Mn ternary system have been obtained or reported, the presented results are a good base for further thermodynamic analysis, which will involve a comparative study of the thermodynamic properties of liquid alloys based on different thermodynamic predicting methods.

The obtained thermodynamic data may be useful as a comparison with some future critical experimental results and for the further thermodynamic optimization of this system, as well as to show the possibility of the application of the employed software for the thermodynamic description of the investigated system.

Acknowledgement. The first author would like to thank the Alexander von Humboldt Foundation, Bonn, Germany, for supporting and sponsoring this research work at the IME Institute for Process Metallurgy and Metal Recycling, RWTH Aachen, Germany.

ИЗВОД

ТЕРМОДИНАМИЧКИ ПРОРАЧУНИ У ТЕРНАРНОМ СИСТЕМУ ТИТАН–АЛУМИНИЈУМ–МАНГАН

АНА И. КОСТОВ[1] и ДРАГАНА Т. ЖИВКОВИЋ[2]

[1]*Институт за бакар Бор, Зелени булевар 35, 19210 Бор* и [2]*Универзитет у Београду, Технички факултет Бор, ВЈ 12, 19210 Бор*

У овом раду приказани су резултати термодинамичких прорачуна у тернарном систему Ti–Al–Mn. FactSage термохемијски софтвер и база података коришћени су за све прорачуне у овом систему у циљу дефинисања термодинамичких величина стања као што су актив-

ности, коефицијенти активности, парцијалне и интегралне вредности за Гибсове енргије мешања и Гибсове енергије у вишку на двема различитим температурама: 2000 и 2100 K. У досадашњој литератури нема публикованих експерименталних података везаних за термодинамичке прорачуне у испитиваном систему, јер се ради о високотемператуном систему. Зато добијени резултати представљају једну добру полазну базу за сваку даљу термодинамичку анализу и могу бити од користи за поређења са неким будућим критичним експерименталним резултатима, као и у термодинамичкој оптимизацији наведеног ситема.

(Примљено 24. маја, ревидирано 15. октобра 2007)

REFERENCES

1. N. Saunders, *Titanium '95: Science and Technology*, P. Bleckinsop, W. J. Evans, H. M. Flower, Eds., Institute of Materials, London, 1996, p. 2167
2. L. Kaufman, H. Nesor, *Calphad* **2** (1978) 325
3. L. Kaufman, Clougherty, *Metallurgy at High Pressures and High Temperatures*, in *AIME Met. Soc. Conf.*, Vol. 22, Gordon and Breach, New York, 1964, p. 322
4. J. P. Gros, I. Ansara, M. Allibert, in *Proceeding of 6th World Conference on Titanium,* Vol. III, P. Lacombe, R. Tricot, G. Beranger, Eds., Les Editions de Physique, Paris, 1989, p. 1553
5. H. M. Lee, J.-R. Soh, Z.-H. Lee, Y.-S. Kim, *Scripta Met.* **29** (1993) 497
6. J. L. Murray, *Metall. Trans. A* **9** (1988) 243
7. I. Ohnuma, Y. Fujita, H. Mitsui, K. Ishikawa, R. Kainuma, K. Ishida, *Acta Mater.* **48** (2000) 3113
8. I. Ansara, *Int. Met. Rev.* **22** (1979) 20
9. U. R. Kattner, W. J. Boettinger, *Mater. Sci. Eng.* **A152** (1992) 9
10. N. Saunders, *CALPHAD XXIV*, Kyoto, Japan, 1995, p. 21
11. L. Jingqi, Q. Jiqin, D. Ren, Z. Yinghong, H. Jinli, *J. Alloys Comp.* **414** (2006) 97
12. C. W. Bale, P. Chartrand, S. A. Degterov, G. Eriksson, K. Hack, R. B. Mahfoud, J. Melancon, A. D. Pelton, S. Petersen, *Calphad* **26** (2002) 189.

Journal of the Serbian Chemical Society
www.shd.org.yu
JSCS@tmf.bg.ac.yu • www.shd.org.yu/JSCS
J. Serb. Chem. Soc. 73 (4) 507–512 (2008)
UDC 543+061.3(4)
EuCheMS news

DIVISION OF ANALYTICAL CHEMISTRY
EUROPEAN ASSOCIATION FOR CHEMICAL AND
MOLECULAR SCIENCES

EUCHEMS NEWS

European analytical column No. 36 from the Division of Analytical Chemistry (DAC) of the European Association for Chemical and Molecular Sciences (EuCheMS)

(January 2008)

BO KARLBERG[1], HENDRIK EMONS[2] and JENS E. T. ANDERSEN[3]*

[1]Department of Analytical Chemistry, Stockholm University, SE-10691 Stockholm, Sweden, [2]Institute for Reference Materials and Measurements (IRMM), Joint Research Centre, European Commission, B-2440 Geel, Belgium and [3]Department of Chemistry, Technical University of Denmark, Building 207, DK-2800 Lyngby Denmark

INSTEAD OF INTRODUCTION – A MESSAGE FROM THE CHAIRMAN OF DAC: "A FOCUS ON EDUCATION"

The European Analytical Column has a somewhat different format this time. From now and on, it is our ambition to invite a guest columnist to give her/his views on various matters related to Analytical Chemistry in Europe. This year we have invited Prof. Hendrik Emons of the Institute for Reference Materials and Measurements (IRMM) to give his perspectives of Analytical Chemistry with inputs obtained from colleagues at the same institute. Recent activities of DAC and changes of its governance are also reported.

Analytical Chemistry in Europe has many facets and the Division of Analytical Chemistry, DAC, is discussing a broad range of them. I would like to focus my introduction of this European Analytical Column to one question:

Do we need analytical chemists with high quality education?

More than every second chemist working outside the educational system in the world is an analytical chemist. This factual circumstance is neglected in most European countries. If Europe wants to be competitive with respect to its industrial activities based on chemistry, then a comprehensive and advanced education of skilled analytical chemists becomes crucial.

---

* Corresponding author. E-mail: jeta@dac-euchems.org

A high quality education in analytical sciences assumes a platform of high quality research. Unfortunately, the various governmental financing of research in analytical sciences in Europe neither reflect nor meet industrial needs. The grants that are given to analytical chemists are marginal and heavily disproportional in comparison with other branches of chemistry. Consequently, there are too few high quality research platforms in analytical chemistry in Europe.

The recruitment of qualified analytical chemistry researchers at universities is hampered by the fact that most industries can offer a skilled Ph.D. in analytical chemistry a much more attractive environment than that of a university.

The recent developments in analytical sciences have provided a broad spectrum of tools and techniques. It is often difficult to find an expert and an appropriate education in a certain analytical discipline in some European countries. The position of analytical chemistry in Europe could be improved through the formation of research networks, arrangement of advanced courses and conferences, *etc*. This is a challenge for us within DAC and EuCheMS during the coming years. A great deal has already been accomplished through the excellent work of Reiner Salzer regarding guidelines for the content of education in analytical chemistry at the B.Sc. level (Eurobachelor).[1]

THE PERSONAL VIEW OF H. EMONS ON PERSPECTIVES FOR ANALYTICAL CHEMISTRY

What an exciting time for analytical chemistry: the demands for information about the interrelations of chemical composition – structure – properties for natural and synthetic materials are exploding. Analytical data are requested in the spatial domain from the atomic/molecular scale within biological structures *etc*., to the scale of global earth observation and in time windows from femtoseconds in laser applications to millions of years for palaeoclimate research. An increasing number of production processes have to be controlled by on-line analysis. The rapid development of technologies with the prefixes "nano" and "bio" could not have occurred without analytical tools from scanning probe microscopies to LC–MS^n.

In particular, the progress in the so-called bio- and nano-sciences is often driven by ideas, as well as by experimental and theoretical approaches, which are based on multidisciplinary knowledge and cross-fertilization among different scientific fields. This has led to "identity" and image problems in traditional scientific disciplines and could complicate the attraction of bright students and junior scientists, as well as research funding and academic positions. Such detrimental effects for analytical chemistry have been observed in several European countries in the last few years.

However, do those phenomena really reflect a downhill trend of analytical chemistry? Let us just look into a few aspects of the bio- or life-sciences: The “omics” are creating more chemical (molecular)-oriented analytical requests from biology and medicine than ever before. For instance, proteomics research is stipulating significantly the further development of mass spectrometry and affinity assays. Analysis at the cellular and tissue level requires the drastic reduction of sample sizes, the controlled preparation of delicate, not very stable samples and improved detection capabilities, including simultaneous multi-analyte quantifycation. The search for crucial human biomarkers is one of the most challenging tasks in clinical chemistry and can only be performed with powerful analytical tools and concepts. New non-invasive methods are required for early tissue diagnosis without biopsy and for the acute monitoring of disease treatments, such as those of cancer therapy.

In addition, the current "nano-wave" is pushing material sciences not only much closer to atomic and quantum physics, but also into many areas of chemistry, including modern analytical chemistry. For instance, the present discussions about possible health effects of some engineered nano-particles cannot be reduced to correlations of toxicological phenomena with morphology characteristics and will certainly in the future involve more chemical surface analysis at the nanoscale.

Obviously, there is not a shortage of exciting problems for analysts in many areas, both with cutting-edge scientific dimensions and with high social and economic relevance. There are, however, awareness issues both within the analytical community and with respect to the perception by scientists from other disciplines, and of regulators, the media, the public *etc*. According to my experience, a "simple" request from an "outsider" to an analytical chemist that he should just perform a "routine" service by analysing a provided sample with respect to pre-specified parameters develops nowadays much more often into a fruitful scientific discussion and collaboration about defining together the analytical problem and on designing the measurement strategy which really could allow the original question to be answered. Consequently, being able to use a mass spectrometer or a DNA sequencer does not make you an analytical chemist! Today, the analyst as a respected and valued scientific partner has to know and apply a range of analytical principles for identifying (often together with other specialists) the crucial measurand(s) for the question of interest, for establishing the metrological traceability and estimating the inherent uncertainty of the provided analytical data. This requires an adequate education on generic principles of analytical chemistry, including the basics of statistical data evaluation, method validation, estimation and use of measurement uncertainties, systems for lab-internal and external quality control, *etc*.

There was – and still is – a strong tendency in many scientific areas, for instance in genomics or proteomics, to establish large collections of analytical data without appropriate assessment of their reliability and/or without sufficient documentation on data validation. Obviously, the efforts towards data quantity and data quality, respectively, have to be re-balanced. This problem should also be considered seriously in the reviewing process of manuscripts prior to publiccation. I am not asking for a revival of the editorial principles of Justus von Liebig in the 19th century, who accepted for the journal "Annalen für Chemie und Pharmacie" only manuscripts in which the described experiments could be successfully repeated in his own laboratory. Nevertheless, there are still too many papers published which claim to establish new analytical methods and procedures but fail to convince the discerning reader about their proper validation or which report analytical data but do not provide convincing quality assurance information.

Obviously, the teaching and practicing of principles of analytical quality assurance and control (QA/QC) should be dealt with in a systematic manner at more European universities. Personally, I do not favour separate courses on QA/QC, but rather would prefer the integration of such generic concepts and procedures into the analytical lecture courses and laboratory exercises that are teaching methods and applications. By this means, a more practical, use-oriented quality knowledge and culture can be embedded in the young generations of analysts, instead of boring them with a definition- and regulation-focused "*l'art pour l'art*" approach to QA/QC. Such an education would also reduce to some extent the difference between curiosity-driven research in academics and the job content of many graduates of analytical chemistry in industrial laboratories or those of regulatory bodies. The latter two often put much more emphasis on quality management and compliance with international standards, such as ISO/IEC 17025, a topic that may not even be known to some university teachers or graduates.

Many projects for analytical chemistry are currently driven by challenges from the implementation and monitoring of legislation. Indeed, there is an increasing demand for scientifically sound, reliable analytical data for regulatory decisions at both the European and the global level. For instance, the new EU Water Framework Directive requires the development of analytical procedures for new specified analytes, such as short-chain chlorinated paraffins, in various types of water. Methods with improved precision are required for measurements around the legal limits – just think about decisions concerning the acceptance or rejection of food imports such as nuts because of their mycotoxin levels. There are needs for robust methods required for controls outside the laboratory (*e.g.*, at customs) or for large-scale screening of products or the environment, as well as for confirmatory/referee laboratory analysis in cases of dispute settlements. As the same analytical procedure is rarely suited for all the different purposes, the demanded variety will keep many of us busy for years to come.

Without being in possession of a crystal ball, near future advances in analytical chemistry can be predicted in a number of general directions. These include the further pushing of performance limits of analytical methods (such as smaller "target" sizes to achieve high spatial resolution, faster analysis for real-time or high-throughput data), simultaneous multi-parameter analysis of increasingly complex systems (living organisms, ecosystems, *etc*.) including their non-target screening, progress of non-invasive methods, provision of "sustainable" analytical data with demonstrated reliability (both precision and trueness) which are suitable for the purpose of making qualified decisions. Moreover, the miniaturesation of devices, laboratory automation and on-line process analysis are likely to continue as trendsetters. Above all the abilities of well-trained and continuously updated analytical chemists to combine their specific competences with interdisciplinary approaches in a problem-solving oriented manner are providing our discipline with a bright future!

NEW DAC GOVERNANCE

Heiner Korte, Germany, resigned as Secretary for the Division of Analytical Chemistry (DAC) after nine years of service. His successor, Jens E. T. Andersen, Denmark, was appointed at the 2007 Annual DAC meeting in Antwerp for the period 2008–2010. Heiner efficiently served under two Chairmen during the period 1999–2007 and due to his professsional contributions to the current structure and organisation DAC has gained wide respect and appreciation in the European analytical chemistry community and amongst his EuCheMS colleagues. The DAC Steering Committee was also appointed at the Annual meeting: George Horvai, Hungary, Wolfgang Buchberger, Austria, Paul Worsfold, UK, Jens E. T. Andersen (Secretary), Denmark, and Bo Karlberg (re-elected Chairman for the period 2008–2010), Sweden. At this meeting, it was also decided that DAC support the continuation of the Study Group of quality assurance. Jens E. T. Andersen took over from Wolfhard Wegscheider after his long-time effort as head of the Study Group. Jens E. T. Andersen was also appointed as the liaison person to EuraChem and to CITAC.

INFORMATION FROM THE **E**U**C**HE**MS** DIVISION OF ANALYTICAL CHEMISTRY

The Euroanalysis conference is the main event of the DAC, and it was excellently organised by Koen Janssens and Luc Van't Dack under the auspices of the Flemish Chemical Society KVCV. The conference was held under the general theme “The role of Analytical Chemistry in the preservation of mankind’s natural and cultural environment”. It was attended by 650 participants from 50 countries worldwide providing more than 800 contributions. The stimulating scientific program, including a fully booked poster sessions, was interspersed with interesting booths of instrument manufacturers and publishers. Prof. Alfredo Sanz-Medel of Oviedo University in Spain gave the “Robert Kellner Lecture”, which was sponsored by the Springer Verlag. “The Merck Award” was awarded to Alexander Makarov of Thermo Finnigan for his development of the orbitrap analyzer of mass spectrometry and to Prof. Shuming Nie of Georgia Institute of Technology for introducing quantum dots to clinical analysis and diagnosis. Euroanalysis XV, with the motto “The impact of Analytical Chemistry on the Quality of Life” is planned for Innsbruck on September 6–11, 2009, and is now accessible at www.Euroanalysis2009.at.

In 2008, the DAC will contribute to the second general conference on Chemistry in Turin, 16–20 September. The DAC focuses on metrology in chemistry and thus promotes its continuing effort within the field of quality assurance. Prof. Manfred Grasserbauer will present a lecture entitled “The Environmental Challenge for Analytical Sciences”. This will continue the process of involving the work of analytical chemists from the public sector, industry and academia in the DAC.

Europe has played a central role over the centuries in developing analytical chemistry and Prof. Duncan Burns continues his effort within the frames of the DAC with "Contributions to the History of Analytical Chemistry in Europe made *via* DAC–EuCheMS". This work resulted in several publications, including, with L. Sabattini, an account of the History of Analytical Chemistry of Italy, publicshed this year preceding the conference in Turin 2008.

It is important to the DAC to maintain networking with the other Divisions of EuCheMS, which are occupied by corresponding scientific issues. The cooperation is fostered by appointing liaison persons who relate to education, history, life sciences, food, environment, electrochemistry, computations, microsystems, IUPAC and Eurachem. The developments of quality assurance and quality control are followed with great interest because these subjects have a profound impact on a wide range of applications that are also considered and supervised by the European commission. Although highly specialised conferences are increasing in numbers and popularity, it is important to communicate actively across the borders defined by technologies, which ensures a high level of science, education and innovation. The contact to other divisions, to supranational boards and to non-European societies is aided by DAC observers. Updated information on DAC activities may be found at www.dac-euchems.org.

Acknowledgements. The authors are indebted to A. Bernreuther, R. Koeber, T. Linsinger, and B. Toussaint, IRMM, for valuable input.

REFERENCE

1. R. Salzer, *Anal. Bioanal. Chem.* **378** (2004) 28.